CogSust

Cognitive Sustainability

June 2025 Vol. 4. No. 2

ISSN 2939 - 5240

Cognitive Sustainability

Cognitive Sustainability (CogSust) is a double-blind peer-reviewed scientific journal published by CogSust Ltd. (H1116 Budapest Putnok u 9.)

The person responsible for publishing: Mária Szalmáné Csete editor@cogsust.com

The person responsible for editing: Ádám Török info@cogsust.com

CogSust is an online quarterly journal, publication frequency: quarterly, by

March, June, September, December.

ISSN 2939-5240

The journal is indexed by:

Library of Hungarian Scientific Works

Repository of the Library of Hungarian Academy of Science

Google Scholar

Sherpa Romeo

RePEc (Research Papers in Economics)

Directory of Open Access Journals

Crossref

Semantic Scholar

ERIH PLUS

Index Copernicus International

Dimensions

Scilit

Lens

https://doi.org/10.55343/CogSust.142

Application of neural networks in vehicle simulation as a substitute for driver models

Tamás Koller
0009-0003-0427-4877
Department of Propulsion Technology
Széchenyi István University
Audi Hungaria Faculty of Automotive Engineering
Győr, Hungary
hu.tamas.koller@gmail.com

Csaba Tóth-Nagy
0000-0001-7825-9133
Department of Propulsion Technology
Audi Hungaria Faculty of Automotive Engineering
Széchenyi István University
Győr, Hungary
toth-nagy.csaba@ga.sze.hu

Abstract

The development and optimization of vehicle simulation models is essential for the virtual validation of new features during vehicle development. New challenges are emerging that require the application and use of innovative solutions. The use and development of artificial intelligence methods can accelerate development processes, which will require a broader investigation of their feasibility. This paper explores the potential of applying a neural network based technology to a driver model within a vehicle simulation instead of the traditional proportional-integral (PI) control methods. The artificial neural network applied here can learn the driving style of the driver and can be used in both simulation and virtual testing scenarios. The aim of this paper is to demonstrate the use of neural network to replace the PI controller throttle signal in a vehicle simulation driver model. In this novel approach, the artificial neural network can learn real driver behavior resulting in a more realistic driver model in vehicle simulation further advancing the accuracy of the simulation.

Keywords

vehicle simulation; neural network; validation; artificial intelligence; virtual test environment; development; vehicle simulation.

1. Introduction

The use of Artificial Intelligence (AI) is vital for contemporary technological progress, particularly in sectors where rapid and efficient development and testing processes are resource-intensive. Digital development enables us to expand our experiential knowledge in most areas of our lives (Zöldy et al., 2022). Tollner et al. (2019) describe an application example in the development of autonomous vehicles, where artificial intelligence assists in decision-making. AI-driven solutions present new opportunities in vehicle simulation development (Rana and Khatri, 2024; MacAdam et al., 1998; Tselentis and Papadimitriou, 2023). Currently, conventional simulation systems demand a significant amount of time and resources. Experimentation under complex conditions and the creation of realistic models present various challenges. AI-enhanced vehicle simulations can be highly effective as these systems can discern intricate patterns and forecast future events (Hermansdorfer et al., 2020; Huang et al., 2018). Artificial intelligence is recognized as a forward-looking technology for improving rail transport, where a key focus is increasing efficiency (Ficzere, 2023). Artificial neural network-based models are reliable and accurate, and accelerate the vehicle development process by making driver models life-like and which act as the real driver of a vehicle. It is possible to train neural networks for different driving styles, making this way of model definition suitable for advancing sustainable development processes.

https://doi.org/10.55343/CogSust.142

A crucial aspect of driving simulation is adjusting the accelerator pedal position, as throttle control is fundamental to driving dynamics. Neural networks enable the identification of complex patterns and allow for reliable data-driven predictions (Conley et al., 2001). Traditionally, vehicles employ Proportional-Integral Controllers for acceleration and deceleration commands (Ioannou and Xu, 1994). However, the rise of AI is paving the way for new control system methodologies, facilitating more sophisticated and adaptive solutions (Lee and Choi, 2021).

MATLAB's Neural Fitting tool is especially suited for learning and optimizing neural networks, predominantly for regression tasks. The focus is to achieve the best possible alignment of input data with output values for driving behavior. When constructing the model, it is crucial to implement the appropriate control mechanisms, as this significantly influences the reliability and precision of the results. If the accelerator pedal signal is generated by neural networks, the vehicle simulation model effectively serves as a substitute for a PI controller, meaning that the model's control is governed by the neural network.

The use of hybrid models in vehicle dynamics simulations presents a significant professional challenge, as they necessitate validation through real measurement data. To facilitate this, the MATLAB Simulink environment offers a highly adaptable toolbox for modeling complex systems, which enhances the design and implementation of simulation models.

This paper demonstrates the functionality of a vehicle simulation model that incorporates a neural network, detailing the learning process and the method for generating the throttle signal. The vision is to replace the traditional accelerator pedal signal, typically driven by a PI-controller, with a neural network in the vehicle simulation model.

2. Methodology

Neural networks are capable of complex pattern recognition and prediction. Building on this capability, the position of the accelerator pedal in the vehicle simulation driver model was first determined, which was examined using a forward-looking simulation method. The term *forward-looking simulation* refers to an approach used in vehicle dynamics studies. This method essentially serves to compute and model the dynamic behavior of various components of a vehicle, such as engine, transmission, final drive, and other various components of the drivetrain (Pettersson et al., 2020). The advantage of forward looking – closed-loop – simulations is that they allow for complex examination and optimization of various parameters and input signals without the need for expensive and time-consuming physical testing. MATLAB Simulink was used for setting up the vehicle simulation model. MATLAB Simulink is an integrated environment that facilitates the modelling and simulation of different dynamic systems..

Based on real-world vehicle measurements conducted on public roads, a vehicle drive cycle of 857 seconds was created, utilizing a real hybrid vehicle. The internal combustion engine of the vehicle was a two-liter, four-cylinder, 110 kW engine that operates in conjunction with a 75 kW electric motor. The vehicle's curb weight was 1950 kg without the driver. The vehicle featured a parallel hybrid configuration, allowing the internal combustion engine and the electric motor to operate either together or independently, thereby optimizing performance and efficiency. The vehicle measurements were carried out at an ambient temperature of approximately 18.75 degrees Celsius, starting from the outskirts and arriving at the center of Győr, Hungary. Among the data obtained from the road measurements, the vehicle speed is provided as an input for the vehicle simulation model. The vehicle's operating modes (electric, hybrid, or pure internal combustion engine), the torque values for the internal combustion and electric motors, and the gearbox gear number have been specified based on calculated values and a look-up table. The dynamics of the vehicle have been parameterized using mathematical equations.

The application of the neural network in the vehicle simulation model began with the training of the neural network. The first step involved determining the input parameters of the training data set, which contains data collected under various driving scenarios. In the driver model, four input parameters (vehicle speed, transmission gear number, vehicle acceleration, and engine RPM) and the target variable (gas pedal position) were trained (Figure 1). The values of the gas pedal position generated by the PI controller from the vehicle simulation model were used for the training of the neural network. In the Matlab Simulink environment, it is necessary to provide the model with an environment that allows the neural network building block to have uninterrupted access to the input data used to run the model. Therefore, the PI controller and the ANN model were run concurrently.

https://doi.org/10.55343/CogSust.142

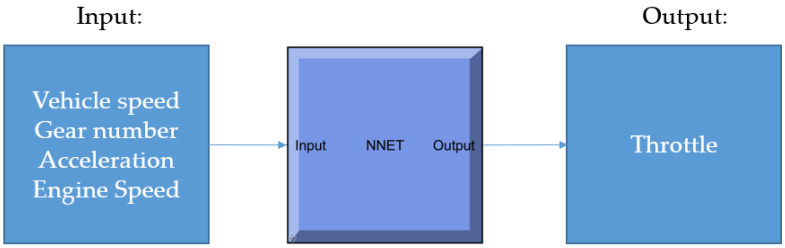

Figure 1. Neural network input and output parameters.

In the vehicle simulation's driver model, the accelerator pedal position was generated by the PI controller to train the neural network, as reintegrating it into the model allows for a clear assessment of the predicted outcomes' value. The brake pedal's function continued to be controlled by the existing PI controller established in the original model, as in this study the focus was on accelerator pedal signal only. Subsequently, the neural network was integrated into the existing simulation environment (Figure 2), where vehicle performance was analysed. The next step involved further fine-tuning the parameters of the neural network to optimize its performance.

By utilizing the MATLAB Neural Fitting toolbox and providing the input parameters, it was possible to determine the target value based on the results generated by the vehicle simulation model. In the subsequent process, the Neural Fitting tool (nftool) was used for setting the ratio of validation and testing data to 15%. The number of the neurons in the single hidden layer was set to 10 that allowed for the optimization of the model's complexity.

For selecting the learning algorithm, the Levenberg–Marquardt method was used, as this technique is well-known for its fast convergence and precise optimization in the training of neural networks. As a next step, a Simulink diagram was generated, which was integrated into the base model. This step enabled the execution of enhanced simulation.

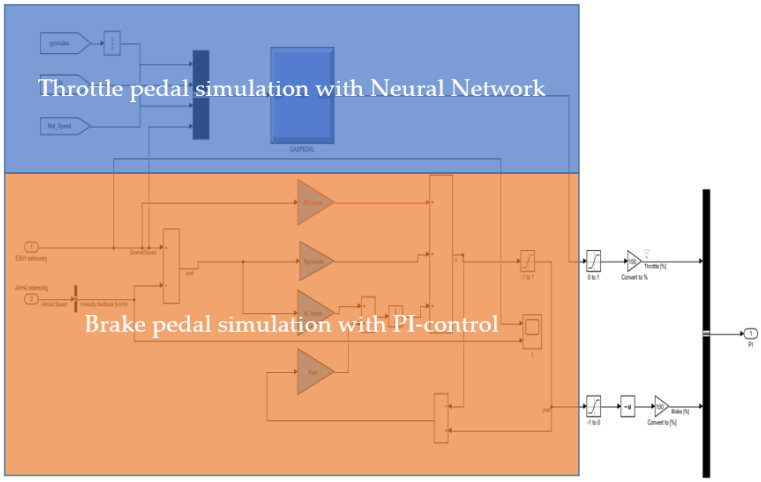

Figure 2. Application of Neural Networks in Driver model.

In summary, the main steps for working with neural networks in the vehicle simulation model are as follows:

- refinement of the vehicle simulation model for training;
- execution of the vehicle simulation and processing of the resulting data;
- training the neural network with the data;
- implementation of the neural network component into the model;
- running the neural network model;
- evaluation, analysis, and comparison of the vehicle simulation model enhanced with the neural network.

https://doi.org/10.55343/CogSust.142

3. Results and discussion

Upon completing the model development, a comparison was made between the driver model created using the new modelling technique and the original driver model used in the vehicle simulation. In simpler terms, the generation of the throttle position was replaced in the original vehicle simulation model by the artificial neural network (ANN) based driver model. Thus, the two different models were compared under the same boundary conditions. It is noteworthy that the engine and electric motor speeds depend on the transmission gear, and an agreement of engine and electric motor speeds were matched as well as the control strategy of the hybrid system.

The results of the simulation were compared to real life measurements for validation purposes. With the application of the new modelling technique, an investigation was conducted to verify the correct functioning of the ANN-based throttle position generation. The results corroborated with the satisfactory performance of the new type of modelling, which is illustrated in Figure 3. The figure displays the vehicle speed as a function of time. Values marked in blue represent the vehicle simulation results operated by the original model, while those in green show the results generated using artificial neural networks.

The comparison between the two driver models not only attracts scientific interest but also contributes to a deeper understanding of driver's behavior and the development of modelling techniques. The Root Mean Square (RMS) was calculated for both vehicle simulation models. The basic model showed an RMS value of 0.776, while the calculation using the new method yielded an RMS value of 0.7411, reflecting the discrepancies between the target speed and the vehicle speed calculated by the simulation.

It is noticeable that throughout the entire simulated period, the new method produced throttle position values corresponding to the required vehicle speed with smaller errors (0.03 RMS value). During the investigation, the hybrid control strategy, as well as the engine speeds and gearbox numbers, were reviewed, demonstrating consistency in both models.

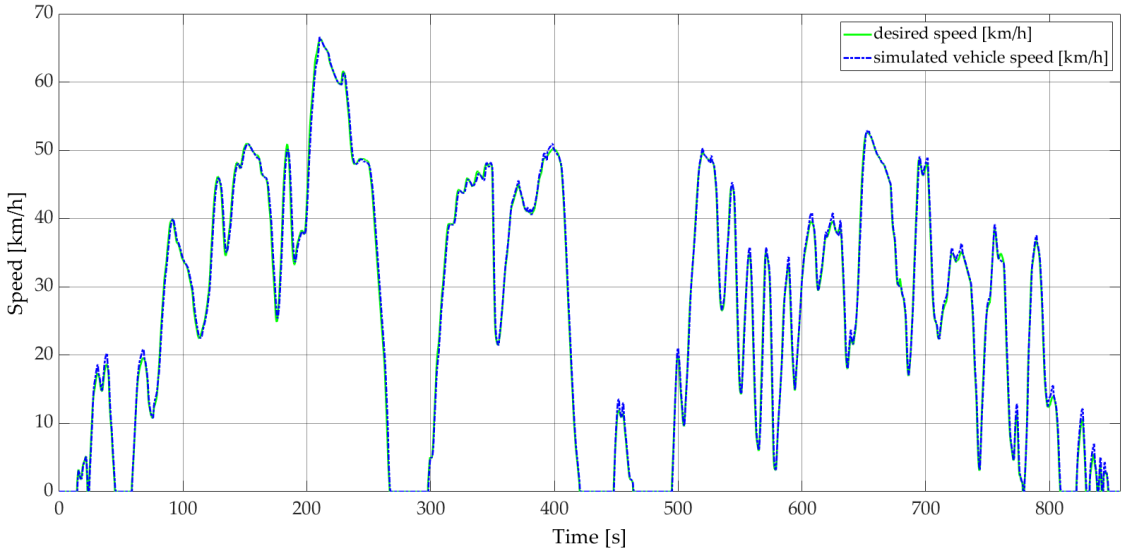

Figure 3. Vehicle speed reached using the PI-based driver model and the ANN-based driver model.

The neural network is capable of responding accurately to unexpected environmental changes and complex driving situations, similarly to traditional PI controllers. The results also indicate that neural networks can learn from the dynamics of the vehicle, thereby autonomously improving the system's efficiency.

https://doi.org/10.55343/CogSust.142

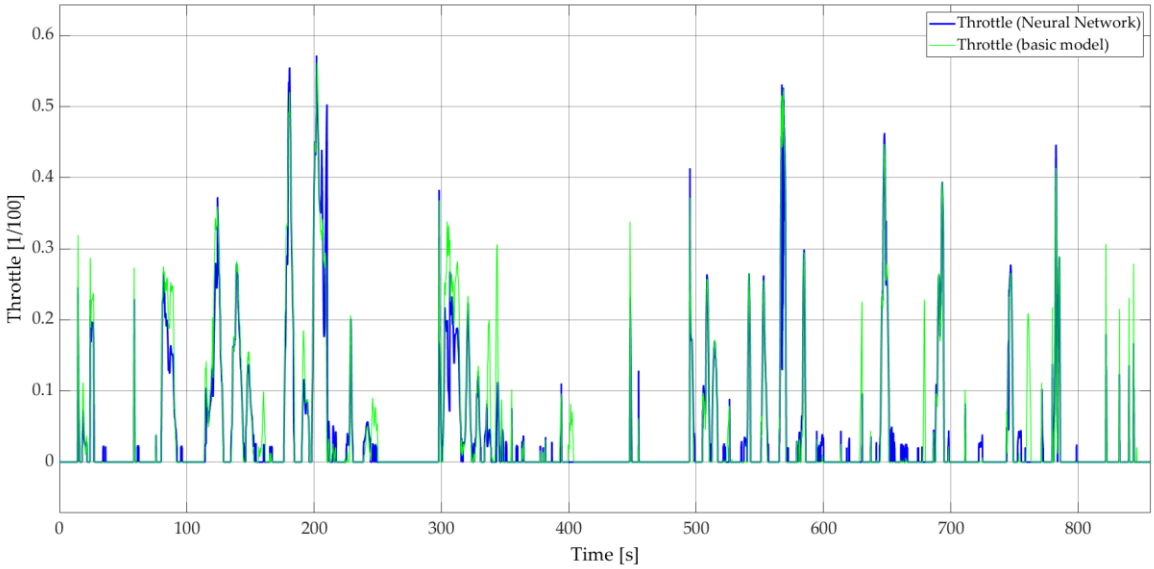

Figure 4. PI-based model and ANN-based driver model generated gas pedal values.

4. Conclusion

This vehicle simulation example is an excellent illustration of how modern AI-based simulation techniques can contribute to the success of automotive developments. Such simulation techniques provide opportunities to optimize vehicle performance while reducing cost and time investment during the development process. Generating gas pedal signals with neural networks can revolutionize vehicle simulation driver modelling, allowing for enhanced control and increased adaptability to real life situations.

In summary, replacing the PI based driver model with a neural network based one in a vehicle simulation model presented an error in RMS values of 0.03, showing that this method can be advantageous in the field of vehicle modelling. This can be used in numerous areas of development such as vehicle architecture and control strategy optimization, as well as performance, fuel consumption, and emissions optimization. This method offers avenues for future advancements, such as more refined and safer control of autonomous vehicles as well. Further research should explore additional refinement opportunities during vehicle development to better leverage the potential of neural networks in the automotive industry.

Replacing the traditional PI-based driver model with a neural network based one presents a practical example in the development of vehicle simulation systems, paving the way for dynamic and intelligent control strategies. Compared to PI controllers, this approach does not only improve performance but also contributes to the development of more sustainable and innovative transportation systems.

The example of hybrid modelling in vehicle dynamic simulation raises several issues that developers encounter, even if the course of development shifts in other directions. The proposed solution is applicable in any vehicle technology environment. Therefore, the application of artificial networks represents an exciting and rapidly evolving field, offering numerous research and development opportunities. Projects of this nature contribute to the innovation and efficiency of future transportation systems.

References

Conley, J., Clay, B., Waters, R., Tóth-Nagy, Cs., Taylor, S., Smith, J., Atkinson, C. M. (2001). The Development of a Fourth Generation Hybrid Electric Vehicle at West Virginia University. *SAE Technical Paper 2001-01-0682*. DOI: 10.4271/2001-01-0682

Ficzere, P. (2023). The role of artificial intelligence in the development of rail transport. *Cognitive Sustainability*, 2(4). DOI: 10.55343/cogsust.81

Hermansdorfer, L., Trauth, R., Betz, J., Lienkamp, M. (2020). End-to-End Neural Network for Vehicle Dynamics Modeling. *2020 6th IEEE Congress on Information Science and Technology (CiSt)*. Agadir–Essaouira, Morocco. 407–412. DOI: 10.1109/CiSt49399.2021.9357196

Huang, X., Sun, J., Sun, J. (2018). A car-following model considering asymmetric driving behavior based on long short-term memory neural networks. *Transportation Research Part C: Emerging Technologies*. 95, 346–362. DOI: 10.1016/j.trc.2018.07.022

Ioannou, P., Xu, Z. (1994). Throttle And Brake Control Systems For Automatic Vehicle Following. *UC Berkeley: California Partners for Advanced Transportation Technology*. URL: https://escholarship.org/uc/item/1vb6380h

https://doi.org/10.55343/CogSust.142

Lee, H., Kim, H., Choi, S. (2021). Driving Skill Modeling Using Neural Networks for Performance-Based Haptic Assistance. *IEEE Transactions on Human-Machine Systems*. 51(3), 198–210. DOI: 10.1109/THMS.2021.3061409

MacAdam, C., Bareket, Z., Fancher, P., Ervin, R. (1998). Using neural networks to identify driving style and headway control behavior of drivers. *Vehicle System Dynamics*. 29 (sup1). DOI: 10.1080/00423119808969557

Pettersson, P., Jacobson, B., Bruzelius, F., Johannesson, P. Fast, L.(2020). Intrinsic differences between backward and forward vehicle simulation models. *IFAC-PapersOnLine*, 53(2), 14292–14299. DOI: 10.1016/j.ifacol.2020.12.1368

Rana, K., Khatri, N. (2024). Automotive intelligence: Unleashing the potential of AI beyond advance driver assisting system, a comprehensive review. *Computers and Electrical Engineering*. 117, 109237. DOI: 10.1016/j.compeleceng.2024.109237

Tollner, D., Cao, H., Zöldy, M. (2019). Artificial Intelligence based Decision Making of Autonomous Vehicles Before Entering Roundabout. *IEEE 19th International Symposium on Computational Intelligence and Informatics and 7th IEEE International Conference on Recent Achievements in Mechatronics, Automation, Computer Sciences and Robotics (CINTI-MACRo)*, Szeged, Hungary. 181–186, DOI: 10.1109/CINTI-MACRo49179.2019.9105322

Tselentis, D. I., Papadimitriou, E. (2023). Driver Profile and Driving Pattern Recognition for Road Safety Assessment: Main Challenges and Future Directions. *IEEE Open Journal of Intelligent Transportation Systems*. 4, 83–100. DOI: 10.1109/OJITS.2023.3237177

Zöldy, M., Szalmáné Csete, M., Kolozsi, P. P., Bordás, P., Török, Á. (2022). Cognitive Sustainability. *Cognitive Sustainability*. 1(1). DOI: 10.55343/cogsust.7

https://doi.org/10.55343/CogSust.138

Sustainable Control of *Fusarium verticillioides* in Wheat Using Plant Extracts and Microorganisms

Asmira Mebdoua
s.mebdoua@univ-bouira.dz
Laboratory of Biotechnology and Protection of Agricultural and Natural Ecosystems
Akli Mohand Oulhadj University of Bouira, Algeria

Nouari SADRATI
n.sadrati@univ-bba.dz
Laboratory of Biotechnology and Protection of Agricultural and Natural Ecosystems
Akli Mohand Oulhadj University of Bouira, Algeria

Saliha Mohammedi
s.mohammedi@univ-bouira.dz
Laboratory of Biotechnology and Protection of Agricultural and Natural Ecosystems
Akli Mohand Oulhadj University of Bouira, Algeria

Amal saidi
amal.saidi@univ-bouira.dz
Laboratory of Biotechnology and Protection of Agricultural and Natural Ecosystems
Akli Mohand Oulhadj University of Bouira, Algeria

Abstract

Fusarium verticillioides is frequently reported as the major pathogen in maize production; however, it has not been previously identified as a causal agent of Fusarium head blight in wheat in Algeria. The aims of this work are to study the pathogenicity of a *Fusarium verticillioides* strain isolated from wheat grains and to perform preliminary assays to control this pathogen using plant extracts from *Rosmarinus officinalis*, *Origanum vulgare* and *Eucalyptus globulus,* and three microorganisms *(Akanthomyces muscarius*, *Pseudomonas fluorescens*, and *Pantoea agglomerans)*. The identity of the strain was confirmed using morphological and molecular methods. The pathogenicity tests were carried out using both durum and bread wheat grains. The agar dilution method was used to evaluate the antifungal activity of the extracts, while the direct confrontation method was used to assess the antifungal activity of the three microorganisms. The results showed that the strain was pathogenic to both durum and bread wheat. Aqueous extracts showed low inhibition rates (14 to 47%), while ethanolic extracts had higher inhibition rates (52 to 65%). Direct confrontation tests revealed inhibition rates of 55% and 52% for *A. muscarius* and *P. fluorescens*, respectively. The fungus *A. muscarius* was also shown to be able to reduce the symptoms of *F. verticillioides* in antagonism tests using wheat seeds. The ethanolic extracts of the three plants, *A. muscarius*, and *P. fluorescens* may offer alternative solutions to the use of fungicides.

Keywords
Fusarium verticillioides, plant extracts, *Akanthomyces muscarius, Pseudomonas fluorescens*

1. Introduction

Wheat is susceptible to attacks by various phytopathogenic fungi in all stages of growth, from seedling to maturity (Pastuszak et al., 2021). Species of the genus *Fusarium* are among these fungi. They are responsible for two important diseases in wheat; the first is Fusarium crown rot (FCR), which causes root system and crown rotting and precocious maturing with sterile white heads. It is mainly caused by *Fusarium acuminatum*, *F. avenaceum*, *F. equiseti*, *F. crookwellense* and *F. culmorum* (Campanella, 2023). The second disease is Fusarium head blight (FHB) causing an important crop loss and reduction of harvested grains quality. The most aggressive FHB species are *F. culmorum*, *F. graminearum* and *F. avenaceum*; while other species are less frequent and less aggressive, such as *F. cerealis*, *F. poae*, *F. equiseti*, *F. solani*, *F. verticillioides* and *F. proliferatum* (Sakr, 2022).

https://doi.org/10.55343/CogSust.138

F. vertillicioides is frequently reported as the major pathogen in maize production (He et al., 2023). It has been associated with several diseases in maize for almost a century, including root rot, stem rot and seedling blight (Yates et al., 2005). In wheat production; however, it was rarely reported as a pathogen or as a grain contaminant. But in the last ten years, it was reported as an emergent pathogen in Finland (Gagkaeva and Yli-Mattila, 2020), as species associated with FHB in South Russia (Gagkaeva et al., 2018) and species associated with FCR in Algeria (Abdallah-Nekache et al., 2019).

The use of synthetic fungicides remains the main tool to control *Fusarium* diseases on wheat (Bachouche et al., 2024). Fungicides used are mainly triazoles like hexaconazole, propiconazole, tebuconazole and triadimenol. Other chemicals can also be applied, such as carbendazim and prochloraz (Dweba et al., 2017; Zhao et al., 2021). However, none of these chemicals provides a complete protection against wheat *Fusarium* diseases (Dweba et al., 2017).

The development of alternative methods to the use of synthetic fungicides has become a necessity in order to better protect crops, environment and humans' health (Seepe et al., 2020). The biocontrol of *Fusarium* by the use of microorganisms such as bacteria and fungi has already been reported by several authors. Dweba et al. (2017) and Matarese et al. (2012) recommended *Brevibacillus* sp. (strain BRC 263), *Streptomyces* sp. (strain BRC87B) and *Trichoderma gamsii* (strain 6085) as potential biocontrol agents of *Fusarium* disease in cereal. *Bacillus* sp. (strain B25) are also effective biocontrol agents against maize *Fusarium* disease (Douriet-Gámez et al., 2018). The biocontrol of *Fusarium* by using the bioactive compounds extracted from plants has been also studied. Dambolena et al. (2012) reported that natural phenolic compounds such as carvacrol, thymol and isoeugenol have a high antifungal activity against *F. verticillioides.* Seepe et al. (2020) studied aqueous and organic extracts of thirteen medicinal plants from South Africa. They found that acetone extracts obtained from *Quercus acutissima*, *Harpephyllum caffrum* and *Combretum erythrophyllum* are the most effective extracts inhibiting the growth of *F. proliferatum, F. graminearum, F. solani* and *F. verticillioides* with minimum inhibitory concentration values less than 0.1 mg/ml. They found also that aqueous extracts of *Olea europaea, Withania somnifera, Combretum molle* and *Lantana camara* are effective and can be used to manage diseases caused by *Fusarium* species.

Based on the aforementioned reports, we hypothesize that plant extracts and beneficial microorganisms can provide an effective approach to controlling *F. verticillioides* while minimizing environmental impacts. The use of plant extracts and microorganisms to combat *F. verticillioides* can significantly reduce reliance on synthetic fungicides, thereby decreasing their undesirable negative effects. These effects might include impacts on non-target organisms and thus on biodiversity, and persistence in the environment. Indeed, while beneficial microorganisms and plant extracts are not entirely specific, their spectrum of action remains much narrower compared to synthetic fungicides (Fenta et al., 2023). Moreover, certain microorganisms, such as *Pseudomonas fluorescens*, can contribute to increasing soil fertility (Martínez et al., 2019). Additionally, plant extracts have the advantage of being biodegradable in the soil. However, the use of exogenous antagonistic microorganisms not native to the treated area can cause significant disruptions to the ecosystem and local microbial populations. The implementation of control methods based on plant extracts and antagonistic microorganisms should be preceded by thorough risk assessments and field trials to guarantee their effectiveness, safety, and optimal application.

The aims of this work are to study the pathogenicity of a *Fusarium verticillioides* strain isolated from wheat grains and to perform preliminary assays to control this pathogen using aqueous and ethanolic extracts of three plants *(Rosmarinus officinalis*, *Origanum vulgare, Eucalyptus globulus)*, the fungus *Akanthomyces muscarius*, and two bacteria *(Pseudomonas fluorescens* and *Pantoea agglomerans).*

2. Data and methods

2.1. Isolation and morphological identification of *Fusarium verticillioides*

The durum wheat seeds (20 samples) used for isolation in this study were provided by the Cooperative of Cereals & Pulses (CCLS) of Bouira Province, Algeria. All the samples came from Bouïra fields characterized by a semi-arid climate. The isolation was performed using the protocol of Ioos et al. (2004). Briefly, wheat grains were superficially disinfected by soaking them in a solution of sodium hypochlorite at 1.5 V/V Cl with the addition of Tween 20 (0.01 V/V%) for 10 minutes. The grains were then placed to dry on sterile filter paper. Among the perfectly dried grains, at least 100 grains were taken at

https://doi.org/10.55343/CogSust.138

random and placed directly on Dichloran Chloramphenicol Peptone Agar (DCPA) medium described by Andrews and Pitt (1986) at the rate of 5 grains per Petri plates. DCPA Petri plates were incubated for 10-12 days at 25 °C.

Typical *Fusarium* colonies were subsequently transferred to PDA (Potato Dextrose Agar) and SNA (Synthetischer Nahrstoffarmer Agar – Synthetic Nutrient Deficient Agar) and were identified after 5 to 10 days of incubation at 25 °C following the protocol of Leslie and Summerell (2008). *F. verticillioides* was detected in two samples.

2.2. Molecular identification and phylogenetic analysis

Genomic DNA was extracted from monosporic *F. verticillioides* S03 strain culture, using a commercial NucleoSpin Plant II kit (Macherey-Nagel, Germany) according to the manufacturer's recommendation. For the S03 strain, segments of ITS (Nuclear ribosomal Internal Transcribed Spacer) region were amplified by the primer pairs ITS1 (CTT GGT CAT TTA GAG GAA GTA A) and ITS4 (TCC TCC GCT TAT TGA TAT GC) as described by Gardes and Bruns (1993); also, segments of TEF-1α (Translocation Elongation factor 1-alpha) region were amplified using the primer pairs EF-728F (CAT YGA GAA GTT CGA GAA GG) and EF2 (GGA RGT ACC AGT SAT CAT GTT) according to Carbone and Kohn (1999). Amplification was performed with a total volume of 25 µL, containing 2 µL of genomic DNA, 1µL of 10µM primers, 5µL of 5X Taq buffer (Promega Corporation, USA), 1.5 µL of 25 mM $MgCl_2$, 0.2µL of d'NTP mixture (25 mM), 0.2µL of 5U/µL of Taq DNA polymerase (Promega Corporation, USA), and 14.10 µL of double-distilled sterile water. PCR conditions for the ITS region were as follow: Initial denaturation at 95 °C for 5 min, 35 cycles of denaturation at 95 °C for 30 s, hybridization temperature of 55 °C for 30 s, extension at 72 °C for 45 s, followed by a final extension at 72 °C for 7 min. The same conditions were used for the TEF1-α region; however, the hybridization temperature was changed to 52 °C. After the PCR reaction, the PCR product was separated into a 1.5% agarose gel (Sigma-Aldrich, USA) and stained with 0.5µg ml^{-1} ethidium bromide. A molecular weight marker of 100 bp (PCR 100 bp low Ladder, Sigma-Aldrich) was used. DNA fingerprints were visualized following exposure to UV light using the Gel Documentation System (Bio-Rad, USA). The PCR products were then purified using the NucleoSpin® Gel and PCR Clean-up kit from Macherey-Nagel (Germany) and sequenced by the Sanger technique using the BigDye v3.1 kit from Applied Biosystems and the same primers used in PCR. The obtained sequences were analyzed and corrected using the CHROMAS PRO software.

The obtained sequences have been compared with those in the National Center for Biotechnology Information (NCBI) database using the programme BLAST. The S03 strain was identified based on percentage homology with published ITS and TEF-1α sequences. Phylogenetic tree has been generated by TEF-1α sequences alignment using MEGA7 software. Maximum likelihood analyzes (ML) were applied using 54 TEF-1α sequences from *Fusarium fujikuroi* species complex. Two sequences from *F. oxysporum* NRRL 22902 and *F. inflexum* NRRL20433 were used as out group. The support of the internal branches of the tree was evaluated by the bootstrap method with 1000 replications.

2.3. Pathogenicity test

In order to evaluate the pathogenicity of *Fusarium verticillioides* strain, seeds of two species of wheat (Bread wheat: cultivar of HD1220; Durum wheat: cultivar of Oued El Bared) were used. For each wheat species and for each treatment, a number of 100 seeds were surface-sterilized by soaking in a 2% NaClO solution for 8 min, then rinsed twice with sterile distilled water. The seeds were placed in Petri plates lined with sterile absorbent paper in triple layer at the rate of 25 seeds per Petri plate. For inoculum preparation, the protocol of Bouanaka et al. (2022) was adopted. Each *Fusarium* strain was cultured on PDA medium at 26 °C. for 15 days. A volume of 10 ml of sterile distilled water with 0.01% (v/v) of Tween-80 was added to the aerial part of *F. verticillioides* 15day-old culture. The culture surface was then carefully scraped until the entire superficial layer of the fungus had been recovered. The resulting suspension, consisting of mycelium and conidia, was filtered through a double layer of sterile cheesecloth and adjusted to 10^6 conidia ml^{-1} using sterile distilled water with 0.01% (v/v) of Tween-80. A volume of 5 ml of the inoculum suspension was sprayed onto each Petri plate containing wheat seeds. Petri dishes were then incubated at 26 °C in total darkness (Bouanaka et al., 2022). Control plates were prepared in the same way by substituting the inoculum suspension with sterile distilled water with 0.01% (v/v) Tween-80. The rate of the seeds germination, the length and the weight of coleoptile were calculated four days after the inoculation.

2.4. Antifungal activity of plant extracts against *F. verticillioides*

https://doi.org/10.55343/CogSust.138

Rosemary *(Rosmarinus officinalis)*, oregano *(Origanum vulgare)* and eucalyptus *(Eucalyptus globulus)* tested were from Bouira Province. Fresh leaves were collected in the April–May period and shade-dried at room temperature. The dried leaves were ground into fine powders using a coffee grinder. Aqueous extracts were obtained by soaking 15 g of leaf powder in 150 ml of distilled water for 24 h with stirring. The extracts were filtered through Whatman No. 1 filter paper and stored at 4 °C. Ethanolic extracts were prepared using a Soxhlet apparatus with 15 g of leaf powder and 150 ml of ethanol (96°V/V%) were used. The extraction was carried out at 70 °C under atmospheric pressure for 3h.

The agar dilution method was used to evaluate the antifungal activity of the extracts (Wilkinson, 2006). For aqueous extracts, a volume of 20 ml were incorporated into PDA medium to prepare 100 ml of final medium volume. For ethanolic extracts, an aliquot of 20 ml of each extract were evaporated using a rotary evaporator and then resolved in 20 ml of water and incorporated into PDA medium to prepare 100 ml of final medium. These media were sterilized at 120 °C for 20 min, and then were poured in sterile Petri dishes.

In order to compare antifungal activity of extracts, two synthetic fungicides were incorporated into the PDA medium in the same way as for the plant extracts. The first was Iprodione at concentration of 7.5 mg per 100 ml of PDA medium: it had been prepared from commercial wettable powder product containing 50% of Iprodione (50% WP). The second was Difenoconazole at 1.5 mg/ 100 ml of PDA medium; it had been prepared from commercial emulsifiable concentrate product containing 25% of Difenoconazole (25% EC)

For inoculation, agar discs (5 mm in diameter) were taken from ten days old culture plates of *F. verticillioides* and then placed on PDA Petri prepared with leaves extracts or with fungicides. The plates were incubated at 26 °C ± 2 °C. The control was carried out under the same conditions without leaves extracts or fungicides. The radial growth was then measured and compared with the control (Wilkinson, 2006). The inhibition percentage of growth was calculated according to this formula (1):

$$\text{Inhibition percentage} = (D_{\text{control}} - D_{\text{test}}) / D_{\text{control}} \times 100 \quad (1)$$

Where D_{control} is the diameter of *F. verticillioides* colony in the control plates, D_{test} is the diameter of *F. verticillioides* colony in the plates amended with plant extracts or fungicides.

2.5. Antifungal activity of *Akanthomyces muscarius*, *Pseudomonas fluorescens*, *Pantoea agglomerans* against *F. verticillioides*

The strains of *Akanthomyces muscarius* (TA01), *Pseudomonas fluorescens* (Ps27), *Pantoea agglomerans* (B21) used in this study were offered by the Plant Microbiology Laboratory of Bouira University.

The antifungal assay of *A. muscarius* against *F. verticillioides* was carried out using direct confrontation method (Hibar et al., 2005). Agar discs (5 mm in diameter) were taken from ten days old culture plates of both fungi and then placed on new PDA Petri; these discs were placed 3 cm apart from each other. As a control, *F. verticillioides* agar disc alone was placed in the center of PDA Petri plate. The fungi were then incubated at 25 °C. The antifungal assays of the two bacteria were carried out using direct confrontation method (Girish and Bhavya, 2018), mycelial disc (5 mm in diameter) of ten days old culture of *F. verticillioides* was placed in the center of PDA plates, bacterial colonies of 48 h old culture were streaked 2.0 cm apart from the fungal discs on both the sides separately. PDA plates inoculated only with *F. verticillioides* served as control.

Radial growth of *F. verticillioides* was measured daily. The inhibition percentage of growth was calculated according to this formula (da Silva et al., 2017)(2):

$$\text{Inhibition percentage} = (\text{D control} - \text{D test}) / \text{D control} \times 100 \quad (2)$$

Where D control is the diameter of *F. verticillioides* colony in the control plates, D test is the diameter of *F. verticillioides* colony in the direction of the antagonist colony in dual culture plates.

2.6. Antagonism tests of *A. muscarius* using wheat seeds

This test was carried out using seeds of two species of wheat (Bread wheat: cultivar of HD1220; Durum wheat: cultivar of Oued El Bared). The disinfection of the wheat seeds and the preparation of the inoculum were carried out in the same way as in the pathogenicity test. Except that for the *F. verticillioides* inoculum the final concentration was adjusted to 2 ×

https://doi.org/10.55343/CogSust.138

10^6 conidia ml^{-1}. For *A. muscarius*, the suspension of conidia was prepared in the same way as for *F. verticillioides*. The final concentration was adjusted to 2×10^6 conidia ml^{-1}.

In each Petri plate containing 25 disinfected wheat seeds, 2.5 ml of antagonist suspension and 2.5 ml of *F. verticillioides* suspension were sprayed at the same time. Control plates were prepared in the same way by substituting *F. verticillioides* inoculum suspension with sterile distilled water with 0.01% (v/v) Tween-80. The notations (germination percentage, length and weight of coleoptiles) are taken after incubation at 26 °C for four days.

2.7. Statistical analysis

Analysis of variance (ANOVA), comparison of means using LSD at the 5% threshold were performed using XLSTAT 2017 software. The graphs were generated using GraphPad Prism 8 software.

3. Results and discussion

3.1.Morphological and molecular identification of *F. verticillioides*

On a PDA medium, colonies of S03 strain grew rapidly (reach 8.3 ± 0.4 cm in 10 days). Mycelium in young cultures was white and turned purplish pink in old cultures. The medium under the culture was pink and became dark purple with age. On SNA medium, microconidia were unicellular oval to club-shaped with a flattened base. They were always formed from monophialides, and were found in long chains. Microconidia size was 6–14 × 2–3.5 µm (Figure 1). Macroconidia were not found in our study. Chlamydospores were absent.

The ITS sequence of S03 strain (Accession: OR610687) showed 99-100% similarity with several strains of *F. verticillioides* available in the NCBI database. However, it also showed high similarity percentages with other species among *Fusarium fujikuroi* species complex such as *F. subglutinans* and *F. fujikuroi.*

The highest percentage of genetic similarity of S03 based on the TEF-1α sequence (Accession: OR611969) was observed within *F. verticillioides*. Of the 100 closest sequences, 98 sequences were within *F. verticillioides.* TEF-1α sequences alone were effective in discriminating *F. verticillioides* from others species with morphological similarity within *Fusarium fujikuroi* species complex such as *F. fujikuroi., F. proliferatum, F. sacchari* and *F. nygamai* (Figure 2).

Figure 1. Microconidia *of F.verticillioides* in the slide mount (a) and in *situ* on SNA medium (b), scale bar = 50 µm

Fusarium head blight and Fusarium crown rot are two important diseases caused by the genus *Fusarium* in wheat. In Algeria, the species primarily responsible for Fusarium head blight are *F. culmorum* and, to a lesser extent, *F. pseudograminearum*. The species associated with Fusarium crown rot include *F. culmorum*, *F. avenaceum*, *F. pseudograminearum*, *F. chlamydosporum*, *F. equiseti*, *F. verticillioides*, and *F. cerealis*, with *F. culmorum* being the dominant species (Abdallah-Nekache et al., 2019; Bouanaka et al., 2022). Notably, *F. verticillioides* has not been previously cited as a causal agent of Fusarium head blight in wheat in Algeria.

https://doi.org/10.55343/CogSust.138

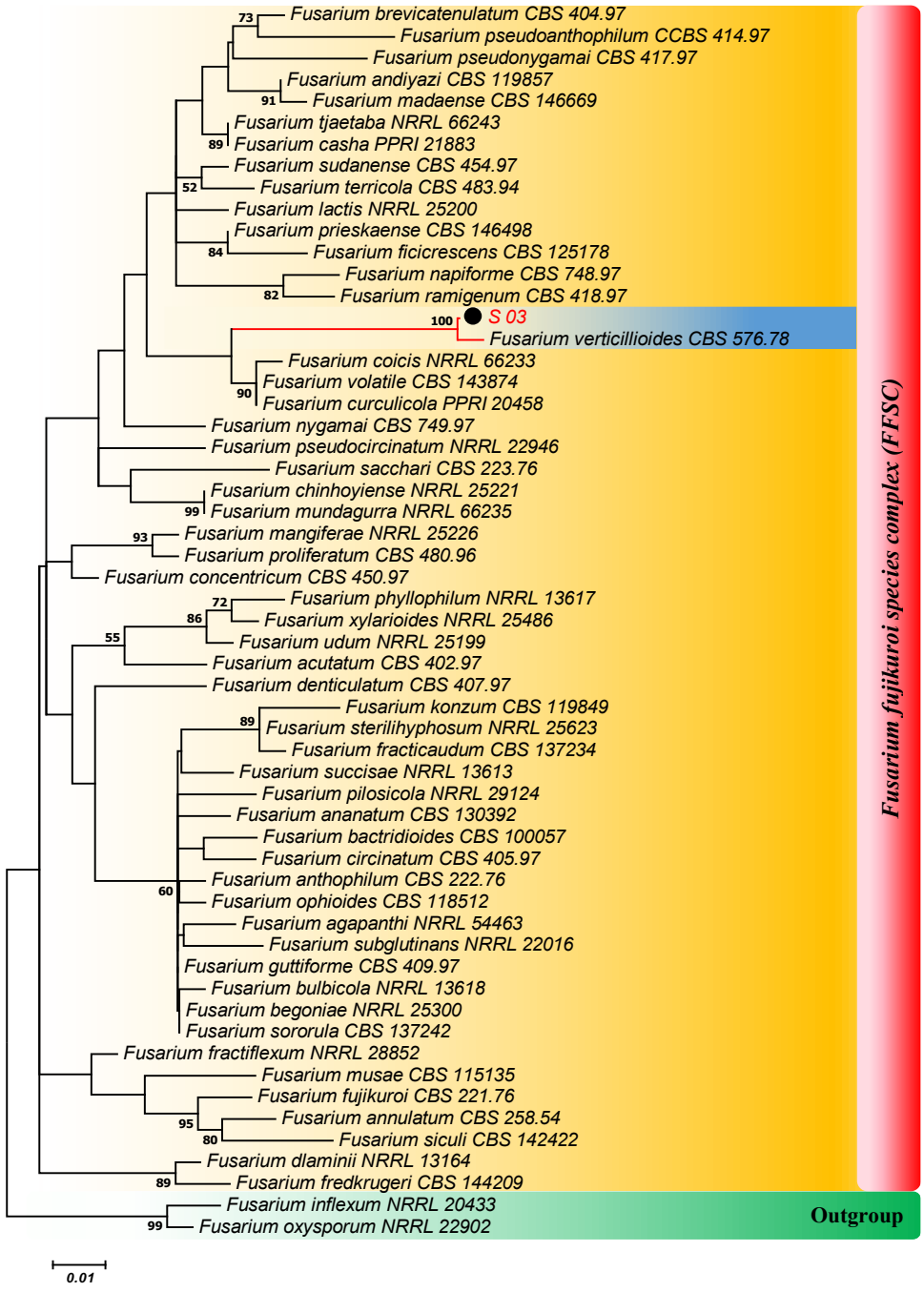

Figure 2. Phylogenetic tree generated from TEF-1α sequences: Numbers on the branches are percentages of 1000 bootstrap replications of MEGA6-maximum likelihood. Maximum likelihood bootstrap values MLBS ≥ 50 % are given at the nodes

In this study, we isolated a strain of *F. verticillioides* from two samples of wheat grain. The morphological characteristics of our strain closely resemble those described by Gagkaeva and Yli-Mattila (2020) who studied *F. verticillioides* newly emerged from winter wheat. Their isolates formed colonies with an average diameter of 58.1–65.8 mm after seven of days incubation on PSA medium at 25 °C. Aerial mycelium was white to violet. Microconidia were formed in chains from simple phialides, with a size range of 5–10 × 1.5–2.8 µm. Fusiform macroconidia were also observed. Sporodochia and

https://doi.org/10.55343/CogSust.138

chlamydospores were absent. In their study, molecular identification was also performed using TEF-1α sequences, and the isolates were identical with several known *F. verticillioides* isolates in GenBank.

3.2. Results of pathogenicity test

The results of pathogenicity tests are presented in Table 1. The germination rates of durum and bread wheat seeds were 96% and 97%, respectively. However, when they were inoculated by *F verticillioides* spores suspension, these rates became 4.0% and 3.1% respectively (Table 1). Spore inoculation also caused a strong reduction on coleoptile length and weight in both durum and bread wheat.

Our strain was found to be pathogenic to both durum and bread wheat, causing a severe reduction in grain germination rates as well as coleoptile weight and length. These findings are consistent with the work of Sakr (2018) who reported a reduction in germination rate and coleoptile length in wheat grains inoculated with four isolates of *F. verticillioides* in Syria.

3.3. Effect of plants extracts and fungicides on radial growth of *F verticillioides*

The diameter of *F. verticillioides* colonies grown on PDA medium alone (control) and PDA medium supplemented with aqueous extracts, ethanolic extracts, and fungicides on the 4th and 7th days of incubation is presented in Figure 3. In the presence of aqueous extracts, a reduction of colony diameter was observed both in 4th and 7th day of incubation, which corresponds to an inhibition rate of 47 ± 2.5% in the case of aqueous oregano extract, 24.5 ± 3.5% in the case of aqueous eucalyptus extract, and 14 ± 4.6% in the case of aqueous rosemary extract. In the presence of ethanolic extracts, a more important reduction of mycelium growth was observed with an inhibition rate of 63.4 ± 2.4%, 57.7 ± 2.6 and 65.2 ± 2.4% in the case of extracts of oregano, eucalyptus and rosemary, respectively (Figure 3). On the other hand, the inhibition rates of mycelium growth recorded with fungicides were 49.8 ± 2.7% and 77.5 ± 2.5% for iprodione and difenoconazole, respectively.

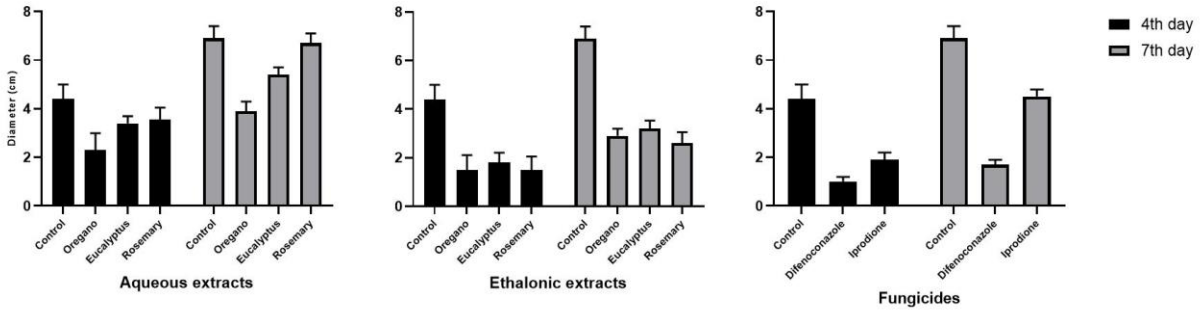

Figure 3. Effect of plants extracts and fungicides on radial growth of *F verticillioides*

In this study, we investigated the antifungal activity of aqueous and ethanolic extracts of three plants. The results showed that ethanolic extracts have a greater inhibitory effect than aqueous extracts. The percentage of inhibition of radial growth of *Fusarium verticillioides* did not exceed 50% with aqueous extracts. Similar findings were reported by Reklaoui et al. (2024); who studied the antifungal activity of aqueous extracts and essential oils of *Rosmarinus officinalis*, *Origanum compactum*, and *Origanum majorana* on ten phytopathogenic fungi, including four species of the genus *Fusarium*. They found that the inhibition rate of mycelial growth was equal to or less than 50% in the case of aqueous extracts.

The ethanolic extracts showed inhibition rates of 63.4 ± 2.4%, 57.7 ± 2.6%, and 65.2 ± 2.4% for oregano, eucalyptus, and rosemary, respectively. This can be attributed to the fact that ethanol is more effective than water in extracting certain secondary metabolites with antifungal properties, such as terpenes, carvacrol, and thymol in oregano; eucalyptol (1,8-cineole) in eucalyptus; and carnosol and camphor in rosemary (Chavan and Tupe, 2014; Coccimiglio et al., 2016; Lakušić et al., 2013; Mączka et al., 2023; Nakagawa et al., 2020; Sabo and Knezevic, 2019). The results obtained for the ethanolic

https://doi.org/10.55343/CogSust.138

extracts are superior to those of the fungicide iprodione (inhibition rate = 49.8%) but remain lower than those achieved with difenoconazole (inhibition rate=77.5%).

3.4. Effect of *A. muscarius*, *P. fluorescens* and *P. agglomerans* on radial growth of *F. verticillioides*

The radial growth of *F. verticillioides* in the absence and presence of antagonistic organisms *(A. muscarius*, *P. fluorescens*, and *P. agglomerans)* is illustrated in Figure 4. The dual confrontation between *A. muscarius* and *F verticillioides* resulted in a reduction of colony diameter of *F. verticillioides* with an inhibition rate of 55 ± 3.3% between the 4th and 8th day of incubation. The strain of *P. fluorescens* was also effective in mycelium growth inhibition with a rate of 52.3 ± 5.1% in the same period. On the other hand, *P. agglomerans* was less effective than *A. muscarius* and *P. fluorescens.* The recorded inhibition rate was 44.7 ± 4%.

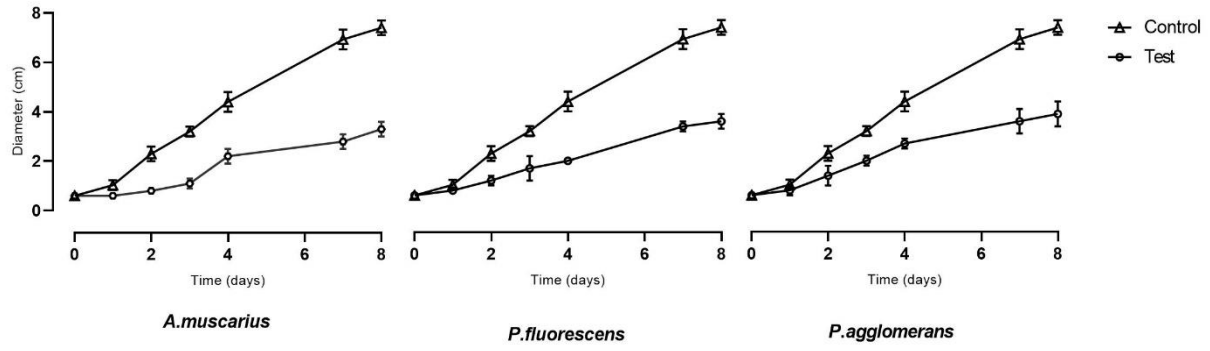

Figure 4. Effect of *A. muscarius*, *P. fluorescens* and *P. agglomerans* on radial growth of *F. verticillioides*

Direct confrontation tests using the entomopathogenic fungus *A. muscarius*, *P. fluorescens*, and *P. agglomerans* showed inhibition rates of 55%, 52%, and 44.7%, respectively. The results obtained with *A. muscarius* and *P. fluorescens* are superior to those recorded with the fungicide iprodione. Saidi et al. (2023), in similar tests, reported inhibition rates of *A. muscarius* against *Fusarium* species ranging between 39% and 52%. According to Turco et al. (2024) and Gomez-de La Cruz et al. (2022), this fungus exhibits antifungal activity against *Hemileia vastatrix*, the causal agent of coffee rust, as well as against the agents of powdery mildew in several plant species. The mechanisms involved include the production of chitinase and the destruction of spores. In the study by Mishra et al. (2022), *P. fluorescens* exhibited an inhibition rate of 69% against *F. verticillioides*. This inhibition was attributed to the synthesis of antifungal molecules such as 2,4-diacetylphloroglucinol. According to Xu et al. (2022), the *P. agglomerans* strain ZJU23 demonstrated efficacy in reducing the growth of *F. graminearum* through the production of Herbicolin A, which binds to and disrupts ergosterol.

3.5. Results of antagonism tests using wheat seeds

The inoculation of wheat seeds with *A. muscarius* at the same time as *F. verticillioides* caused an improvement in the germination rate, which increased from 4% to 22% in the case of durum wheat and from 3.1% to 25.3% in the case of bread wheat. This improvement in the germination rate was also accompanied by an improvement in the other two parameters (length and weight of coleoptile in germinated seeds). It should be noted that inoculation of grains with *A. mucarius* alone caused a slight decrease in the three parameters studied compared to those recorded in the control. In our study, the treatment of wheat grains inoculated with *F. verticillioides* using a suspension of *A. muscarius* moderately improved germination rates as well as the length and weight of the coleoptile. In other studies, treating wheat grains with entomopathogenic fungi such as *Beauveria bassiana* and *Metarhizium brunneum* ten days prior to inoculation with the phytopathogen *Fusarium culmorum* has been shown to effectively protect wheat plants. This protective effect is attributed to the colonization of both the roots and aerial parts of the plants by these entomopathogens (Jaber, 2018).

Table 1. Results of pathogenicity test and antagonism test using wheat seeds

https://doi.org/10.55343/CogSust.138

	Treatment	Seeds germination rate (%)	Average coleoptile length (mm)	Average coleoptile weight (mg)
Durum wheat	Control	96.0 ± 1	23.3 ± 4.2	24.2 ± 4.9
	A. muscarius	92.0 ± 1	21.5 ± 4.1	20.44 ± 5.1
	F. verticillioides	4.0 ± 4	3.1 ± 1.78	1.46 ± .1.01
	F. verticillioides + *A. muscarius*	22.0 ± 6	7.68 ± 1.66	3.9 ± 2
Bread wheat	Control	97.0 ± 3	21.0 ± 2.1	20.3 ± 2.9
	A. muscarius	97.3 ± 3.5	18.53 ± 1.5	14.54 ± 2.1
	F. verticillioides	3.1 ± 2.8	2.5 ± 0.5	1.35 ± 0.6
	F. verticillioides + *A. muscarius*	25.33 ± 9.6	14.1 ± 1.7	11.1 ± 3

4.Conclusion

Isolate *S03 (F. verticillioides)* is pathogenic to wheat, causing a significant reduction in grain germination rates as well as decreases in coleoptile weight and length. The use of ethanolic extracts from oregano, eucalyptus, and rosemary, along with the fungus *A. muscarius* and the bacterium *P. fluorescens*, can inhibit the growth of this strain in vitro as effectively as fungicides. These alternatives may therefore represent an organic and less harmful solution. However, more extensive trials under field conditions are required before progressing to formulation trials.

References

Abdallah-Nekache, N., Laraba, I., Ducos, C., Barreau, C., Bouznad, Z., Boureghda, H. (2019). Occurrence of Fusarium head blight and Fusarium crown rot in Algerian wheat: Identification of associated species and assessment of aggressiveness. *European Journal of Plant Pathology*. 154(3), 499–512. DOI: https://doi.org/10.1007/s10658-019-01673-7

Andrews, S., Pitt, J. I. (1986). Selective medium for isolation of *Fusarium* species and dematiaceous hyphomycetes from cereals. [Comparative Study]. *Applied and Environmental Microbiology*. 51(6), 1235–1238. DOI: https://doi.org/10.1128/AEM.51.6.1235-1238.1986

Bachouche N., Abbas F., Berghout K., Lamri N., Metna F. A. A. (2024). Assessing the phytosanitary protection of cereal crops in the Bouira region (Northern Algeria). *Cognitive Sustainability*. 3(3). DOI: https://doi.org/10.55343/cogsust.113

Bouanaka, H., Bellil, I., Khelifi, D. (2022). First report on *Fusarium cerealis*, identification and virulence as causal agents of crown rot on wheat in Algeria. *Archives of Phytopathology and Plant Protection*. 55(5), 597–614. DOI: https://doi.org/10.1080/03235408.2022.2035557

Campanella, V. (2023). Fusarium foot rot: Monitoring and characterization of soil-rhizosphere populations in durum wheat. *Applied Soil Ecology*. 191, 105051. DOI: https://doi.org/10.1016/j.apsoil.2023.105051

Carbone, I., Kohn, L. M. (1999). A method for designing primer sets for speciation studies in filamentous ascomycetes. *Mycologia*. 91(3), 553–556. DOI: https://doi.org/10.1080/00275514.1999.12061051

Chavan, P. S., Tupe, S. G. (2014). Antifungal activity and mechanism of action of carvacrol and thymol against vineyard and wine spoilage yeasts. *Food Control*. 46, 115–120. DOI: https://doi.org/10.1016/j.foodcont.2014.05.007

Coccimiglio, J., Alipour, M., Jiang, Z.-H., Gottardo, C., Suntres, Z. (2016). Antioxidant, antibacterial, and cytotoxic activities of the ethanolic *Origanum vulgare* extract and its major constituents. *Oxidative Medicine and Cellular Longevity*. 2016(1), 1404505. DOI: https://doi.org/10.1155/2016/1404505

da Silva, J. A. T., de Medeiros, E. V., da Silva, J. M., Tenório, D. d. A., Moreira, K. A., da Silva Nascimento, T. C. E., Souza-Motta, C. (2017). Antagonistic activity of *Trichoderma* spp. against *Scytalidium lignicola* CMM 1098 and antioxidant enzymatic activity in cassava. *Phytoparasitica*. 45(2), 219–225. DOI: https://doi.org/10.1007/s12600-017-0578-x

Dambolena, J. S., López, A. G., Meriles, J. M., Rubinstein, H. R., Zygadlo, J. A. (2012). Inhibitory effect of 10 natural phenolic compounds on *Fusarium verticillioides*. A structure–property–activity relationship study. *Food Control*. 28(1), 163–170. DOI: https://doi.org/10.1016/j.foodcont.2012.05.008

Douriet-Gámez, N. R., Maldonado-Mendoza, I. E., Ibarra-Laclette, E., Blom, J., Calderón-Vázquez, C. L. (2018). Genomic analysis of *Bacillus* sp. strain B25, a biocontrol agent of maize pathogen *Fusarium verticillioides*. *Current Microbiology*. 75, 247–255. DOI: https://doi.org/10.1007/s00284-017-1372-1

Dweba, C., Figlan, S., Shimelis, H., Motaung, T., Sydenham, S., Mwadzingeni, L., Tsilo, T. (2017). Fusarium head blight of wheat: Pathogenesis and control strategies. *Crop Protection*. 91, 114–122. DOI: https://doi.org/10.1016/j.cropro.2016.10.002

Fenta L., Mekonnen H., Kabtimer N. (2023). The exploitation of microbial antagonists against postharvest plant pathogens. *Microorganisms*. 11(4), 1044. DOI: https://doi.org/10.3390/microorganisms11041044

Gagkaeva, T. Y., Orina, A., Gavrilova, O., Ablova, I., Bespalova, L. (2018). Characterization of resistance of winter wheat varieties to Fusarium head blight. *Вавиловский журнал генетики и селекции – Vavilov Journal of Genetics and Breeding*. 22(6), 685–692. DOI: https://doi.org/10.18699/VJ18.411

Gagkaeva, T. Y., Yli-Mattila, T. (2020). Emergence of *Fusarium verticillioides* in Finland. *European Journal of Plant Pathology*. 158(4), 1051–1057. DOI: https://doi.org/10.1007/s10658-020-02118-2

Gardes, M., Bruns, T. D. (1993). ITS primers with enhanced specificity for basidiomycetes-application to the identification of mycorrhizae and rusts. *Molecular Ecology*. 2(2), 113–118. DOI: https://doi.org/10.1111/j.1365-294X.1993.tb00005.x

Girish, K., Bhavya, B. (2018). Antifungal activity of *Lantana camara* L., rhizosphere bacteria. *EurAsian Journal of BioSciences*. 12(2), 245–251. URL: https://www.researchgate.net/publication/332154823_Antifungal_activity_of_Lantana_camara_L_rhizosphere_bacteria

Gomez-de La Cruz, I., Guillén-Navarro, K., Huerta-Palacios, G., García-Fajardo, L. V., Martínez-Bolaños, M. (2022). Enzyme activity of three mycoparasite isolates and their effect on Coffee Leaf Rust (*Hemileia vastatrix* Berk. & Br.). *Symbiosis*. 88(1), 47–59. DOI: https://doi.org/10.1007/s13199-022-00885-6

He, D., Shi, J., Qiu, J., Hou, Y., Du, Y., Gao, T., Huang, W., Wu, J., Lee, Y-W., Mohamed, S. R., Liu, X., Xu,. J. (2023). Antifungal activities of a novel triazole fungicide, mefentrifluconazole, against the major maize pathogen *Fusarium verticillioides*. *Pesticide Biochemistry and Physiology*. 192, 105398. DOI: https://doi.org/10.1016/j.pestbp.2023.105398

Hibar, K., Daami-Remadi, M., Khiareddine, H., El Mahjoub, M. (2005). Effet inhibiteur in vitro et in vivo du *Trichoderma harzianum* sur *Fusarium oxysporum* f. sp. *radicis-lycopersici*. *Biotechnology, Agronomy, Society and Environment*. 9(3), 163–171. URL: https://www.researchgate.net/publication/26411084_Effet_inhibiteur_in_vitro_et_in_vivo_du_Trichoderma_harzianum_sur_Fusarium_oxysporum_f_sp_Radicis-lycopersici

Ioos, R., Belhadj, A., Menez, M. (2004). Occurrence and distribution of *Microdochium nivale* and *Fusarium* species isolated from barley, durum and soft wheat grains in France from 2000 to 2002. *Mycopathologia*. 158, 351–362. DOI: https://doi.org/10.1007/s11046-004-2228-3

Jaber, L. R. (2018). Seed inoculation with endophytic fungal entomopathogens promotes plant growth and reduces crown and root rot (CRR) caused by *Fusarium culmorum* in wheat. *Planta*. 248, 1525–1535. DOI: https://doi.org/10.1007/s00425-018-2991-x

Lakušić, D., Ristić, M., Slavkovska, V., Lakušić, B. (2013). Seasonal variations in the composition of the essential oils of rosemary (*Rosmarinus officinalis*, Lamiaceae). *Natural Product Communications*. 8(1), 1934578X1300800132. DOI: https://doi.org/10.1177/1934578X1300800

Leslie, J. F., Summerell, B. A. (2006). *The Fusarium Laboratory Manual*. Blackwell. DOI: https://doi.org/10.1002/9780470278376

Mączka, W., Twardawska, M., Grabarczyk, M., Wińska, K. (2023). Carvacrol: A natural phenolic compound with antimicrobial properties. *Antibiotics*. 12(5), 824. DOI: https://doi.org/10.3390/antibiotics12050824

Martínez J. I., Gómez-Garrido M., Gómez-López M. D., Faz Á., Martínez-Martínez S., Acosta J. A. (2019) Pseudomonas fluorescens affects nutrient dynamics in plant-soil system for melon production. *Chilean Journal of Agricultural Research*. 79(2), 223–233. DOI: http://doi.org/10.4067/S0718-58392019000200223

Matarese, F., Sarrocco, S., Gruber, S., Seidl-Seiboth, V., Vannacci, G. (2012). Biocontrol of Fusarium head blight: Interactions between *Trichoderma* and mycotoxigenic *Fusarium*. *Microbiology*. 158(1), 98–106. DOI: https://doi.org/10.1099/mic.0.052639-0

Mishra, J., Mishra, I., Arora, N. K. (2022). 2, 4-Diacetylphloroglucinol producing *Pseudomonas fluorescens* JM-1 for management of ear rot disease caused by *Fusarium moniliforme* in *Zea mays* L. *3 Biotech*. 12(6), 138. DOI: https://doi.org/10.1007/s13205-022-03201-7

Nakagawa, S., Hillebrand, G. G., Nunez, G. (2020). *Rosmarinus officinalis* L.(rosemary) extracts containing carnosic acid and carnosol are potent quorum sensing inhibitors of *Staphylococcus aureus* virulence. *Antibiotics*. 9(4), 149. DOI: https://doi.org/10.3390/antibiotics9040149

Pastuszak, J., Szczerba, A., Dziurka, M., Hornyák, M., Kopeć, P., Szklarczyk, M., Płażek, A. (2021). Physiological and biochemical response to *Fusarium culmorum* infection in three durum wheat genotypes at seedling and full anthesis stage. *International Journal of Molecular Sciences*. 22(14), 7433. DOI: https://doi.org/10.3390/ijms22147433

Reklaoui, L., Bzazou Elouazzani, Z. E. A., Annaz, H., Kasmi, M., Rfaki, A., Ghazal, H., Essalmani, H., Barrijal, S. (2024). Antifungal Activity of Essential Oils and Aqueous Extracts of Three Moroccan Plants: A Study on Ten Phytopathogenic Fungi. *Tropical Journal of Natural Product Research*. 8(8). DOI: https://doi.org/10.26538/tjnpr/v8i8.14

Sabo, V. A., Knezevic, P. (2019). Antimicrobial activity of *Eucalyptus camaldulensis* Dehn. plant extracts and essential oils: A review. *Industrial Crops and Products*. 132, 413–429. DOI: https://doi.org/10.1016/j.indcrop.2019.02.051

Saidi, A., Mebdoua, S., Mecelem, D., Al-Hoshani, N., Sadrati, N., Boufahja, F., Bendif, H. (2023). Dual biocontrol potential of the entomopathogenic fungus *Akanthomyces muscarius* against *Thaumetopoea pityocampa* and plant pathogenic fungi. *Saudi Journal of Biological Sciences*. 30(8), 103719. DOI: https://doi.org/10.1016/j.sjbs.2023.103719

Sakr, N. (2018). Aggressiveness of Fusarium head blight species towards two modern Syrian wheat cultivars in an *in vitro* Petri-dish. *Cereal Research Communications*. 46(3), 480–489. DOI: https://doi.org/10.1556/0806.46.2018.031

Sakr, N. (2022). Adaptation of phytopathogenic fungi to quantitative host resistance: in vitro selection for greater aggressiveness in Fusarium head blight species on wheat. *Cytology and Genetics*. 56(3), 261–272. DOI: https://doi.org/10.3103/S0095452722030112

Seepe, H., Amoo, S., Nxumalo, W., Adeleke, R. (2020). Sustainable use of thirteen South African medicinal plants for the management of crop diseases caused by *Fusarium* species: An in vitro study. *South African Journal of Botany*. 130, 456–464. DOI: https://doi.org/10.1016/j.sajb.2020.01.038

Turco, S., Drais, M. I., Rossini, L., Di Sora, N., Brugneti, F., Speranza, S., Contarini, M., Mazzaglia, A. (2024). Genomic and pathogenic characterization of *Akanthomyces muscarius* isolated from living mite infesting hazelnut big buds. *Genes*. 15(8), 993. DOI: https://doi.org/10.3390/genes15080993

Wilkinson, J. M. (2006). Methods for testing the antimicrobial activity of extracts. In: Ahmad, I., Aquil, F., Owais, M. (eds): *Modern Phytomedicine: Turning Medicinal Plants into Drugs*. 157–171. DOI: https://doi.org/10.1002/9783527609987

Xu, S., Liu, Y.-X., Cernava, T., Wang, H., Zhou, Y., Xia, T., Cao, S., Berg, G., Shen, X-X., Wen, Z., Li, C., Ruan, H., Chai, Y., Zhou, X., Ma, Z., Shi, Y., Bai, Y., Chen, Y. (2022). Fusarium fruiting body microbiome member *Pantoea agglomerans* inhibits fungal pathogenesis by targeting lipid rafts. *Nature Microbiology*. 7(6), 831–843. DOI: https://doi.org/10.1038/s41564-022-01131-x

Yates, I., Widstrom, N., Bacon, C., Glenn, A., Hinton, D., Sparks, D., Jaworski, A. (2005). Field performance of maize grown from *Fusarium verticillioides*-inoculated seed. *Mycopathologia*. 159, 65–73. DOI: https://doi.org/10.1007/s11046-004-8402-9

Zhao, B., He, D., Wang, L. (2021). Advances in *Fusarium* drug resistance research. *Journal of Global Antimicrobial Resistance*. 24, 215–219. DOI: https://doi.org/10.1016/j.jgar.2020.12.016

https://doi.org/10.55343/CogSust.154

Possibilities for determining the energy consumption of electric locomotives during acceleration and constant-speed traction

Szabolcs FISCHER
https://orcid.org/0000-0001-7298-9960
Department of Transport Infrastructure and Water Resources Engineering, Széchenyi István University
Győr, Hungary
fischersz@sze.hu

Bence HERMÁN
https://orcid.org/0009-0005-4620-5022
Department of Vehicle Manufacturing and Technology, Széchenyi István University
Győr, Hungary
herman.bence@sze.hu

Szabolcs KOCSIS SZÜRKE
https://orcid.org/0000-0001-5639-8116
Department of Automotive and Railway Engineering, Széchenyi István University
Győr, Hungary
kocsis.szabolcs@ga.sze.hu

Abstract

Electric locomotives are integral to sustainable railway transportation, where optimizing energy consumption is crucial for efficiency and environmental impact reduction. This study investigates energy usage during acceleration and constant-speed traction in Siemens Taurus 0470-series locomotives operating on the Sopron–Győr railway line (Line 8 in Hungary). Using empirical data from onboard computer displays, video recordings, and Optical Character Recognition (OCR), the research applies statistical correlation methods to analyze energy consumption trends. The study identifies key influencing factors, including acceleration energy correction coefficients (α_1 = 1.2981, α_2 = 1.3151) and specific energy consumption values at constant speeds, averaging 0.00204 kWh/kN/km at 120 km/h with a 21.12% relative standard deviation value. Heatmaps illustrate energy consumption patterns, highlighting peak usage near stations and track turnouts. The findings support refining energy models and driving strategies while emphasizing the potential benefits of regenerative braking, timetable optimization, and advanced driver assistance systems. By integrating these insights, railway operations can achieve enhanced energy efficiency and long-term sustainability.

Keywords

electric locomotive, Siemens Taurus locomotive, energy consumption, acceleration, traction with constant speed

1. Introduction

Cognitive sustainability in transportation, particularly within the railway sector, involves the interplay between cognitive processes and sustainable practices to enhance operational efficiency and user experience (Zöldy and Baranyi, 2023; Zöldy et al., 2024; Zöldy, 2024). It emphasizes understanding how cognitive factors influence decision-making and behavior in sustainable transport systems. For example, cognitive mapping techniques can visualize and analyze users' mental representations of transport challenges, leading to improved strategies for promoting sustainable travel behaviors (Waleghwa and Ioannides, 2024). Integrating cognitive decision-making frameworks into railway planning and management can identify key performance indicators and sustainability criteria, enhancing transport infrastructure effectiveness (Oraegbune and

https://doi.org/10.55343/CogSust.154

Ugwu, 2020). This approach addresses immediate operational challenges and aligns with broader sustainability goals by fostering awareness and responsibility among stakeholders.

In railways, cognitive sustainability also considers the mental workload and cognitive performance of train operators, which are critical for safety and efficiency. Prolonged tasks and high mental workloads can lead to cognitive underload, decreasing attention and increasing error rates among train crew members (Currie et al., 2023). Cognitive load management strategies and advanced technologies, such as eye-tracking systems, can enhance staff cognitive performance, improving safety and sustainability in railway operations (Madleňák et al., 2023). Fostering a cognitive understanding of sustainable practices among operators and passengers can encourage environmentally friendly behaviors, such as using public transport instead of private vehicles, reducing emissions and improving urban air quality (Macassa, 2023). Cognitive sustainability also addresses public perceptions and attitudes towards sustainable transport, which shape travel behaviors. Cognitive dissonance arises when travel choices conflict with environmental values, leading to reluctance to shift towards sustainable modes of transport (Bina and Biassoni, 2023). Targeted educational programs and awareness campaigns can address this dissonance, empowering users to make informed decisions aligned with sustainability objectives. Integrating cognitive sustainability principles into transport planning and policy-making can create a resilient and sustainable railway system that meets current mobility needs and anticipates future challenges related to climate change and urbanization (de la Torre et al., 2021). This holistic approach fosters a sustainable transport culture prioritizing cognitive engagement and environmental stewardship. Although slightly outside the focus of the current research, it is worth mentioning – to provide a broad perspective on cognitive mobility – that some researchers have discussed the noises and vibrations of electric vehicles and their reduction possibilities (Zöldy and Pathy-Nagy, 2022; Zöldy and Dömötör, 2022), as well as the effects of long-term utilization on vehicle battery performance (Tollner and Zöldy, 2022).

Cognitive sustainability in railways enhances operational efficiency, decision-making, and broader sustainability objectives, including optimizing energy consumption in electric locomotives to reduce environmental impact and improve economic viability. Understanding and accurately calculating energy consumption is essential for designing efficient railway systems.

This study explores methodologies and technologies for determining energy consumption during acceleration and constant-speed traction, linking cognitive sustainability principles with technical advancements in railway energy management. The calculation of consumed energy in electric locomotives involves various methodologies, technologies, and operational practices. First, a literature review synthesizes studies on energy consumption, focusing on mathematical modeling, technological advancements, operational factors, and environmental implications.

The energy required to move trains depends on infrastructure effects such as traction and vehicle characteristics (Dižo et al., 2022; Mikhailov et al., 2021), permanent way characteristics (Kuchak et al., 2020; 2021; Ézsiás et al., 2024; Fischer et al., 2024; Fischer, 2025), transportation organization effects, for example speed, marshaling, stop plans, seat capacity utilization, handling, signal displays, logistics (Volkov et al., 2020; Saukenova et al., 2022), and external environmental impacts including altitude, climate and barometric pressure (Ren et al., 2020; Fischer, 2015; Fischer and Kocsis Szürke, 2023; Fischer et al., 2025). Train energy consumption includes operational energy (traction energy and regenerative braking energy) and auxiliary energy used by onboard service equipment, like air conditioning, lighting, and ventilation (Fischer and Kocsis Szürke, 2023)).

Mathematical modeling is crucial for estimating energy consumption. Rodriguez-Cabal et al. (2022) developed a methodology for estimating electrical power on undocumented railroad tracks, emphasizing accurate data collection and model validation. Liang et al. (2023) used machine learning to enhance prediction models for locomotive traction energy consumption, improving accuracy by incorporating operational variables. Technological advancements, such as modern multi-engine traction drives (Zarifyan et al., 2021) and hybrid systems, fpr example fuzzy PID control systems for mining electric locomotives (Ma et al., 2024), optimize energy use. Regenerative braking systems (Lu et al., 2019; Yan et al., 2018) improve energy recovery during braking, reducing overall consumption. Environmental considerations, such as carbon-neutral technologies (Lu and Allen, 2024) and battery technology (Kaleybar et al., 2022; Chen et al., 2013), align with global sustainability goals.

Operational factors (e.g., track conditions, load variations, driving behaviors) significantly influence energy consumption (Istomin, 2018; Cheremisin et al., 2020). Digital technologies and data analytics enable real-time monitoring and

https://doi.org/10.55343/CogSust.154

optimization of energy use (Istomin et al., 2018). Alternative energy sources, such as hydrogen fuel cells and battery technologies (Cole et al., 2023; Kaleybar et al., 2022) and energy storage systems (Domanov et al., 2019) enhance efficiency. Research on power losses (Nikitenko et al., 2022) and control strategies for traction converters (Rajibayev et al., 2023) further optimize energy consumption in electric locomotives.

The future of electric locomotives will likely involve a combination of these various approaches, integrating advanced modeling, innovative technologies, and operational best practices to optimize energy consumption. The ongoing research in this field will continue to shape the development of more efficient and sustainable electric locomotives, contributing to the broader goals of reducing greenhouse gas emissions and enhancing the efficiency of rail transport.

In the international literature, many articles and studies deal with the determination of the consumed energy of electric railway vehicles (i.e., locomotives and electric multiple units (EMUs)). Rochard and Schmid (2000) primarily examined the validity of train resistance formulae, by analyzing those developed by Davis, Armstrong and Swift, and others. They found that, typically, air resistance is the most important part of train resistance calculation. This makes the streamlined design of trains critical. The mass of trainsets (and hence their calculated weight) and their effect on train resistance are of particular interest and importance for freight trains. They go through the French, German and Japanese calculation formulae. Rochard and Schmid (2000) provide practical formulae for train resistance using second order polynomial functions (the detailed explanation of the railway resistances is discussed in Ihme (2022)). Lukaszewicz (2007) conducted full-scale tests in Sweden and derived train resistance equations related to several locomotive and wagon configurations. The considered formulae are also second order polynomial functions. The calculation possibilities of the consumed energy are detailed by Mandić et al. (2009), Ihme (2022), and Fischer (2015).

The present paper addresses the key research gap in the field of energy consumption analysis for electric locomotives, which is related to the refinement of energy consumption models. Therefore, this study suggests that the correlation functions and correction factors used in energy prediction models should be further refined to enhance forecasting accuracy (Fischer, 2015).

The structure of the paper is as follows: Section 2 summarizes the data and data processing methodologies, Section 3 presents the results and the discussion, and Section 4 provides the conclusions.

2. Data and methods

2.1. Data sources and collection

The data was collected by the authors through their measurements on intercity (IC) trains hauled by Siemens Taurus 0470-series locomotives between Sopron and Győr along the Sopron–Budapest and Budapest–Sopron routes. A total of five days of measurements were conducted, covering seven train runs:

- On November 28, 2024, Scarbantia IC train No. 997 operated between Sopron and Győr with locomotive 470 501 (91430470501-7) – Sisi – hauling 4 IC passenger wagons, with a total weight of 298 tons.
- On November 28, 2024, Scarbantia IC train No. 984 operated between Sopron and Győr with locomotive 470 503 (91430470503-3) – Wagner – hauling 4 IC passenger wagons, with a total weight of 300 tons.
- On December 13, 2024, Scarbantia IC train No. 997 operated between Sopron and Győr with locomotive 470 501 (91430470501-7) – Sisi – hauling 5 IC passenger wagons, with a total weight of 345 tons.
- On December 13, 2024, Scarbantia IC train No. 984 operated between Sopron and Győr with locomotive 470 503 (91430470503-3) – Wagner – hauling 5 IC passenger wagons, with a total weight of 345 tons.
- On December 16, 2024, Scarbantia IC train No. 987 operated between Sopron and Győr with locomotive 470 502 (91430470502-5) hauling 4 IC passenger wagons, with a total weight of 298 tons.
- On January 24, 2025, Scarbantia IC train No. 987 operated between Sopron and Győr with locomotive 470 502 (91430470502-5) hauling 5 IC passenger wagons, with a total weight of 351 tons.
- On January 31, 2025, Scarbantia IC train No. 987 operated between Sopron and Győr with locomotive 470 502 (91430470502-5) hauling 6 IC passenger wagons, with a total weight of 387 tons.

https://doi.org/10.55343/CogSust.154

The data were collected by the following methods:

- During the measurements conducted on November 28, 2024, December 13and 16, 2024, GoPro 11 action cameras were used for visual recording, while GoPro 13 action cameras were employed during the measurements on January 24 and 31, 2025. The cameras recorded the display of the locomotives' onboard computers, which showed the exact time, train number, consumed and regenerated energy values (in kWh), as well as the total traction force (considering all four traction electric motors/engines together) in kN. Additionally, the catenary voltage was displayed. Three data points were recorded using the GoPro cameras at 60 fps. The GPS data from the GoPro cameras was utilized for location identification, and the timestamps were synchronized according to the GoPro camera's internet-based time updates.
- The video records captured by the GoPro cameras were subsequently processed on a desktop computer, where they were converted into individual frames and downsampled to a 1 Hz sampling rate (from 60 fps). Optical Character Recognition (OCR) technology was applied to extract the data, which was then saved in CSV format.
- The applied software and processing motors are controlled by custom-written Python routines.

Fig. 1 shows some parts of the measurement setup.

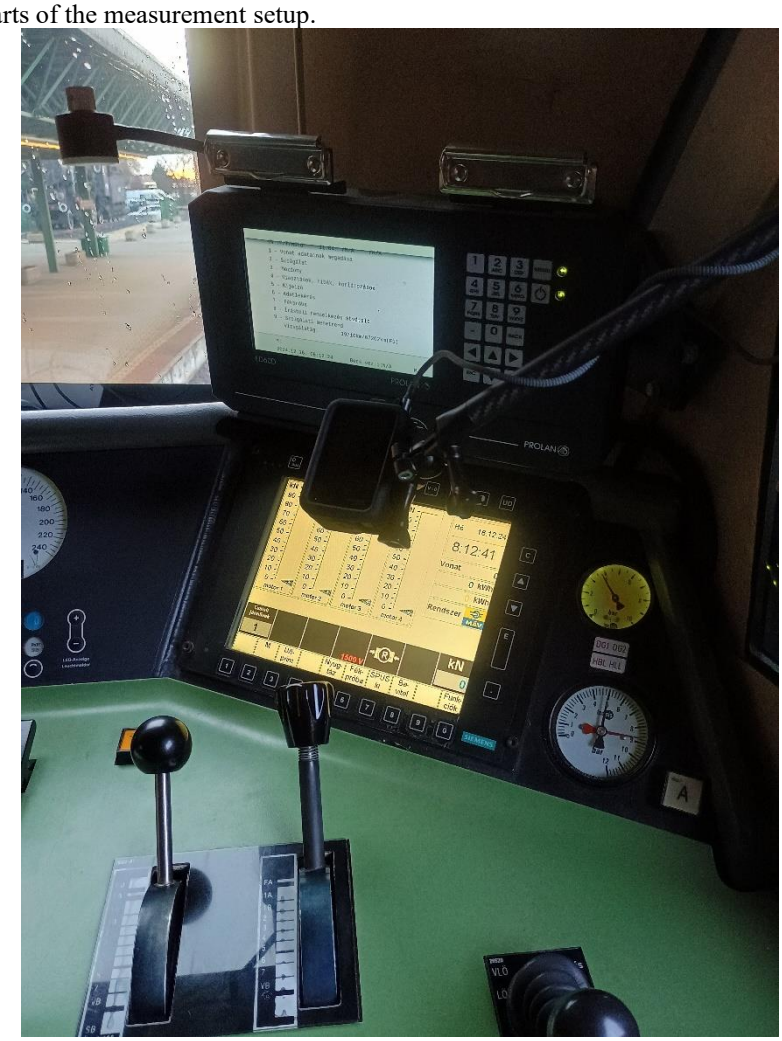

Figure 1. The measurement setup (there is the GoPro camera in front of the displays; here its display is in stand-by mode because the energy consumption is much less than with switched on display)

https://doi.org/10.55343/CogSust.154

2.2. Data processing

The data collected, as described in Section 2.1, was imported into an MS Excel environment and analyzed according to the following methodology:

- As mentioned at the end of Introduction, the primary objective of this study was to conduct a statistical correlation comparison between two different calculation methods for the measured acceleration energy values, as well as to estimate energy consumption during constant-speed traction.
- To achieve the above, it was necessary to document and implement detailed calculation procedures, which are defined by Eqs. (1–3).

$$E_{calc.,me,i,j} = 0.5 \cdot m_i \sum_{j=1}^{n} \left(v_{j+1}^2 - v_j^2\right)/(3.6 \cdot 10^6) \quad (1)$$

$$E_{calc.,tf,k,l} = \sum_{k=1}^{p} \sum_{l=1}^{q} [0.5 \cdot (v_{k+1} + v_k) \cdot (v_{k+1} - v_k) \cdot s_l]/(3.6 \cdot 10^6) \quad (2)$$

$$E_{meas.,i,j} = E_{calc.,me,i,j} \cdot \alpha_1 = E_{calc.,tf,k} \cdot \alpha_2 \quad (3)$$

where,

- $E_{calc.,me,i,j}$ is the calculated acceleration energy of the train mass m_i [kg] in [kWh] based on the equation of the motion energy (of course, during a given acceleration, the m_i does not change);
- v_j and v_{j+1} are the values of acceleration speed step in [m/s];
- $E_{calc.,tf,k,l}$ is the calculated acceleration energy of the train mass m_i [kg] in [kWh] based on the equation of traction force $F_{traction}$;
- v_k is the so-called specific acceleration force of the considered locomotive at the speed (v_k [m/s]) that hauls the train mass m_i [kg], for the determination of v_k the traction force of the locomotive ($F_{traction}$ [kN]) as a function of the speed (v [m/s]), as well as the train resistance (μ_{train} [N/kN]) and the weight of the whole train (Q_{train} [kN]) should be taken into consideration;
- s_l is the driven distance between the points [m] where there are the considered train at speed values v_{k+1} and v_k (the frequency of the data was 1 Hz in the current study);
- let us consider that $E_{calc.,me,i,j}$ and $E_{calc.,tf,k,l}$ are related to the same acceleration between v_j and v_{j+1}, which can be measured with $E_{meas.,i,j}$ in [kWh];
- the values of i, j, k and l indexes are shown differently because more sub-distances and subparts can be during an acceleration according to the traction force measurements; it is the reason for the consideration of the n, p and q values;
- α_1 and α_2 are correction parameters (factors) that should be determined from the correlation calculation between the calculated and the measured acceleration energies.

The parameter μ_{train} can be determined by many equations and formulas (Rochard and Schmid, 2000; Lukaszewicz, 2007; Ihme, 2022; Mandić et al., 2009), from which the one shown in Eq. (4) is applied in the current study, using the Hungarian Railways for passenger trains (Fischer, 2015):

$$\mu_{train} = 2.0 + 0.047 \cdot 3.6 \cdot \frac{v}{100} \quad (4)$$

The traction with constant speed was defined by the unit [kWh/kN/km] related to Q_{train} [kN] and S [km] (i.e., the distance driven with the constant speed (v [m/s]) in question). For this parameter, no calculation was executed; only the data processing of the measurements was done.

Data processing consists of two methodologies: first, using unfiltered data pairs (i.e., the calculated and the measured energy values in the case of accelerations and measured energy values in the case of traction with constant speed); and second, using filtered data pairs. In the case of accelerations, the filter eliminates data pairs that fall outside the mean ±20%. For traction with constant speed, contiguous section lengths shorter than 3 km are filtered out. In the latter case, it was necessary to apply this method, which is not entirely accurate, due to the absence of an accurate calculation method. The specified filtering criteria assume that the measurement error margin of ±20% is acceptable; these are primarily engineering assumptions and approximations that include the simplifications detailed in Section 2.3. These limitations should, of course, be clarified in future research and publications.

Heatmaps are also presented in Section 3, which illustrate not only the consumed energy but the regenerative braking energies considering both the Sopron–Győr and the Győr–Sopron runs. When the heatmap is created, it sets a color scale based on the difference in consumption considering 1.0 second timesteps, i.e., it determines the intensity (local average). It

https://doi.org/10.55343/CogSust.154

places the points with the differences in consumption on the map. In turn, the interpretation of the colors on the heatmap is the averaged density (weighted average) of the values of the points within a given area. As the map is zoomed in or out, it contracts the colors of the points in a given area, with the colors around the points contracting by 10 pixels, i.e., the intensity increases. Zooming the map out, larger areas are several points higher on average.

2.3. Limitations

The following limitations were considered during the research:

- Measurements were conducted exclusively with Siemens Taurus 0470-series locomotives (502 "green-yellow" Taurus locomotive, and ones with nicknames Sisi and Wagner).
- Only the Sopron–Győr and Győr–Sopron segments of Railway Line 8 were considered for analysis due to two main reasons (this railway line is a single track line):
  1. In the Kisalföld region, gradient values (longitudinal-vertical inclinations) are relatively low, with a maximum of 5.8‰ between Kapuvár and Fertőendréd, as well as between Sopron and Fertőboz. Typical gradient values range between 3‰ and 5‰; however, the gradient signs were not available for the study.
  2. After Győr, intercity trains departing from Sopron continue on Railway Line 1, where significantly steeper gradients are characteristic of the Győr–Budapest section.
- It is important to note that for trains departing from Sopron towards Budapest, acceleration from 0 to 100 km/h at Győr Station was included in the analysis. For trains in the opposite direction, only the segment from the stop at Győr Station to Sopron was examined.
- Curve resistance was not considered. The minimum curve radius on the Győr–Sopron section is R = 410 m (at Fertőboz Station), while curves with $R \leq 500$ m are the most common in this section.
- Constant-speed segments were analyzed at predefined values of $V_{const.}$ = 60…80…100…120 km/h, with 120 km/h being the most frequently occurring and longest-sustained speed (approximately 50% of the total Győr–Sopron section is covered at this speed).
- In the case of acceleration, all identifiable acceleration events within the measured train runs were analyzed.
- Only electrical energy consumption values were considered and included in further analysis; regenerative braking energy was not taken into account.
- A single train resistance equation was applied – see Eq. (4) –, which is specified for passenger trains (Fischer, 2015).
- The effects of temperature, humidity, and variations in the adhesion-friction coefficient at the wheel-rail interface were not considered.
- The influence of locomotive sanding during acceleration was omitted.
- Train weight values were taken exclusively from GYSEV (ROeEE, i.e., the Győr–Sopron–Ebenfurt Railways Ltd.) records. Variations in train car types between different runs and their potential impact were not analyzed.
- Track and track geometry defects were not considered.
- The influence of locomotive drivers' driving styles was disregarded.
- In some cases, locomotive 0470 502 was subject to a service-imposed speed restriction of V = 140 km/h due to transformer oil cooling issues. The impact of this restriction on acceleration and traction energy consumption was not analyzed.
- It is crucial to mention that the recorded energy values relied solely on the onboard computer system of the Siemens Taurus 0470-series locomotives, including its update frequency and accuracy, which were not precisely verified.
- The timetable optimization was currently neglected; however, in the Conclusions the related recommendations are determined.

3. Results and discussion

Figs. 2–7 depict the results of the analyses. Figs. 2–3 (unfiltered) and Figs. 5–6 (filtered according to the method described in Section 2.2) deal with the measurement of acceleration energies and their determination by linear regression functions, taking into account the kinetic energy and the traction force curve. In each graph, the values of the parameters alpha1 (Figs. 2 and 5) and alpha2 (Figs. 3 and 6) are given. In the unfiltered cases, the coefficient of determination (R^2) was above 0.95, while values above 0.99 were obtained for the filtered data set. If the filtering criterion defined by the engineering approach (see Section 2.2) is acceptable, it can be stated that for passenger trains hauled by Siemens Taurus 0470 locomotives (considering hauled IC wagons), α_1 = 1.2981, while α_2 = 1.3151. The number of data points is lower for Figs. 3 and 5 because, during measurements on 13.12.2024 and 31.01.2025, there were unfavorable lighting conditions that made it impossible to evaluate the bright (yellow) traction data displayed on the locomotive's on-board computer display, so they were neglected (omitted from the evaluations).

Figs. 4 and 7 show that there is significant variation in the specific energy consumption data for each (constant) speed (V = 60...100...120 km/h). For V = 60 km/h, since only one measurement data point is available, this calculation was not performed. In contrast, for V = 100 km/h, for the unfiltered data set, the mean value is 0.00138 kWh/kN/km and the standard deviation is 0.00077 kWh/kN/km, while the relative standard deviation is 56.02%; the same values for V = 120 km/h – for

https://doi.org/10.55343/CogSust.154

the same unfiltered data set – the mean value is 0.00197 kWh/kN/km, the standard deviation is 0.00052 kWh/kN/km, while the relative standard deviation is 26.36% – all are shown in Fig. 4. For filtered datasets (see Fig. 7) the results are as follows: for $V = 100$ km/h, the previously reported results remain valid, with no changes observed); for $V = 120$ km/h, the mean value is 0.00204 kWh/kN/km, the standard deviation is 0.00043 kWh/kN/km, while the relative standard deviation is 21.12%. For both the unfiltered and filtered datasets, the coefficient of determination (R^2) was above 0.92.

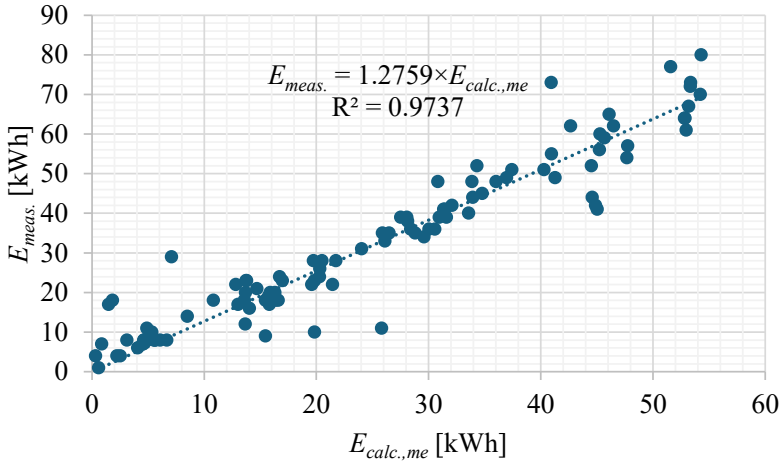

Figure 2. Regression function and determination of α_1 considering unfiltered dataset, for runs between both Sopron–Győr and Győr–Sopron (total: 105 data points)

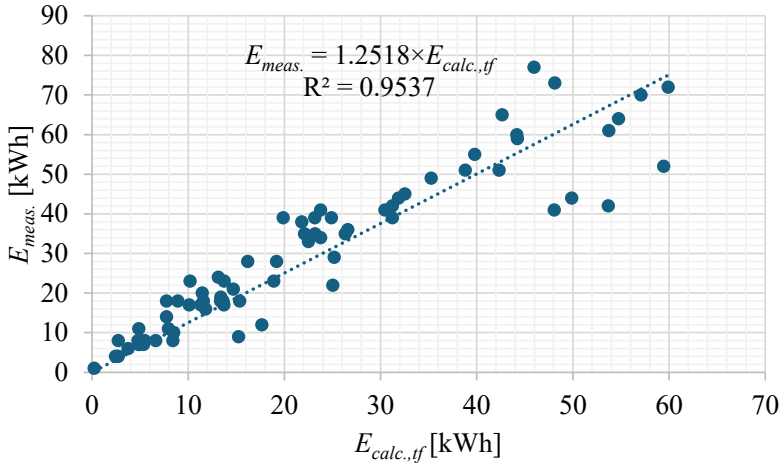

Figure 3. Regression function and determination of α_2 considering unfiltered dataset, for runs between both Sopron–Győr and Győr–Sopron (total: 75 data points)

https://doi.org/10.55343/CogSust.154

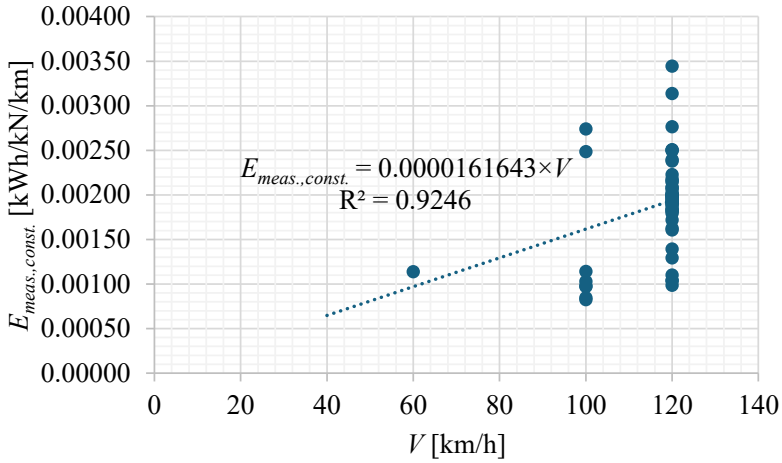

Figure 4. Regression function for traction with constant speed considering unfiltered dataset, for runs between both Sopron–Győr and Győr–Sopron (total: 52 data points)

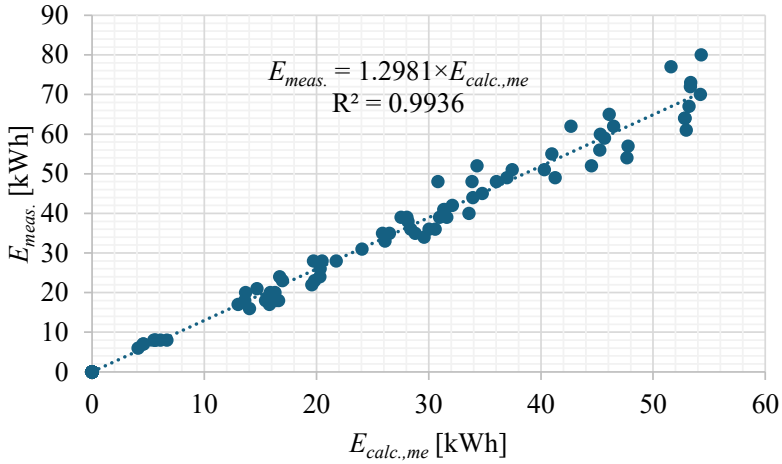

Figure 5. Regression function and determination of α_1 considering filtered dataset, for runs between both Sopron–Győr and Győr–Sopron (total: 76 data points)

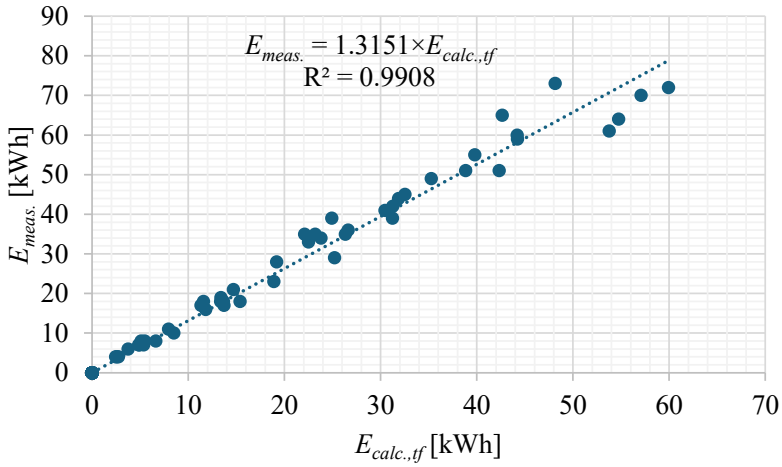

Figure 6. Regression function and determination of α_2 considering unfiltered dataset, for runs between both Sopron–Győr and Győr–Sopron (total: 48 data points)

https://doi.org/10.55343/CogSust.154

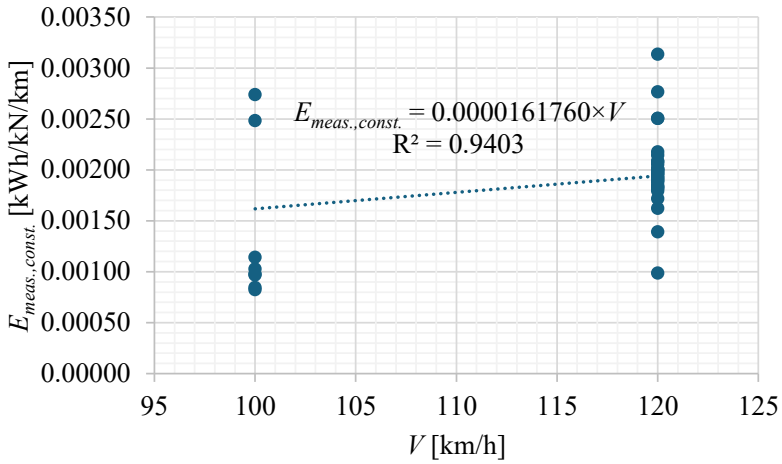

Figure 7 Regression function for traction with constant speed considering filtered dataset, for runs between both Sopron–Győr and Győr–Sopron (total: 40 data points)

Figs. 8–11 show the above results in heat maps. Figs. 8 and 10 connect to Figs. 2–3 and Figs. 5–6, hence Figs. 9 and 11 represent the parallel measured regenerative braking energies. The meaning of the colors in Figs. 8–11 are detailed in Section 2.2. The heatmaps clearly show that the peak consumption values are concentrated around railway stations and possible turnout tracks (yellowish colors) but also appear in purple between stations due to constant speed traction along the whole section – see. Fig. 8 and Fig. 10. In Figs. 9 and 11, the regenerative braking energies are concentrated around the stations. This also indicates that the intermediate sections are typically not subject to speed restrictions – likely because train crossings at turnout tracks and/or other traffic reasons for the train to slow down occur mainly near stations.

Based on the observations made during the measurements, the train drivers preferred to use the electric brake instead of traditional pneumatic-mechanic brake (the regenerative energy can be recovered by using electric brake), despite the limited braking force of the Siemens Taurus locomotives, which is only 150 kN (Baur, 2003) for safety and derailment protection reasons. In this respect, it would be more advantageous to use Siemens Vectron locomotives, because they can be equipped with an electric braking force of double that amount, i.e., 300 kN (or in some countries, 240 kN) (Siemens, 2024). In the case of Siemens Vectron locomotives, the measurement procedure is not available for small time-frames, because the onboard computer of the locomotive shows the measured data only every (approx.) 20 seconds, which is not appropriate for detailed and accurate analysis.

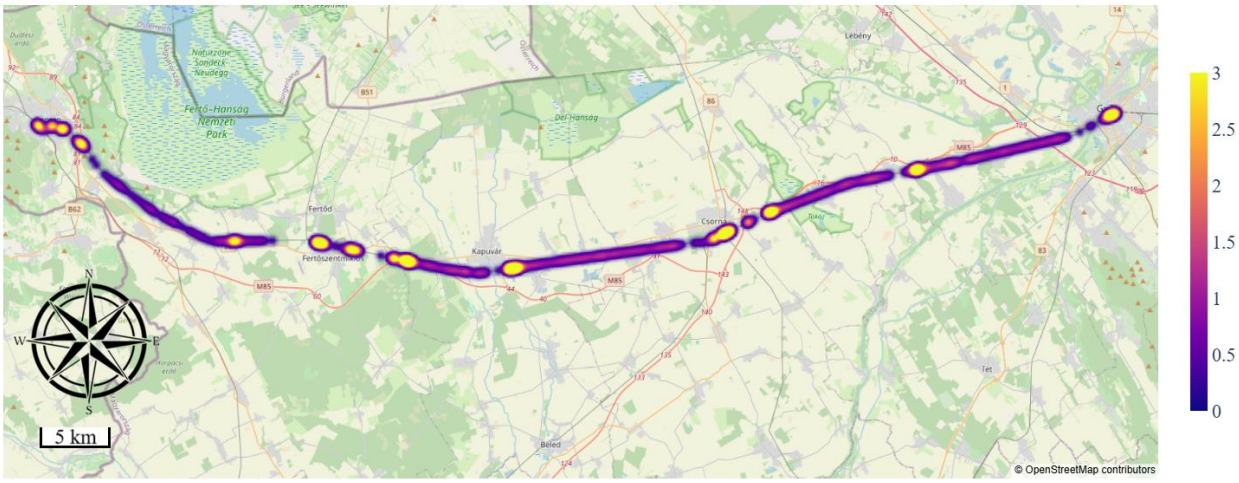

Figure 8. Consumed energy heatmap, Sopron (left) –Győr (right) route, date: 28 November 2024

https://doi.org/10.55343/CogSust.154

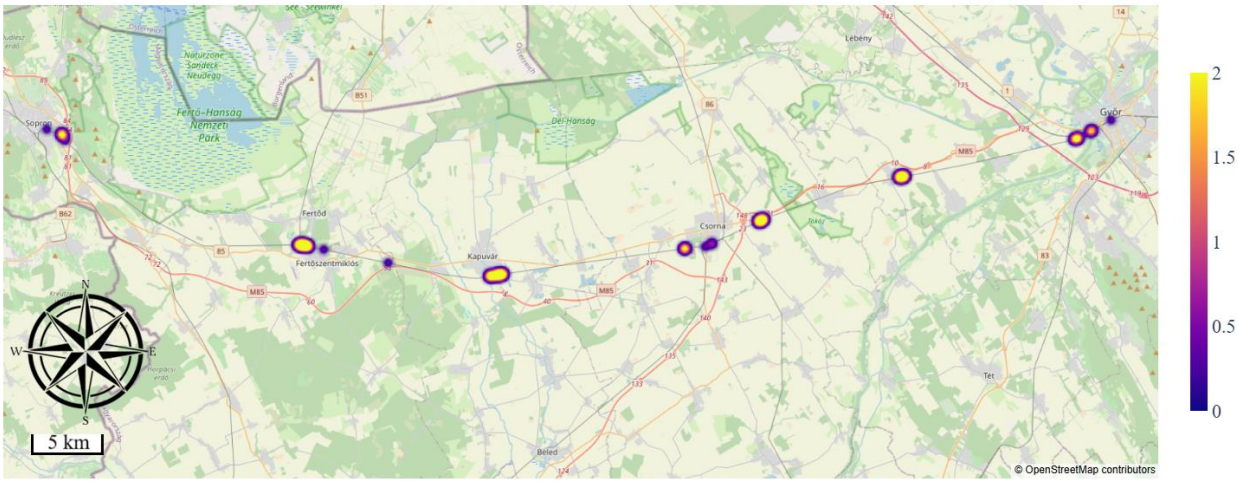

Figure 9. Regenerative braking energy heatmap, Sopron (left) –Győr (right) route, date: 28 November 2024

Figure 10. Consumed energy heatmap, Győr (right) – Sopron (left) route, date: 28 November 2024

https://doi.org/10.55343/CogSust.154

Figure 11. Regenerative braking energy heatmap, Győr (right) – Sopron (left) route, date: 28.11.2024

It is worth mentioning that these results can be compared with Fischer (2015). The value of α_2 in Fischer (2015) is 1.331, while the current study found 1.2759 (without filtering, see Fig. 2) and 1.2981 (with filtering, see Fig. 5). Similar results are contained in Fischer (2015) related to earlier investigations: 1.415. If the filtering is taken into account, the current article results in approx. 2.5% and 8.3% lower calculation factors than previous studies (i.e., 1.2981 vs. 1.331; 1.2981 vs. 1.415, respectively). The assumed reason for the differences is the effect of less accurate measurement possibilities and manual measurements, as well as train weights calculated from braking forces (Fischer (2015)). These two factors caused/could cause significant differences in the results obtained.

4. Conclusion

The following conclusions can be drawn from the obtained results:

- Cognitive sustainability and energy efficiency: frequent acceleration due to speed restrictions increases energy consumption. Long-term investments in track improvements could enhance efficiency and reduce operational costs.
- Energy consumption findings:
  1. Acceleration and constant-speed traction energy use can be estimated with correction factors α_1 = 1.2981 and α_2 = 1.3151 for Siemens Taurus 0470-series locomotives. The results were compared with earlier studies. Based on them, there is a 2.5…8.3% difference.
  2. At 120 km/h, the average specific energy consumption is 0.00204 kWh/kN/km (filtered dataset).
  3. Heatmaps of energy consumption and regenerative braking show peak energy use around stations and turnout tracks, reflecting the impact of frequent acceleration and deceleration.
- Regenerative braking concerns:
  1. It remains unclear whether regenerative braking energy is credited at full value.
  2. There is potential to redirect unused regenerative energy to power auxiliary systems.
  3. Siemens Vectron locomotives, with 300 kN regenerative braking force (compared to 150 kN in Taurus models), could improve energy recapture, reduce brake wear, and lower maintenance costs.
- Operational improvements for energy efficiency:
  1. Implementing driver assistance systems (DAS) could optimize train operation and reduce energy use.
  2. Timetable optimization should be explored to minimize unnecessary acceleration and braking.
  3. Expanding the Sopron–Győr railway line to a double-track system could reduce delays caused by passing loops and enhance overall efficiency.
  4. Analyzing train operators' driving styles is crucial, as stress from schedule adherence affects energy consumption.
  5. Incentive programs could be introduced to reward energy-efficient driving and regenerative braking performance; it is one of the authors' future research plans.

https://doi.org/10.55343/CogSust.154

- Infrastructure and locomotive modernization:
  1. Upgrading locomotives and passenger cars, along with regular maintenance, can reduce rolling resistance and improve energy efficiency; it is one of the authors' future research plans.
  2. The derived correlation functions and correction coefficients from this study provide a more precise framework for energy consumption calculations and forecasting.

Acknowledgement

This paper was supported by the János Bolyai Research Scholarship of the Hungarian Academy of Sciences. The paper was technically supported by the SZE-RAIL Research Team. The research has not received any financing for the article process charge. The authors express their most profound respect for the technical support of the Raaberbahn Hungary, especially Endre Lőkkös and Bálint Huszár.

References

Baur, K. G. (2003). *Taurus-Lokomotiven für Europa*. EK-Verlag, Freiburg im Breisgau.

Bina, M., Biassoni, F. (2023). Travel experience and reasons for the use and nonuse of local public transport: A case study within the community interregional project SaMBA (Sustainable Mobility Behaviors in the Alpine Region). *Sustainability*. 15(24), 16612. DOI: 10.3390/su152416612

Chen, W., Peng, F., Liu, Z., Li, Q., Dai, C. (2013). System integration of China's first PEMFC locomotive. *Journal of Modern Transportation*. 21(3), 163–168. DOI: 10.1007/s40534-013-0020-0

Cheremisin, V., Istomin, S., Perestenko, A. (2020). Artificial intelligence methods to control the energy efficiency of electric rolling stock online. *E3S Web of Conferences*. 175, 05046. DOI: 10.1051/e3sconf/202017505046

Cole, C., Sun, Y. Q., Wu, Q., Spiryagin, M. (2023). Exploring hydrogen fuel cell and battery freight locomotive options using train dynamics simulation. *Proceedings of the Institution of Mechanical Engineers, Part F: Journal of Rail and Rapid Transit*. 238(3), 310–321. DOI: 10.1177/09544097231166477

Currie, G., Reynolds, J., Logan, D., Young, K. (2023). "Tram wrong way" international experience and mitigation of track switch errors. *Transportation Research Record*. 2677(6), 631–643. DOI: 10.1177/03611981221149432

Dižo, J., Blatnický, M., Harušinec, J., Suchánek, A. (2022). Assessment of dynamics of a rail vehicle in terms of running properties while moving on a real track model. *Symmetry*. 14(3), 536. DOI: 10.3390/sym14030536

Domanov, K., Shatohin, A., Nezevak, V., Cheremisin, V. (2019). Improving the technology of operating electric locomotives using electric power storage device. *E3S Web of Conferences*. 110, 01033. DOI: 10.1051/e3sconf/201911001033

Ézsiás, L., Tompa, R., Fischer, S. (2024). Investigation of the possible correlations between specific characteristics of crushed stone aggregates. *Spectrum of Mechanical Engineering and Operational Research*. 1(1), 10–26. DOI: 10.31181/smeor1120242

Fischer, S. (2015). Traction energy consumption of electric locomotives and electric multiple units at speed restrictions. *Acta Technica Jaurinensis*. 8(3), 240–256. DOI: 10.14513/actatechjaur.v8.n3.384

Fischer, S. (2025). Investigation of the settlement behavior of ballasted railway tracks due to dynamic loading. *Spectrum of Mechanical Engineering and Operational Research*. 2(1), 24–46. DOI: 10.31181/smeor21202528

Fischer, S., Kocsis Szürke, S. (2023). Detection process of energy loss in electric railway vehicles. *Facta Universitatis, Series: Mechanical Engineering*. 21(1), 81–99. DOI: 10.22190/FUME221104046F

Fischer, S., Harangozó, D., Németh, D., Kocsis, B., Sysyn, M., Kurhan, D., Brautigam, A. (2024). Investigation of heat-affected zones of thermite rail weldings. *Facta Universitatis, Series: Mechanical Engineering*. 22(4), 689–710. DOI: 10.22190/FUME221217008F

Fischer, S., Hermán, B., Sysyn, M., Kurhan, D., Kocsis Szürke, S. (2025). Quantitative analysis and optimization of energy efficiency in electric multiple units. *Facta Universitatis, Series: Mechanical Engineering*, accepted manuscript in Online first. DOI: 10.22190/FUME241103001F

Ihme, J. (2022). Running Resistances of Rail Vehicles. In: *Rail vehicle technology*. Springer, Wiesbaden. 31–50. DOI: https://doi.org/10.1007/978-3-658-36969-9

Istomin, S. (2018). The use of correlation and regression analysis for assessment of the energy effectiveness of the DC electric locomotives auxiliary equipment. *MATEC Web of Conferences*. 239, 01038. DOI: 10.1051/matecconf/201823901038

Istomin, S., Perestenko, A., Dang, C. T. (2018). Development of the system of visual control of electric power consumption by electric rolling stock. *MATEC Web of Conferences*. 239, 01035. DOI: 10.1051/matecconf/201823901035

Kaleybar, H. J., Brenna, M., Li, H., Zaninelli, D. (2022). Fuel cell hybrid locomotive with modified fuzzy logic based energy management system. *Sustainability*. 14(14), 8336. DOI: 10.3390/su14148336

Kuchak, A. T. J., Marinkovic, D., Zehn, M. (2020). Finite Element Model Updating: Case Study of a Rail Damper. *Structural Engineering and Mechanics*. 73, 27–35. DOI: 10.12989/sem.2020.73.1.027

Kuchak, A. T. J., Marinkovic, D., Zehn, M. (2021). Parametric investigation of a rail damper design based on a lab-scaled model. *Journal of Vibration Engineering & Technologies*. 9, 51–60. DOI: 10.1007/s42417-020-00209-2

Liang, H., Zhang, Y., Yang, P., Wang, L., Gao, C. (2023). Comparison and analysis of prediction models for locomotive traction energy consumption based on the machine learning. *IEEE Access*. 11, 38502–38513. DOI: 10.1109/access.2023.3268531

Lu, A. Allen, J. G. (2024). Intermittent electrification with battery locomotives and the post-diesel future of North American freight railroads. *Transportation Research Record: Journal of the Transportation Research Board*. 2678(11), 1691–1718. DOI: 10.1177/03611981241245996

Lu, Q., He, B., Gao, Z., Che, C., Wei, X., Ma, J., Zhang, Z., Luo, J. (2019). An optimized regulation scheme of improving the effective utilization of the regenerative braking energy of the whole railway line. *Energies*, 12(21), 4166. DOI: 10.3390/en12214166

Lukaszewicz, P. (2007). Running resistance: Results and analysis of full-scale tests with passenger and freight trains in Sweden. *Proceedings of the Institution of Mechanical Engineers, Part F: Journal of Rail and Rapid Transit*. 221(2), 183–193. DOI: 10.1243/0954409JRRT89

Ma, C., Huang, B., Basher, M. K., Rob, M. A., Jiang, Y. (2024). Fuzzy PID control design of mining electric locomotive based on permanent magnet synchronous motor. *Electronics*, 13(10), 1855. DOI: 10.3390/electronics13101855

Macassa, G. (2023). Public perceptions of sustainable physical activity and active transportation: a pilot qualitative study in Gävle and Maputo. *Sustainability*. 15(21), 15354. DOI: 10.3390/su152115354

Madleňák, R., Masek, J., Madleňáková, L., Chinoracký, R. (2023). Eye-tracking investigation of the train driver's: A case study. *Applied Sciences*. 13(4), 2437. DOI: 10.3390/app13042437

Mandić, M., Uglešić, I., Milardić, V. (2009). Electric railway power consumption. *Journal of Energy – Energija*. 58(4), 384–407. DOI: 10.37798/2009584306

Mikhailov, E., Semenov, S., Shvornikova, H., Gerlici, J., Kovtanets, M., Dižo, J., Blatnický, M., Harušinec, J. (2021). A study of improving running safety of a railway wagon with an independently rotating wheel's flange. *Symmetry*. 13(10), 1955. DOI: 10.3390/sym13101955

Nikitenko, A., Kostin, M., Mishchenko, T., Hoholyuk, O. (2022). Electrodynamics of power losses in the devices of inter-substation zones of AC electric traction systems. *Energies*. 15(13), 4552. DOI: 10.3390/en15134552

Oraegbune, O., Ugwu, O. (2020). Delivering sustainable transport infrastructure projects (railway) in Nigeria: Frameworks, indicators, method and tools. *Nigerian Journal of Technology*. 39(3). DOI: 10.4314/njt.v39i3.4

Rajibayev, D., Miryakubov, A., Mavlanov, A. (2023). Study of the traction converter control system of the uzelr series of electric locomotives. *E3S Web of Conferences*. 458, 03016. DOI: 10.1051/e3sconf/202345803016

Ren, J., Zhang, Q., Liu, F. (2020). Analysis of factors affecting traction energy consumption of electric multiple unit trains based on data mining. *Journal of Cleaner Production*. 262, 121374. DOI: 10.1016/j.jclepro.2020.121374

Rochard, B. P., Schmid, F. (2000). A review of methods to measure and calculate train resistances. *Proceedings of the Institution of Mechanical Engineers, Part F: Journal of Rail and Rapid Transit*. 214(4), 185–199. DOI: 10.1243/0954409001531306

Rodriguez-Cabal, M. Á., Herrera-Jaramillo, D. A., Bastidas-Rodríguez, J. D., Ceballos, J. P. V., Montes-Villa, K. S. (2022). Methodology for the estimation of electrical power consumed by locomotives on undocumented railroad tracks. *Energies*. 15(12), 4256. DOI: https://doi.org/10.3390/en15124256

Saukenova, I., Oliskevych, M., Taran, I., Toktamyssova, A., Aliakbarkyzy, D., Pelo, R. (2022). Optimization of schedules for early garbage collection and disposal in the megapolis. *Eastern-European Journal of Enterprise Technologies*, 1(3), 13–23. DOI: 10.15587/1729-4061.2022.251082

Siemens (2024). VECTRON 230 km/h, Travel high speed flexibly across Europe. URL: https://assets.new.siemens.com/siemens/assets/api/uuid:c0d82542-6247-4cad-925a-c4a6d260530d/siemens-mobility-vectron-datasheet-230kmh.pdf (Accessed: 10 March 2025)

Tollner, D., Zöldy, M. (2022). Long term utilisation effect on vehicle battery performance. In *2022 IEEE 1st International Conference on Cognitive Mobility (CogMob)*. IEEE. 79–84. DOI: 10.1109/CogMob55547.2022.10118087

de la Torre, R., Corlu, C. G., Faulín, J., Onggo, B. S., Juan, A. A. (2021). Simulation, optimization, and machine learning in sustainable transportation systems: Models and applications. *Sustainability*. 13(3), 1551. DOI: 10.3390/su13031551

Volkov, V., Taran, I., Volkova, T., Pavlenko, O., Berezhnaja, N. (2020). Determining the efficient management system for a specialized transport enterprise. *Naukovyi Visnyk Natsionalnoho Hirnychoho Universytetu*. 2020(4), 185–191. DOI: 10.33271/nvngu/2020-4/185

Waleghwa, B., Ioannides, D. (2024). "Everyone wants to drive there": Challenges to transport sustainability in rural tourism destinations. *International Journal of Tourism Research*. 26(6), e2810. DOI: 10.1002/jtr.2810

Yan, J., Wang, H., Zhong, S., Lan, Y., & Huang, K. (2018). Control strategy for the energy optimization of hybrid regenerative braking energy utilization system used in electric locomotive. *Mathematical Problems in Engineering*. 2018, 1–13, 510487. DOI: 10.1155/2018/2510487

https://doi.org/10.55343/CogSust.154

Zarifyan, A., Mustafin, A., Valentseva, E., Shapshal, A. (2021). Capacity utilization level of freight electric locomotives and evaluation of expense reduction on consumed energy due to modernization. *Transport Problems*, 16(4), 5–14. URL: https://www.researchgate.net/publication/357333160_CAPACITY_UTILIZATION_LEVEL_OF_FREIGHT_ELECTRIC_LOCOMOTIVES_AND_EVALUATION_OF_EXPENSE_REDUCTION_ON_CONSUMED_ENERGY_DUE_TO_MODERNIZATION (Accessed: 10 March 2025)

Zöldy, M. (2024). Changes at mobility space use in the cognitive mobility era. *Acta Technica Jaurinensis*, 17(4), 163–168. DOI: 10.14513/actatechjaur.00750

Zöldy, M., Baranyi, P. (2023). The Cognitive Mobility Concept. *Infocommunications Journal*. 2023(Special Issue), 35–40. DOI: 10.36244/ICJ.2023.SI-IODCR.6

Zöldy, M., Dömötör, F. (2022). Noise and vibration test of electric drive cars. *In 2022 IEEE 1st International Conference on Cognitive Mobility (CogMob)*. IEEE. 121–124. DOI: 10.1109/CogMob55547.2022.10118037

Zöldy, M., Pathy-Nagy, Z. (2022). Evaluating of E-Vehicle Gear Noise. In *2022 IEEE 1st International Conference on Cognitive Mobility (CogMob)*. IEEE. 93–96. DOI: 10.1109/CogMob55547.2022.10117985

Zöldy, M., Baranyi, P., Török, Á. (2024). Trends in Cognitive Mobility in 2022. *Acta Polytechnica Hungarica*. 21(7), 189–202. DOI: 10.12700/APH.21.7.2024.7.11

https://doi.org/10.55343/CogSust.150

Implementation of an optimised autonomous Arduino-based car

Dr. Clio Vossou
0000-0002-4665-7759
Postdoctoral researcher, Vehicles Laboratory, National Technical University of Athens
Athens, Greece
klvossou@mail.ntua.gr

Ioanna Konstantinou
School of Mechanical Engineering, National Technical University of Athens
Athens, Greece
joanna_constantinou@hotmail.com

Prof. Dimitrios Koulocheris
0000-0002-1379-5805
Director of Vehicles Laboratory, National Technical University of Athens
Athens, Greece
dbkoulva@mail.ntua.gr

Abstract

Autonomous vehicles can be a key feature to sustainable mobility since they promise optimised routes, more efficient fuel consumption, safer road transport, and the ability to alter the perception of driving. This paper describes the implementation of a low-cost, self-navigating Arduino-based model car. The model car utilises an Arduino Uno mainboard. Four DC motors with their corresponding wheels are embedded in the model car to ensure its movement. Furthermore, the model car has an ultrasonic sensor to detect and avoid obstacles. Moreover, the model car hosts an action camera to record its environment, and more features may be added later for artificial cognition. Its chassis is designed and optimised to accommodate all the electronic components and ensure movement. Different versions of the chassis were fabricated using 3D printing technology. The performance of the model car was assessed while navigating in three different scenarios, during which the effect of the speed of the model car and the efficiency of its ultrasonic sensor were evaluated. The paper concludes with the topology optimisation of the chassis of the model car to optimise the chassis compliance and consequently improve the navigation characteristics of the model car.

Keywords

autonomous vehicle, sustainability, Arduino, ultrasound sensor, topology optimisation

1. Introduction

Sustainability, in general, is a term associated with economy, environment and society (Ketter et al., 2023). Transportation is an important economic sector that is rapidly changing to keep up with policymakers' sustainability goals, especially in the EU (Bao et al., 2023; Buzási and Csete, 2015). This can be translated to efficient, zero-emission and safe vehicles in road transport. Enhancing vehicles with artificial cognition can optimise road transport sustainability.

According to the statistics for the greenhouse gas emissions in the European Union (Eurostat, 2024a), although between 2008 and 2023 the level of greenhouse gas (GHG) emissions from all economic activities decreased by approximately 25%, GHG emissions from transportation and storage activities remained almost unaltered. Furthermore, the number of registered passenger cars in the EU shows an increasing trend regarding passenger road transport. In 2023, the number of registered passenger cars reached almost 257 million, corresponding to an increase of 6.5% compared to 2018 (Eurostat, 2024b). As

https://doi.org/10.55343/CogSust.150

the number of passenger vehicles increases, and since most road accidents can be attributed to human error (Fathy et al., 2020), one can also expect an increase in road accidents. Hence, for the road transportation to become sustainable, it must be optimised in terms of environmental footprint and safety. At a system level, this could be achieved utilising artificial intelligence and cognitive info-communication (Orynycz, 2024). Electric, autonomous and connected road vehicles seem to enhance transportation sustainability and lead to the development of smart cities (Sheeba et al., 2021). Furthermore, the introduction of connected road vehicles with on-board sensors could lead to vehicle-level mobility decisions based on sustainability (Zöldy et al., 2022).

An autonomous road vehicle is a computer-controlled car with artificial cognition capabilities that can guide itself, familiarise itself with the surroundings, make decisions and fully operate without human interaction (Das et al., 2024). According to the Standard SAE J3016, driving automation has six levels, from Level 0 (No Driving Automation) to Level 5 (Full Driving Automation). While Level 1 (Driver Assistance) and Level 2 (Partial Driving Automation) have been successfully commercialised with features like lane-centring and Adaptive Cruise Control (ACC), achieving full driving automation (Level 5) remains the ultimate goal (SAE, 2018).

Autonomous cars' presence has also become imminent in public and industrial transport, including buses, taxis, trucks, and couriers. Especially for trucks, applications such as platooning seem to be gaining attention, although there are many challenges ahead before fully autonomous vehicles can become the main mode of transportation across the globe. Safety, ethics, psychology, and other profound fields will undoubtedly involve decision-making and policy formulation (Ciuciu et al., 2017).

In order to test concepts applied in cars that enhance transport sustainability, scale model cars can be developed. Due to their small size, scale model cars have a lower environmental footprint during production and operation stages than full-scale cars. The concepts of embedded automation systems can especially be tested on such scale models since they require lower financial effort and offer quick and reliable results, provided the model is properly built.

In the literature, several Arduino-based model cars exist with various capabilities. Some of these models are controlled via Bluetooth (Gandotra et al., 2016; Patil et al., 2022; Vijayalakshmi, 2019; Ankit et al., 2016; Chen et al., 2018; Simatupang et al., 2016; Tang et al., 2019; Yilmaz and Tariyan, 2019). The models designed by Ankit et al. (2016) and Yılmaz and Tariyan Özyer (2019) also have the capability of autonomous movement. The model cars described in Fathy et al. (2020), Claes et al. (2013) and Walke et al. (2022) host a camera for obstacle detection and incorporate more capabilities such as lane detection. However, the majority of the model vehicles utilise one or more (Ciuciu et al., 2017) ultrasonic sensors since they have emerged as a prevalent choice for measuring distances and facilitating obstacle avoidance in autonomous vehicles (Bhatia and Panchal, 2024). Table 1 summarises the capabilities of the Arduino-based model cars found in the literature:

Table 1. Arduino-based model cars in the literature

	Control via Bluetooth	Autonomous movement	Camera	Ultrasonic sensor(s)
Ankit et al. (2016)	✓	✓		✓
Bhatia and Panchal (2024)		✓		✓
Chen et al. (2018)	✓			✓
Ciuciu et al., 2017		✓		✓
Claes et al. (2013)		✓	✓	
Das et al. (2024)		✓		
Fathy et al. (2020)		✓	✓	
Gandotra et al., (2016)	✓			
He et al. (2020)		✓		✓
Patil et al. (2022)	✓			✓
Rosen et al. (2014)		✓		✓
Simatupang et al., (2016)	✓			
Tang et al. (2019)	✓	✓		✓
Vairavan et al. (2018)		✓		✓
Vijayalakshmi (2019)	✓			
Walke et al. (2022)		✓	✓	
Yılmaz and Tariyan Özyer (2019)	✓	✓		✓

https://doi.org/10.55343/CogSust.150

It is worth mentioning that the typical design of model cars was described only in the works of Ankit et al. (2016), Yılmaz and Tariyan Özyer (2019) and Bhatia and Panchal (2024), and only a few results of their operation are described. Furthermore, little can be found concerning the performance evaluation of autonomous model cars or their use for developing real-scale autonomous vehicles. The use of scaled autonomous vehicles in the research and development of autonomous vehicles is illustrated by Ferencz and Zöldy (2021; 2022), who used scaled radio-controlled vehicle models to validate autonomous vehicles' movement in a roundabout.

The present paper presents the design and implementation of a self-navigating model car, and its performance in different navigation scenarios is evaluated. Additionally, the topology optimisation of its chassis in terms of mass is addressed. The paper begins with the description of the design methodology of the autonomous model car, which includes the selection of the electronic components, the mounting of hardware parts and the development of the necessary software code. Afterwards, the behaviour of the model car is monitored in different navigation manoeuvres, and the results are presented. Finally, the design of an optimised chassis is presented, considering the typical dimensions of normal-scale vehicles and the principles of topology optimisation.

2. Design methodology

In order to manufacture the proposed autonomous model car, the electronic components were first carefully selected. Then, a preliminary design of the chassis was created, taking into consideration the electronic components' shape and weight characteristics, and it was manufactured using 3D printing. Subsequently, the electronic components were mounted on the chassis. Finally, the software code was written and uploaded to the board.

2.1. Electronic components

As the central processing unit, the Arduino UNO R3 was selected. This board incorporates the ATmega328P 8-bit microcontroller. For the movement of the model car, the motor wheel kit was selected, consisting of 4 DC geared motors, four wheels and four holders. In order to control the DC geared motors, the Adafruit Motor/Stepper/Servo Shield for Arduino was utilised. This motor shield can control up to 4 DC motors or up to 2 stepper motors. For the model car to have an obstacle avoidance capability and be autonomous, the ultrasonic module distance sensor HC-SR04 was selected. The HC-SR04 is a proximity sensor with an input voltage of 5 VDC, which provides a 2 to 400 cm non-contact measurement function, and its ranging accuracy can reach up to 3 mm. Its measuring angle is 30°. Since the measuring angle of the HC-SR04 sensor is 30°, it was decided to mount it on the servomotor KS0194 with a rotation angle range of 180°. Finally, two 9 V rechargeable Li-ion batteries were used for the model car's power supply.

2.2. Chassis design and manufacturing

For the preliminary design of the chassis, the dimensions of the electronic components were taken into consideration, and an effort was made to reduce the chassis weight by removing material from areas which would not host any components. This led to the design (Design1) presented in Figure 1.

https://doi.org/10.55343/CogSust.150

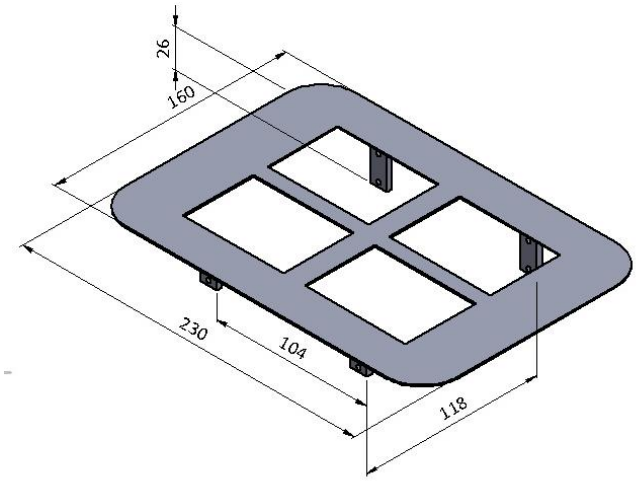

Figure 1. Chassis – preliminary design (Design 1)

The chassis was designed in Solidworks® and manufactured using fused deposition modelling in an Ultimaker S5 3D printer. The Ultimaker's Polylactic Acid (PLA) was selected as chassis material. The chassis is symmetric along the longitudinal (left–right) and the lateral (front–rear) axes. The outer dimensions of the chassis are 230 × 160 mm, with a wheelbase of 104 mm and a track width of 118 mm. Figure 2 presents the preliminary implementation of the autonomous model car.

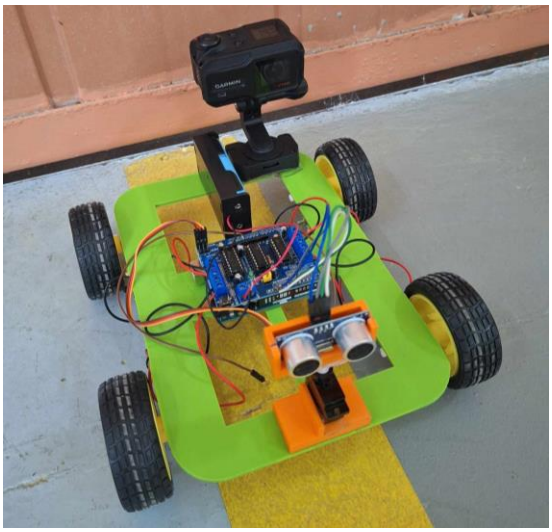

Figure 2. Preliminary implementation of the autonomous model car (Design 1)

The wheels' motors are mounted on the chassis. A DC motor controls each wheel without suspension and has a camber angle 0°. All the wheels are in contact with the ground and non-slipping conditions are hypothesised (Luu et al., 2019).

In Figure 2, the Garmin Virb action camera, used to monitor the movement of the model car, is visible at the rear of the model car. Furthermore, the placement of the battery pack can be observed. Additionally, the positioning of the ultrasonic distance sensor is crucial, as it correlates with the performance of the model car in obstacle detection and avoidance. Therefore, a special mounting can be observed. During the operation of this preliminary implementation, unwanted movement of the wheels around the vertical axis (Z-axis) was observed. Also, the influence of the non-symmetric placement of the action camera was observed. Therefore, the chassis was redesigned to ensure that the movement around the Z-axis of the four DC motors is restricted and that the battery pack can be hosted horizontally, lowering the centre of mass of the model car, improving its performance. Figure 3 presents the improved design (Design 2) of the chassis.

https://doi.org/10.55343/CogSust.150

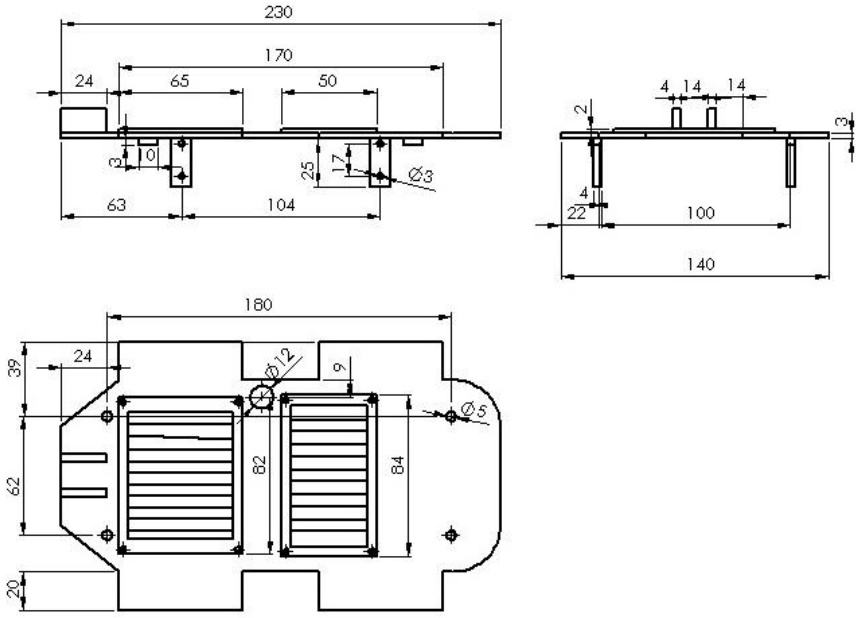

Figure 3. Chassis – improved design (Design2)

As Figure 3 demonstrates, the chassis's overall shape was changed to reduce its weight without emptying vast areas. Furthermore, the width of the chassis was set to 140 mm, and its track width was reduced to 100 mm. Finally, two areas with reduced material were designed: one measuring 82 × 65 mm to host the Arduino board and the motor shield, and another measuring 84 × 50 mm to host the battery pack.

2.2.1. centre of mass

The height of the centre of mass of a vehicle affects its handling; thus, before the construction of the model car, its centre of mass was calculated. The mass of each component was measured with an electronic scale, Kern FCB24K1, with a weighing range of 24 kg and readability equal to 1 g. Thereafter, the assembly of the model car was designed using Solidworks software, and the position of each component and its centre of mass was estimated computationally. Table 2 presents the mass of each component and its computationally estimated position of the centre of mass on the improved model car.

Table 2. Mass and coordinates of the centre of mass of each component of the autonomous model car

Component	Mass (g)	Centre of mass		
		X Coordinate	Y Coordinate	Z coordinate
Ultrasonic module & servo motor	24	70.0	31.2	214.4
Battery pack	102	70.0	9.5	90
Board & motor shield	60	70.0	6.0	167.5
DC motor 1	31	7.5	-13.5	64.0
DC motor 2		7.5	-13.5	166.0
DC motor 3		132.5	-13.5	166.0
DC motor 4		132.5	-13.5	67.0
Wheel 1	41	-19.0	-13.5	36.0
Wheel 2		-16.0	-13.5	36.0
Wheel 3		156.0	-13.5	194.0
Wheel 4		150.0	-13.5	194.0
Action Camera	199	70.0	67.6	17.5
Chassis	71	70.1	-1.8	115.6

https://doi.org/10.55343/CogSust.150

As Table 2 illustrates, the heaviest component is the action camera, followed by the battery pack. The total mass of the model car is 744 g, and the coordinates of its centre of mass are presented in Table 3.

Table 3. Mass and coordinates of the centre of mass of the improved model car

Mass (g)	Centre of mass		
	X Coordinate	Y Coordinate	Z Coordinate
744	69.9	15.5	93.1

2.3. Autonomous model car implementation

All the electronic components were mounted on the chassis and then interconnected as indicated in Figure 4 (a). Figure 4 (b) shows the complete autonomous Arduino-based improved model car (Design2).

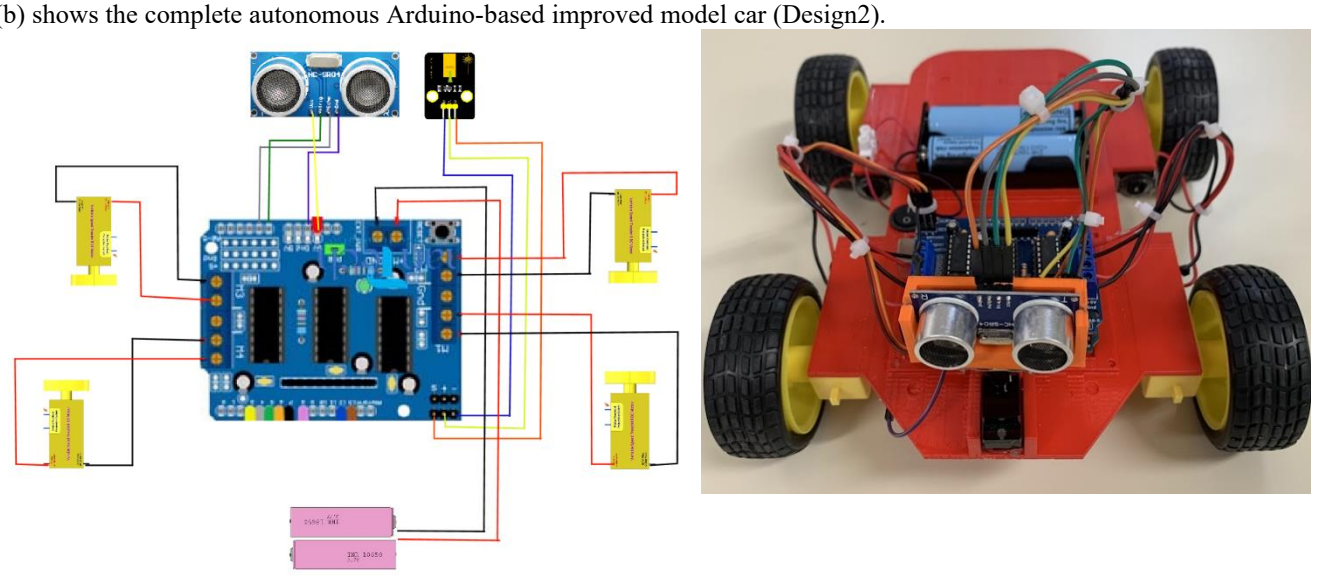

(a) (b)

Figure 4. Improved model car (Design2): (a) Circuit diagram of the electronic components and (b) Implementation of Design2

The software code must be written and uploaded to the main board for the prototype of the Arduino-based autonomous model car to become functional. The software code was developed in the Arduino IDE environment, and the libraries for the motor shield (AFMotor.h), the servomotor (Servo.h) and the ultrasonic module (NewPing.h) were added. In Figure 5, the flow chart of the algorithm is presented.

https://doi.org/10.55343/CogSust.150

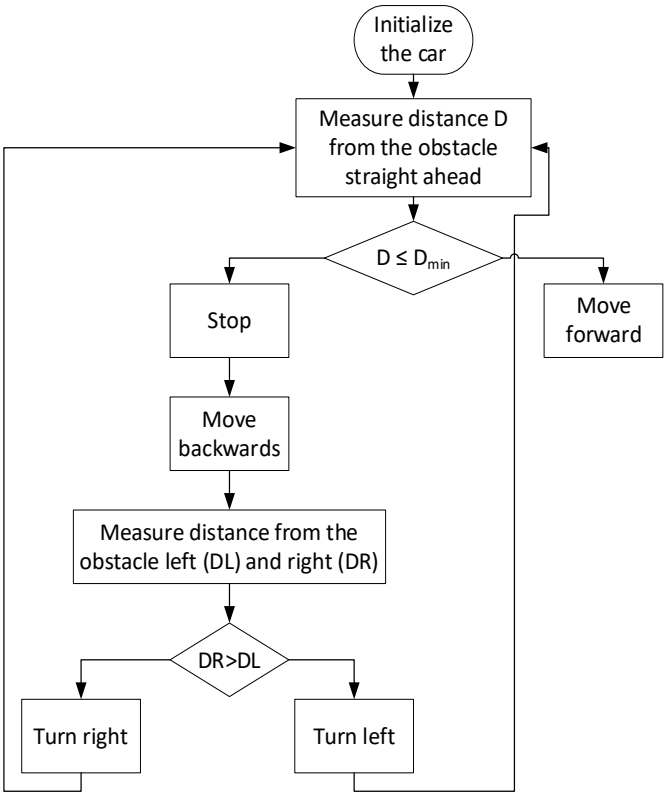

Figure 5. Flow chart of the software of MC2

During the initialisation of the model car, all four DC motors are started along with the servomotor and the ultrasonic sensor. After initiation, the DC motors move with a defined rotational speed. The servomotor starts at 0° angle. Then, the first measurement of the distance D from the nearest obstacle in the forward direction is performed. If the measured distance is more than D_{min}, the model car moves in the forward direction. The ultrasonic sensor measures this distance repetitively. When this distance becomes less than D_{min}, the model car stops for 0.1 s, moves backwards for 0.2 s and stops again. Then, using the servomotor, the ultrasonic sensor turns first to the right and measures the distance from the closest obstacle in this direction (D_R), and then turns left to measure the corresponding distance (D_L) from the closest obstacle. Finally, the autonomous model car moves in the direction with the highest distance from the obstacle. If $D_R = D_L$ The model car chooses to move to the left. The cornering of the model car is achieved by altering the speeds of the inner wheel motors compared to the outer ones. In general, the software code incorporates the control of the speed and the movement of the motors, the processing of sensor data and navigation decisions.

3. Test of the prototype

In order to test the prototype, three different manoeuvres were designed. The autonomous model car had to move on a straight line for 3000 mm during the first manoeuvre. For the second manoeuvre, the model car navigated in a straight lane with a width of 500 mm and a length of 3000 mm, defined using discrete obstacles of height 500 mm at distances of 200 mm. For the final manoeuvre, the model car had to navigate in a square free space of 2000 × 2000 mm, bounded by discrete obstacles of a height of 500 mm. In Figure 6, the setups for all three manoeuvres are presented.

https://doi.org/10.55343/CogSust.150

(a)

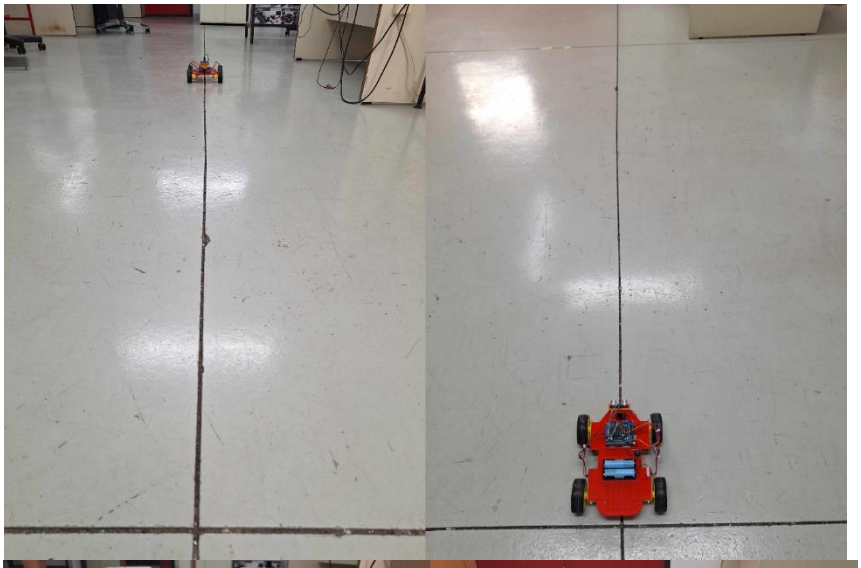

(b)

https://doi.org/10.55343/CogSust.150

(c)

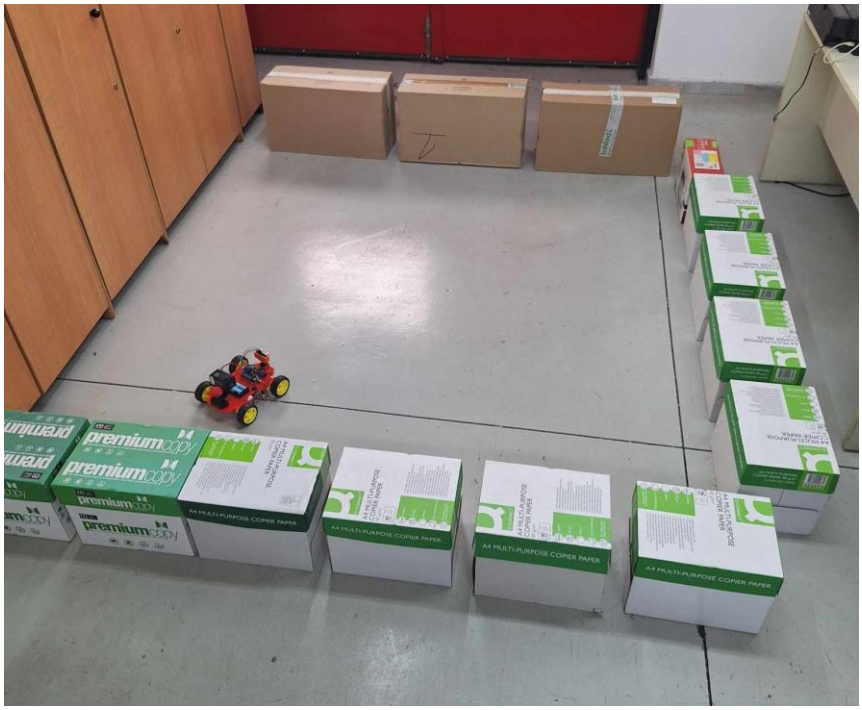

Figure 6. Manoeuvre setups (a) Test 1, (b) Test 2 and (c) Test 3

In Figures 6 (a) and (b), the model car is presented at each test's start and end. The first test was performed with three different DC motor speeds to evaluate their effect on navigation skills. The speed of the DC motors is defined through a dimensionless number that ranges from 0 to 255. In each test, the value of the dimensionless speed was set to 150, 200 and 250, respectively. In Tests 2 and 3, the value of D_{min} To evaluate its effect, it was set to 250 mm, 500 mm and 1000 mm, respectively. Care was taken for the road surface to have a low friction coefficient for all test manoeuvres.

3.1. Results

In this section, the results of the navigation of the model car are presented for all manoeuvres.

3.1.1. Test 1

Regardless of the DC motors' speed, the model car could complete Test 1. Nevertheless, it was noticed that the movement of the model car deviated from the straight line towards the left, as it is presented in Figure 7. The value of the deviation differed for different DC motor speeds.

https://doi.org/10.55343/CogSust.150

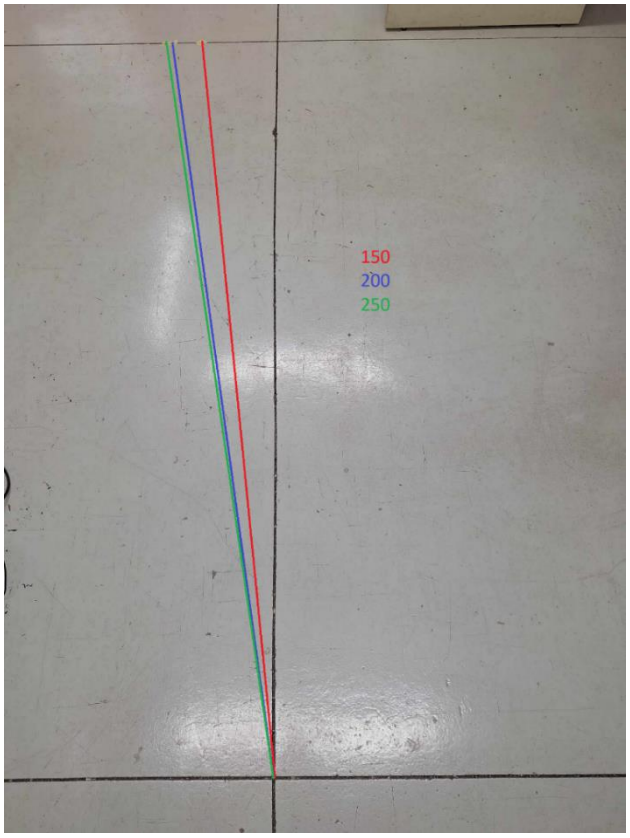

Figure 7. Model car trail for different speeds.

Table 4 presents the time needed for the model car to complete Test 1 and the measured resulting deviation.

Table 4. Results for Test 1

Dimensionless speed	Time (s)	Deviation (cm)
150	10	31
200	8	43
250	6	42

3.1.2. Test 2

During Test 2, the movement of the model car was restricted by a barrier. When the model car moves towards the barrier, it changes its orientation to avoid it. The influence of D_{min} was evaluated along with the speed of the model car, leading to different versions of the same test manoeuvre. It was noticed that not all test manoeuvres were completed.

Table 5 presents the complete (✓) and incomplete (X) test manoeuvres.

Table 5. Test 2 was performed with different DC motor speeds and D_{min}

Dimensionless speed	150	200	250
D_{min} (mm)			
250	X	X	✓
500	✓	✓	✓
1000	X	X	X

Furthermore, in Table 6, the number of orientation changes of the model car are presented for the completed test manoeuvres, along with the total time needed to complete each test manoeuvre.

https://doi.org/10.55343/CogSust.150

Table 6. Total time and number of orientation changes for the completed manoeuvres in Test 2

D_{min} (mm)	Dimensionless Speed	Number of orientation changes	Total time to completion (s)
250	**250**	1	9
500	**150**	2	16
500	**200**	4	22
500	**250**	4	20

3.1.3. Test 3

In Test 3, the model car was placed in the centre of a square space with dimensions of 2000 × 2000 mm and allowed to move within it. The square space was bounded by discrete obstacles as presented in Figure 6 (c). Both the DC motor speed and D_{min} were altered in order to monitor the model car's dynamic behaviour. For each combination of D_{min} and DC motor speed, the movement of the model car was monitored with the action camera for a total of 60 s. When D_{min} was set to 250 mm, regardless of the speed of the model car, it was not using the whole space, but its movement was restricted near one of the corners of the square space. When D_{min} was set to 500 mm, the model car could cover all the space in the square for the DC motor speed of 200 and 250. Finally, when D_{min} was set to 1000 mm, the movement of the model car was restricted in the central area of the square space.

3.2. Discussion

Each test was designed to simulate a special movement condition. Therefore, Test 1 was designed to review the ability of the model car to navigate in a straight line free from obstacles. It was shown that the model car moved without changing its orientation, but it deviated from the intended direction slightly due to the quality of the wheels, the friction between the tires and the road surface, which was not smooth enough, and the position of the centre of mass of the model car. Table 7 presents the correlation between the DC motor's dimensionless speed and the model car speed for Test 1.

Table 7. Correlation between the DC motor's dimensionless speed and the model car speed

Dimensionless speed	Calculated model car speed (m/s)
150	0.30
200	0.38
250	0.50

Figure 8 presents the correlation between the dimensionless speed of the DC motors and the actual speed of the model car as it was calculated in Test 1.

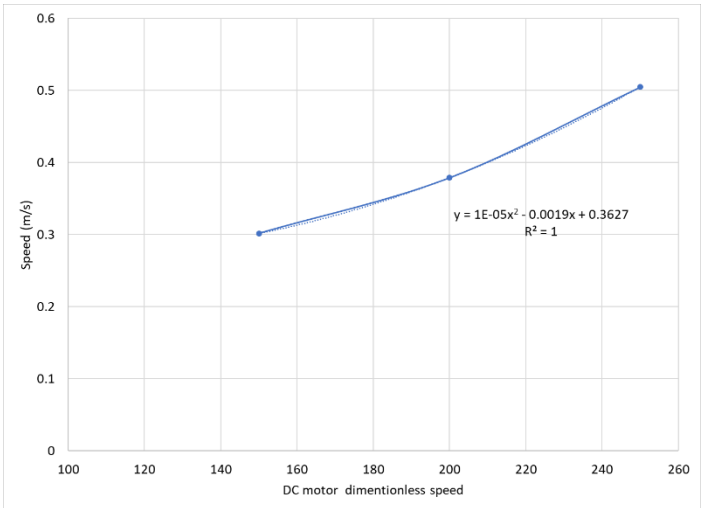

Figure 8. Correlation between the dimensionless speed of the DC motors and the speed of the model car

https://doi.org/10.55343/CogSust.150

As shown in Figure 8, the correlation between the DC motors' speed and the model car's speed is not linear. Moreover, it can be seen that increasing the DC motor speed reduces the deviation from the straight line.

Test 2 was designed to review the ability of a model car to navigate between obstacles. In this test, the influence of both the model car speed and the minimum allowed distance from an obstacle (D_{min}) was crucial to completing the manoeuvre as shown in Table 5. In Table 6, it was shown that as the DC motor speed increases, the number of orientation changes during the movement of the model car increases, regardless of the value of D_{min}. Furthermore, keeping the DC motor speed constant, the number of changes in the orientation of the model car increases with D_{min}.

Finally, Test 3 was designed to observe the free movement of the model car in a given space. Through this test, it was shown that the only combination of DC motor speed and D_{min} that led to full space utilisation was when the dimensionless speed was set to 200 and D_{min} was 500 mm. In addition, it was noticed that a low value of D_{min} restricts the movement of the model car in a corner of the square space. On the other hand, if the value of D_{min} is comparable to the overall dimensions of the free space, and the movement of the model car is restricted to the centre of the square space.

4. Chassis topology optimisation

Reviewing the performance of the autonomous model car in the test manoeuvres, the benefit of improving its response during cornering, acceleration, and braking, hence its handling characteristics, is obvious. In order to alter the handling characteristics of the model car, without adding any components, the weight of the chassis can be minimised and its dimensions can be changed. At the same time, a reduction in the weight of the chassis will reduce the total weight of the model car, lowering its environmental footprint during both construction and function phases and increasing its sustainability.

In order to ensure that the weight of the chassis can be reduced, a static finite element (FE) analysis was performed in SolidWorks Simulation Software. In Table 8, the loads applied from the electronic components, due to their weight, on the chassis are presented.

Table 8. Applied loads

Component	Force (N)
Ultrasonic module & servo motor	0.24
Battery pack	1.00
Board & motor shield	0.59
Action Camera	1.95

The areas of the attachment of the DC motors to the chassis were considered fixed supports where all the nodes' degrees of freedom were considered equal to 0. The boundary conditions of the FE model are presented in Figure 9.

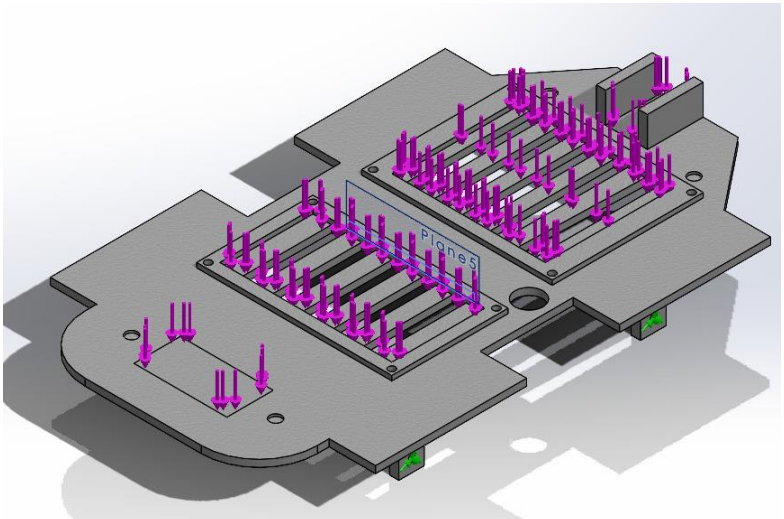

https://doi.org/10.55343/CogSust.150

Figure 9. Boundary conditions of the FE model.

In Figure 10, the mesh of the FE model is presented. The mesh was blended curvature-based, and the maximum element size was set to 5 mm, resulting in a solid mesh of 14115 FE and 28195 nodes.

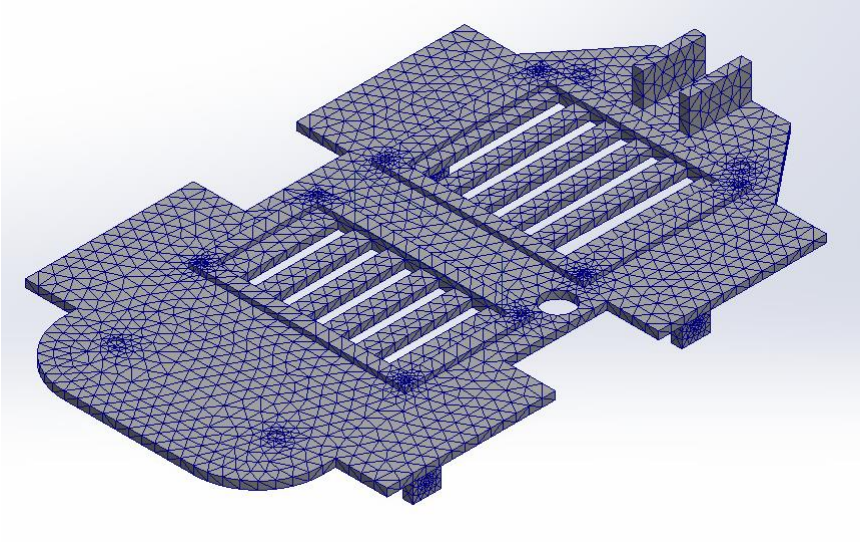

Figure 10. Mesh of the FE mode

The chassis was printed from Polylactic Acid (PLA). The physical and mechanical properties used for PLA were retrieved from the literature (Hodžić et al., 2020) for Ultimaker's PLA and are presented in Table 9.

Table 9. Physical and mechanical properties of Ultimaker's PLA (Hodžić et al., 2020)

Density (kg/m^3)	1020
Young's modulus (GPa)	2.9
Yield strength (MPa)	36.3
Tensile strength (MPa)	57.6

Figure 11 presents the Equivalent Von Mises stress (SEQV) on the chassis in an isometric and a side view.

(a)

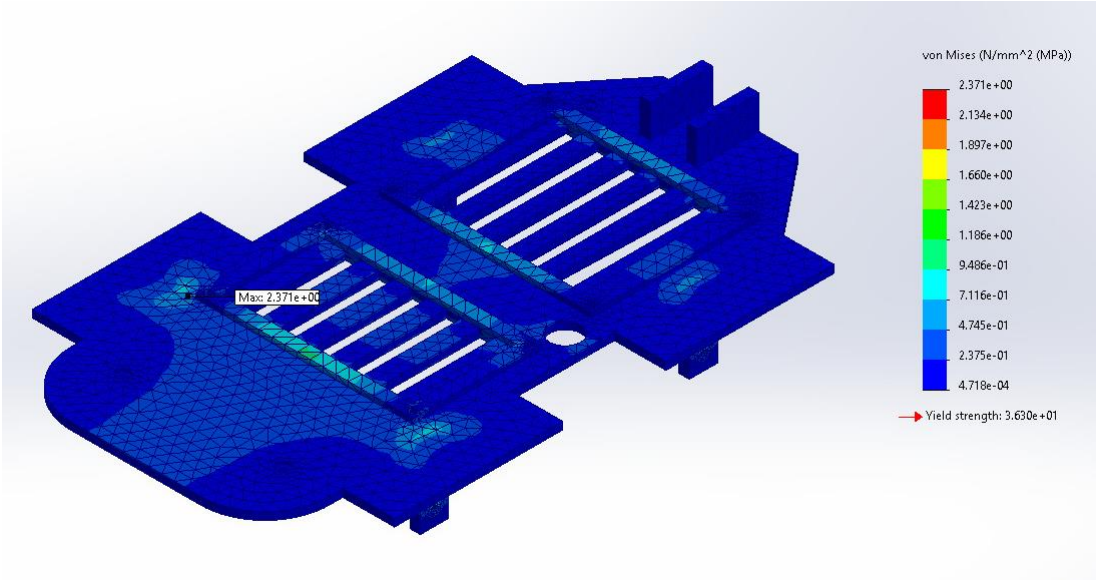

https://doi.org/10.55343/CogSust.150

(b)

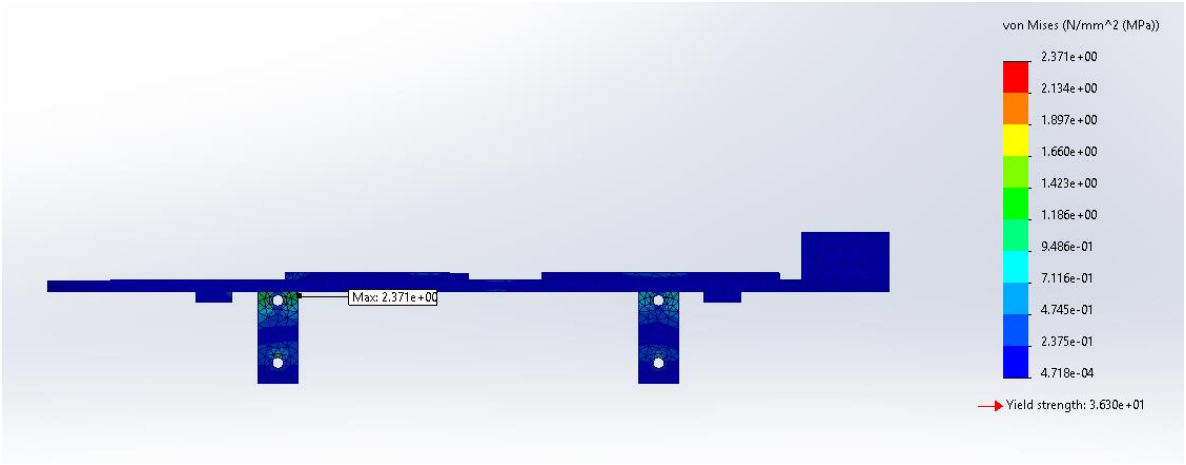

Figure 11. SEQV contour in isometric and side view

The maximum value of SEQV is located on the rear protruding structure used to support the DC motor, where it reaches 2.4 MPa. In Figure 12, the total deformation of the model is presented.

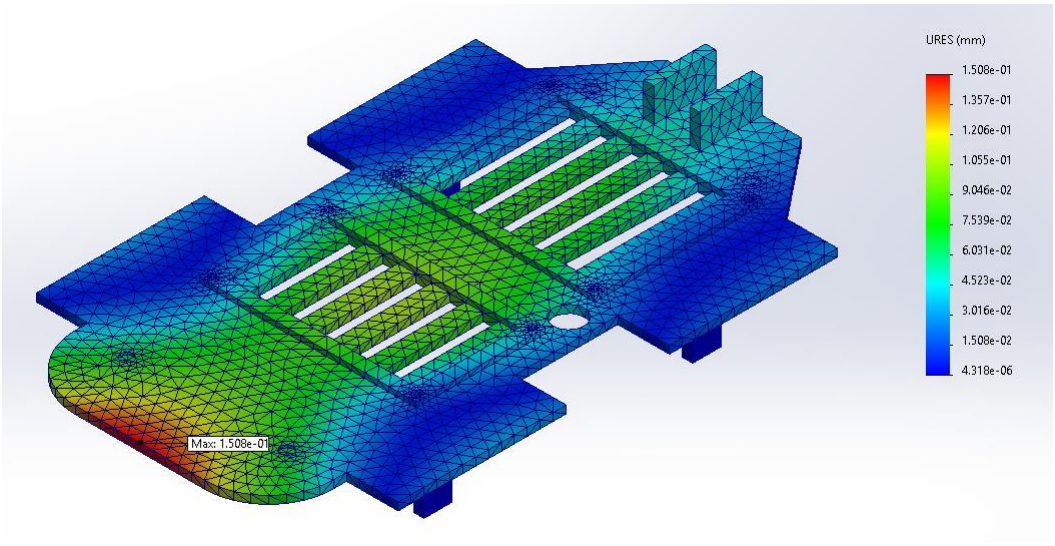

Figure 12. Total deformation contour

The maximum value of total deformation is 0.15 mm, located on the rear end of the chassis, where the action camera is mounted. The fact that the maximum value of SEQV is 6.6% of the yield strength of the material and that the displacement is less than 0.2 mm indicates that the weight of the chassis can be reduced without loss of structural integrity.

Using Design2 as the initial design of the chassis, topology optimisation was performed using the best stiffness to weight ratio as a goal, with the constraints of mass reduction by 50% and of a safety factor equal to 1.3. In Figure 13, the topology optimisation result (Design2_OPTI) is presented.

https://doi.org/10.55343/CogSust.150

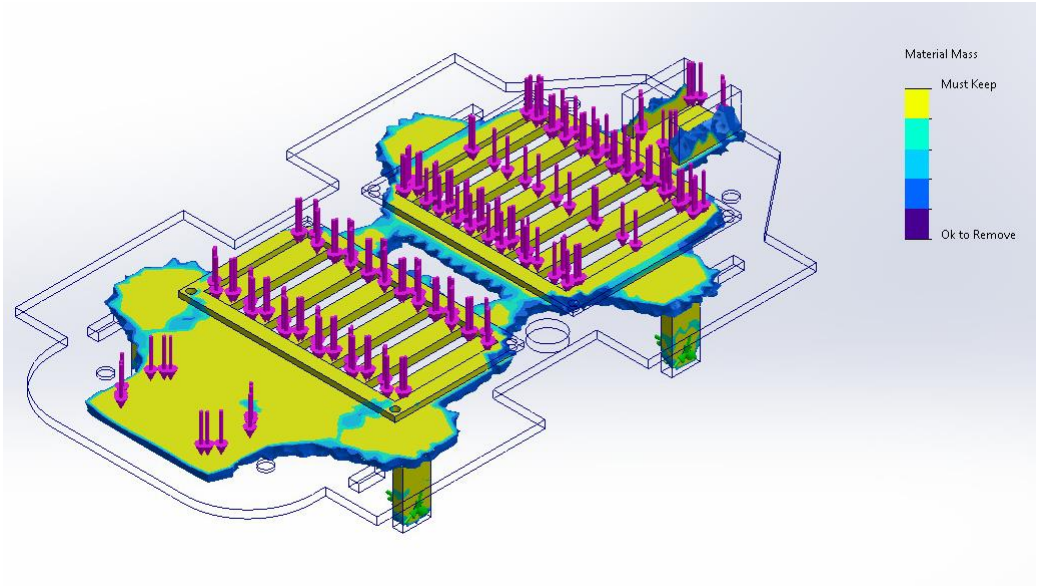

Figure 13. Results of the topology optimisation (Design2_OPTI)

As Figure 13 shows, it is obvious that material can be removed from the area in-between the structures that host the board and the battery pack, and from the rear part of the chassis. Additionally, the supporting structures of the wheels can profit from filets, but no material can be removed from those areas.

In order to further improve the dynamic behaviour of the model car, a new chassis (Design3) design was proposed based on the mean dimensions of typical vehicles. According to Zhang et al. (2022), the most common dimensions of passenger cars are presented in Table 10.

Table 10. Mean dimensions of passenger cars

	Length (mm)	Width (mm)	Height (mm)
Sedan	5100	1890	1560
SUV	4950	1940	1850
MPV	5150	1930	1900

As can be observed in Table 10, SUV vehicles are the widest, hence their dimensions were selected as a baseline for the new design of the chassis of the Arduino-based autonomous model car. Furthermore, the mean length of the wheelbase of an SUV is 2.75 m, while the mean length of the track width is 1.60 m. A typical scale for model cars that results in dimensions close to the ones of Design2 is 1:18, leading to the dimensions presented in Table 11.

Table 11. Scaled dimensions of an SUV for the Design3

Length (mm)	275
Width (mm)	108
Height (mm)	103
Wheelbase (mm)	153
Track width (mm)	89

This results in a 20% longer and 23% narrower chassis design (Design3), presented in Figure 14.

https://doi.org/10.55343/CogSust.150

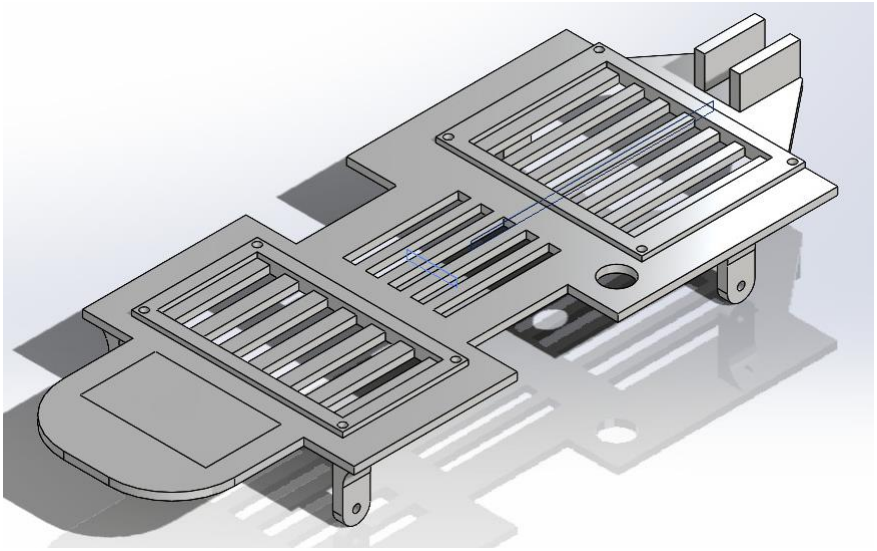

Figure 14. Chassis design based on a scaled SUV (Design3)

Figure 15 presents the topology optimisation results for the design of the chassis (Design3_OPTI). The topology optimisation was performed using the same goal, constraints, and boundary conditions as in Design2.

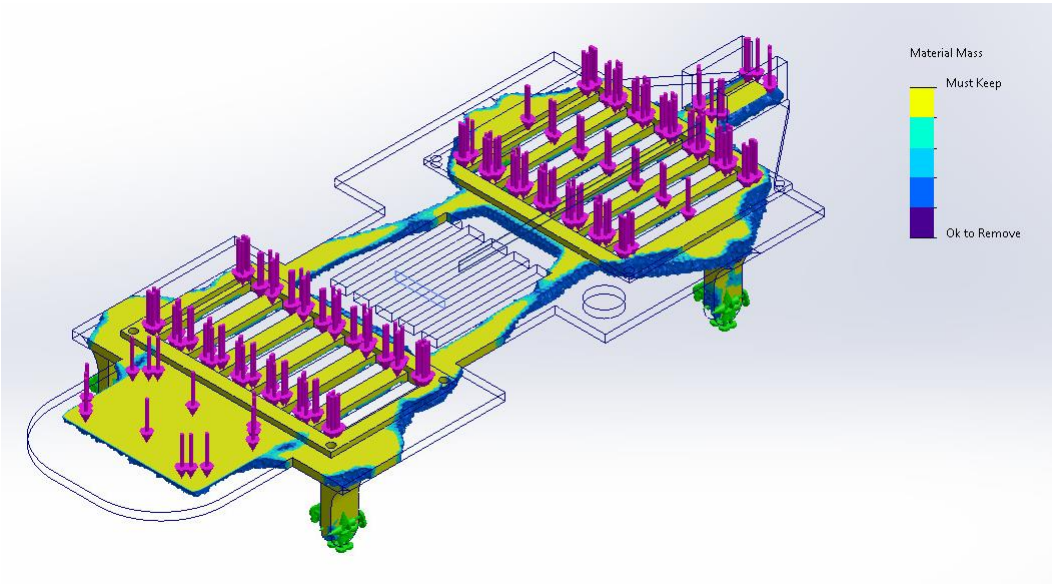

Figure 15. Results of the topology optimisation (Design3_OPTI)

In Table 12, the weight of all chassis designs is presented.

Table 12. Mass of different chassis versions

Chassis Versions	Mass (g)
Design1	74
Design2	71
Design2_OPTI	46
Design3	69
Design3_OPTI	37

https://doi.org/10.55343/CogSust.150

As depicted in Table 12, the lightest design version of the chassis is Design3_OPTI, with a weight of 37 g, which is 50% lighter than the initial design (Design1).

5. Conclusions

In this paper, the procedure of the implementation of an optimised Arduino-based, autonomous model car is described. The selection of electronic components and the design process are presented in detail. Furthermore, the dynamic behaviour of the model car is investigated through various tests simulating different navigation conditions. Finally, alternatives for an optimised chassis design, regarding handling and sustainability, were provided using topology optimisation in Solidworks software.

Altogether, the tests of the prototype model car demonstrated that the Arduino-based autonomous model car (Design2) responded efficiently to different navigation scenarios by taking appropriate actions such as moving forward, turning left or right, and stopping to avoid collision with obstacles. Its functionality was proven more efficient for higher DC motor speed values and the minimum accepted distance from an obstacle. D_{min} depending on this speed and the mean distance of the obstacles.

In the future, this Arduino-based model car can host more ultrasonic sensors to enhance its decision-making ability. Other types of sensors can be added related to its sustainability, i.e., electric power consumption. Future research directions include testing the different chassis designs, evaluating the energy consumption of the model car, integrating additional sensors, and exploring machine learning techniques for advanced decision-making. Conclusively, this Arduino-based model car can be used as a starting point to decrease true scale testing, which uses high energy resources.

References

Ankit, V., Jigar, P., Savan, V. (2016). Obstacle avoidance robotic vehicle using ultrasonic sensor, android and Bluetooth for obstacle detection. *International Research Journal of Engineering and Technology*. 3(2), 339–348. URL: https://www.irjet.net/archives/V3/i2/IRJET-V3I257.pdf

Bao, L., Kusadokoro, M., Chitose, A., Chen, C. (2023). Development of socially sustainable transport research: A bibliometric and visualisation analysis. *Travel Behaviour and Society*. 30(2), 60–73. DOI: 10.1016/j.tbs.2022.08.012

Bhatia, A., Panchal, P. (2024). Development of an Arduino-Based Smart Robot Car for Object Detection and Navigation. *International Journal of Research in Aeronautical and Mechanical Engineering*. 12(3), 1–7. DOI: 10.5281/zenodo.10802365

Buzási, A., Csete, M. (2015). Sustainability indicators in assessing urban transport systems. *Periodica Polytechnica: Transportation Engineering*. 43(3), 138–145. DOI: 10.3311/PPtr.7825

Chen, L., Zhang, J., Wang, Y. (2018, May). Wireless car control system based on ARDUINO UNO R3. *2nd IEEE Advanced Information Management, Communicates, Electronic and Automation Control Conference (IMCEC)*. 1783–1787. DOI: 10.1109/IMCEC.2018.8469286

Ciuciu, C., Bărbuță, D., Săsăujan, S., Șipoș, E. (2017). Autonomous scale model car with ultrasonic sensors and Arduino board. *Acta Technica Napocensis*. 58(4), 6–11. DOI: https://users.utcluj.ro/~atn/papers/ATN_4_2017_2.pdf

Claes, D., Fossel, J., Broecker, B., Hennes, D., Tuyls, K. (2013). Development of an Autonomous RC-car. *Intelligent Robotics and Applications: 6th International Conference, Proceedings, Part II.* Springer, Berlin–Heidelberg. 108–120. DOI: 10.1007/978-3-642-40849-6_10

Das, N., Bhuyan, A., Sonowal, P. P., Lama, A., Boruah, N. 2024. Design and Implementation of Arduino based low cost Autonomous Car. *6th International Conference on Energy, Power and Environment (ICEPE)*. IEEE. DOI: 10.1109/ICEPE63236.2024.10668936

Eurostat (2024a). Greenhouse gas emission statistics – air emissions accounts. URL: https://ec.europa.eu/eurostat/statistics-explained/index.php?title=Archive:Greenhouse_gas_emission_statistics_-_air_emissions_accounts

Eurostat (2024b). Passenger cars in the EU. URL: https://ec.europa.eu/eurostat/statistics-explained/index.php?title=Passenger_cars_in_the_EU

Fathy, M., Ashraf, N., Ismail, O., Fouad, S., Shaheen, L., Hamdy, A. (2020). Design and implementation of self-driving car. *Procedia Computer Science*. 175, 165–172. DOI: 10.1016/j.procs.2020.07.026

Ferencz, C., Zöldy, M. (2021). Autonomous driving cycle modeling, simulation and validation on 1: 10 scale vehicle model platforms. *International Journal for Traffic and Transport Engineering (IJTTE)*. 11(4), 565–579. DOI: 10.7708/ijtte2021.11(4).06

Ferencz, C., Zöldy, M. (2022). Simulation and validation with radio-controlled (RC) autonomous vehicles in roundabout situation. *Periodica Polytechnica Transportation Engineering*. 50(3), 252–259. DOI: 10.3311/PPtr.15730

Gandotra, S., Sharma, B., Mahajan, S., Motup, T., Choudhary, T., Thakur, P. (2016). Bluetooth controlled RC car using Arduino. *Imperial Journal of Interdisciplinary Research*, 2(9), 144–147.

He, Z., Zhang, Y., Zheng, H., Zhang, Y., Yu, H., Luo, M. (2020, May). New Design of All-terrain Smart Car Based on Arduino. *IOP Conference Series: Materials Science and Engineering*. 853(1), 012046. DOI:10.1088/1757-899X/853/1/012046

Hodžić, D., Pandžić, A., Hajro, I., Tasić, P. (2020). Strength comparison of FDM 3D printed PLA made by different manufacturers. *TEM Journal*. 9(3), 966–970. DOI: 10.18421/TEM93-18

https://doi.org/10.55343/CogSust.150

Ketter, W., Schroer, K., Valogianni, K. (2023). Information systems research for smart sustainable mobility: A framework and call for action. *Information Systems Research*. 34(3), 1045–1065. DOI: 10.1287/isre.2022.1167

Luu, D. L., Lupu, C., Chirita, D. (2019, June). Design and development of smart cars model for autonomous vehicles in a platooning. *15th International Conference on Engineering of Modern Electric Systems (EMES)*. IEEE. 21–24. DOI: 10.1109/EMES.2019.8795199

Orynycz, O. (2024). Cognitive tools for enhancing sustainability in liquid fuel and internal combustion engine development. *Cognitive Sustainability*. 3(4). DOI: 10.55343/cogsust.135

Patil, V. P., Gohatre, U., Matey, S., Jadhav, R., Kantekar A. (2022). Design and Development of Bluetooth control car based on Arduino UNO. *International Research Journal of Modernization in Engineering Technology and Science.* 4(8), 608–614. URL: https://www.irjmets.com/uploadedfiles/paper/issue_8_august_2022/29186/final/fin_irjmets1660556771.pdf

Rosen, W., Ertekin, Y., Carr, M. E. (2014, June). An autonomous Arduino-based racecar for first-year engineering technology students. *ASEE Annual Conference & Exposition*. 24–153. DOI: 10.18260/1-2--20044

SAE (2018). SAE International Recommended Practice, Taxonomy and definitions for terms related to driving automation systems for on-road motor vehicles. SAE Standard J3016_201806, Revised June 2018, Issued January 2014. DOI: 10.4271/J3016_201806

Sheeba, H., Gaur, D., Kumar Shukla, V. (2021, October). Impact of Emerging Technologies on Future Mobility in Smart Cities by 2030. *Proceedings of the 2021 9th International Conference on Reliability, Infocom Technologies and Optimisation (Trends and Future Directions)(ICRITO)*. 8–10). DOI: 10.1109/ICRITO51393.2021.9596095

Simatupang, J. W., Yosua, M. (2016). A remote controlled car using wireless technology. *Journal of Electrical And Electronics Engineering*. 1(2), 56–61. DOI: 10.33021/jeee.v1i2.192

Tang, L., Huang, W., You, J. (2019, August). The design of the intelligent car based on the Arduino UNO and Lab VIEW. *Journal of Physics Conference Series*. 1288(1):012071. DOI: 10.1088/1742-6596/1288/1/012071

Vairavan, R., Kumar, S. A., Ashiff, L. S., Jose, C. G. (2018). Obstacle avoidance robotic vehicle using ultrasonic sensor, Arduino controller. *International Research Journal of Engineering and Technology (IRJET)*. 5(2). URL: https://www.irjet.net/archives/V5/i2/IRJET-V5I2457.pdf

Vijayalakshmi, S. (2019). Robotic Car Using Arduino with Bluetooth Controller. or wirelessly controlled. *International Journal of Intelligence in Science and Engineering*. 1(1). URL: https://papers.ssrn.com/sol3/papers.cfm?abstract_id=3353197

Walke, T., Agnihotri, A., Gohate, R., Mane, S., Pande, S., Pendke, K. (2022). Miniature model of autonomous vehicle using Arduino UNO and open CV. *Ijraset Journal For Research in Applied Science and Engineering Technology*. 10(4), 3294–3305. DOI: 10.22214/ijraset.2022.42074

Yılmaz, E., Tarıyan Özyer, S. (2019). Remote and autonomous controlled robotic car based on Arduino with real time obstacle detection and avoidance. *Universal Journal of Engineering Science*. 7(1), 1–7 DOI: 10.13189/ujes.2019.070101

Zhang, J., Yang, H., Chen, Z., Yu, T., Liu, H. (2022). Probability distribution and recommended values of passenger car external dimensions in mechanical parking garage design. *Journal of Asian Architecture and Building Engineering*. 21(5), 1942–1958. DOI: 10.1080/13467581.2021.1971995

Zöldy, M., Szalmáné Csete, M. S., Kolozsi, P. P., Bordás, P., Török, Á.. (2022). Cognitive sustainability. *Cognitive Sustainability*. 1(1). DOI: 10.55343/cogsust.7

https://doi.org/10.55343/CogSust.185

Adaptation of economic intervention effect on mobility model in Far East environment

Mate ZOLDY
mate.zoldy@gtk.bme.hu
Budapest University of Technology and Economics
Budapest, Hungary

Li Aijuan
liajuan@sdjtu.edu.cn
Shandong Jiaotong University
Shandong, China

Abstract

Mobility is a key pillar of the 21st century, connecting people and information while presenting sustainability challenges. This paper aims to evaluate the impact of economic interventions on urban mobility, specifically through the introduction of parking fees in Jinan, China. The study employs a refined mobility model that categorises road usage into downtown, city, rural, and motorway environments and adapts European baseline data to the Far Eastern context. Data and methods include the development of a model measuring individual utility by average speed and social utility by CO_2 emissions per passenger kilometre. The model is adapted to reflect Far Eastern cities' unique urbanisation and energy mix. Results indicate that the introduction of parking fees in Jinan has significantly reduced traffic congestion, increased public transportation usage by 20%, and decreased CO_2 emissions by 8%. The tiered pricing system has improved urban space utilisation and economic efficiency. In conclusion, the study highlights the effectiveness of economic tools in promoting sustainable urban mobility and underscores the need for region-specific adaptations. Future research should explore additional economic interventions and expand the model's applicability to other regions.

Keywords

Sustainable Mobility, Economic Interventions, Urbanisation, CO_2 Emissions, Public Transportation

1. Introduction

Mobility is a key pillar of the third millennium. It connects and helps to be informed but also has several externalities (Buzási and Csete, 2015). One of the most challenging tasks is influencing or changing mobility to serve society and be sustainable (Zoldy et al., 2022; Kocziszky, 2023). Several researchers are trying to find engineering solutions to improve the sustainability dimension of mobility (Buzási and Jäger, 2020). Research today focuses on more sustainable energy sources (Torok et al., 2014; Orynycz et al., 2025), alternative solutions in the automotive drivetrain, new tendencies regarding modal split (Zamprogno and Esztergár-Kiss, 2024), improvements in vehicle dynamics, a new solution in safety and cyber security, more secure connection between the vehicle and the infrastructure, applications on the internet of the things (Nguyen et al., 2025) smart infrastructure, and cognitive traffic management (Zöldy et al, 2024). Although these and several other studies have tangible outcomes; it is more and more clear that without involving the governmental toolkit to force the changes (Szalmáné Csete et al., 2024; Wengritzky et al., 2024)), not all of these opportunities will be part of the future mobility system. Governmental subsidies and tax effectiveness depend at least on the internal structure of mobility (Zöldy and Kolozsi, 2025) the share of performances. A new model describes the urban mobility modal split and mobility forms to clearly show the governmental action's effects (Gaal et al., 2015; M. Zöldy, 2024).

While investigating the parking fee introduction in Jinan, China, it was clear that Chinese metropolises have a different modal split from the European cities. This research presents the framework of the developed modelling space and analyses the Chinese metropolises to include them into the model. In the last part of this study, an economic tool, namely the parking fee introduction effect, is shown with the help of the updated model.

https://doi.org/10.55343/CogSust.185

2. The method

A model was developed to show the effects of different economic interventions on individual and social utility in the context of mobility. In this model, average speed, measured in meters per secundum, is used as an indicator of individual utility within mobility. If the average speed increases, the individual utility increases as well, as it implies that mobility goals can be reached faster. Meanwhile, social utility is measured by emissions, specifically the CO_2 emitted in grams over passenger kilometres [gCO_2/pkm]. If the amount of emitted CO_2 over passenger kilometres increases, it lowers the model's social utility.

The model uses a space model for mobility: it divides mobility into four layers: downtown, city, rural and highway. These four levels better characterise the mobility of the cognitive era, which is influenced heavily by more and more urbanisation. Previous research introduced a refined classification of road mobility (Zöldy, 2024) by expanding the traditional three categories – urban, rural, and motorway – with a fourth: downtown. This new category reflects the evolving nature of mobility in highly urbanised environments.

The downtown category represents the innermost parts of large cities, often historic centres or traffic-calmed zones. These areas are characterised by very low speeds, typically around 10 km/h, and a high level of interaction with pedestrians and micromobility devices like scooters and bicycles. There are usually no lane separations, and the infrastructure is not designed for high vehicle throughput. Instead, the focus is on sustainability, with very low emissions and energy consumption per participant. Vehicle dynamics are limited, and the environment is optimised for walking, cycling, and public transport.

In contrast, the urban category covers general city traffic in densely populated areas. Here, vehicles move at slightly higher speeds – under 30 km/h – but still face frequent stops, turns, and interactions with diverse road users. The traffic is complex and turbulent, with high emissions and energy use. This category reflects traditional city driving, where private cars, buses, and delivery vehicles share the road.

The rural category includes roads in less populated areas like small towns and the countryside. These roads typically support moderate speeds of around 75 km/h and have fewer intersections and interactions than urban roads. The traffic mix, including agricultural vehicles and bicycles, is diverse, but the dynamics are more stable. Emissions and energy use are moderate, and the infrastructure is simpler than in urban areas.

Finally, the motorway category refers to high-speed roads like highways and expressways. These roads are designed for efficient, long-distance travel, with average speeds around 110 km/h. They feature physically separated lanes, no level crossings, and minimal vehicle interaction. The traffic is homogeneous, mostly cars and trucks, and vehicle dynamics are stable. However, this efficiency comes at the cost of high emissions and energy consumption.

Additionally, our model uses four passenger mobility categories. It is easy to associate them with mobility forms. The four modes are: walking, micromobility (roller, bike, e-bike, scooter, e-scooter), public transport (bus, tram, metro), and passenger cars. These four categories describe mostly the mobility modes of the 21st century.

Visualisation of the model is shown in Figure 1. It represents the average European mobility patterns.

https://doi.org/10.55343/CogSust.185

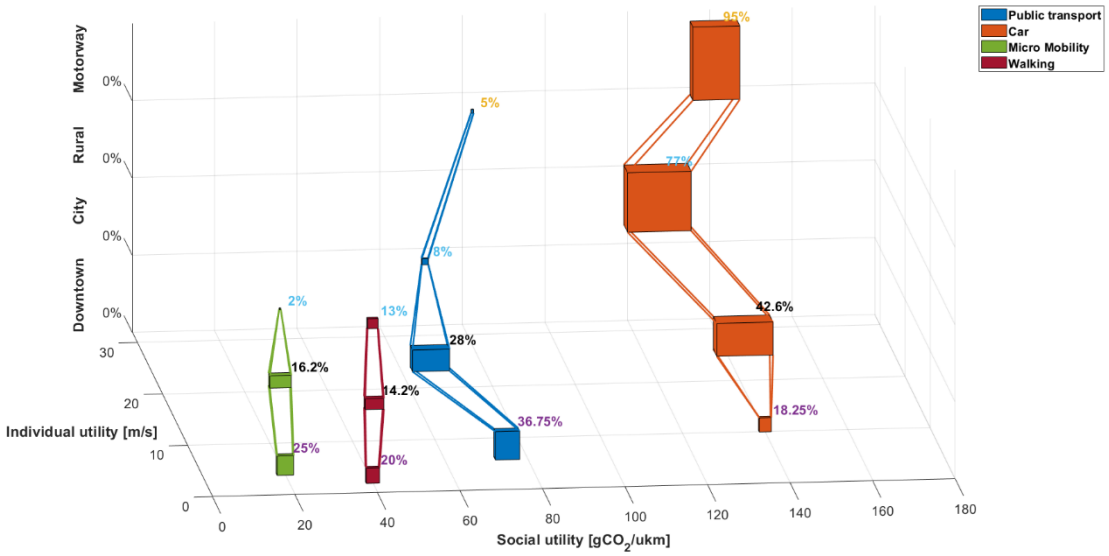

Figure 1. Model visualisation for a European mobility scenario

One key element of the model is the modal split between transport modes.

3. Far East context

During the investigation of the model's adaptability, all dimensions were checked and validated. The first assumption was that European average data could be good for evaluating governmental economic intervention's effect on sustainable mobility. It was recognised that all aspects should be rechecked and corrected if needed. The following aspects were investigated:

Table 1. Model adaptation from European context to far-east context

aspect of the model	adaptation need	remark
social utility [gCO_2/ukm]*	to keep	common measure worldwide
measure of social utility by mobility categories	to review	In the Far East, micro-mobility is based on electric vehicles with a lower CO_2 impact.
personal utility [m/s]	to keep	common measure worldwide
measure of social utility by mobility categories	to keep	traffic flow is similar around the globe
space use categories [downtown, city, rural, motorway]	to keep	common measure worldwide
mobility categories	to keep	common measure worldwide
mobility modal split %	to review	different urbanisation in the far-east resulted in different modal split
economical interventions	to keep	similar toolkit worldwide

*please note CO_2/ukm: ukm is the Hungarian abbreviation of passenger kilometre performance indicator

Based on the reviewed literature, the following adaptations were carried out according to the Far East cities' specialities, presented in Table 2. The adaptation is based on two main pillars. First, the Chinese energy mix differs from the European one, as it has a higher carbon footprint. It appears to have higher CO_2 emissions in the model (Bieker (2021), IEA (2020) and Transport & Environment (2020). This adaptation will help improve the baseline model's punctuality, new data used to refine the CO_2 footprint of European micro-mobility across different space utilisations.

Table 2. Adaptation of social utility baseline values

measure of social utility [gCO_2/ukm]	European baseline [gCO_2/ukm]	Far-east baseline [gCO_2/ukm]
Micro-mobility/downtown	20	40
Micro-mobility/city	20	35
Micro-mobility/rural	20	45

The mobility split ratios have to be adopted as well. Based on the overviewed literature, the main difference between the mobility split of the two regions is based on the urbanisation differences (He et al. 2011, Yang et al. 2017). Based on a synthesis of academic literature, government reports, and World Bank studies, we can outline the estimated modal split

https://doi.org/10.55343/CogSust.185

across different urban zones in the largest far east cities (World Bank, 2018; Pengjun and Shengxiao, 2018). Downtown areas like Beijing and Shanghai are heavily transit-oriented due to dense metro networks and car restrictions (e.g., license plate lotteries and congestion pricing). Micromobility (especially e-bikes) is widely used for first/last-mile connections and short trips, particularly in suburban and peri-urban zones. Motorways are almost exclusively used by private vehicles and freight, with minimal public transport presence except intercity buses. Walking remains significant in historic cores and older residential districts, where urban form supports pedestrian activity. Table 3 shows the new baseline values for Far-East cities (PT: public transport, MM: micromobility).

Table 3. Adaptation of Far East modal split ratios

BASELINE		European ratio %	Far-east ratio
down-town	PT	34	56
	Car	25	12
	MM	23	12
	walking	18	20
City	PT	23	45
	Car	48	25
	MM	16	12
	walking	14	17
rural	PT	7,65	26
	Car	77,5	46
	MM	2,1	16
	walking	13,1	12
motor-way	PT	5	5
	Car	95	95
	MM	0	0
	walking	0	0

https://doi.org/10.55343/CogSust.185

4. Factors that influence mobility - Evaluation of parking fee: case study in Jinan

The introduction of parking fees in Jinan, which began in early 2023, was a pivotal measure in addressing the city's chronic traffic congestion and promoting sustainable urban mobility. The local government implemented a tiered pricing system, where parking fees vary based on the location and duration of parking. In high-demand areas, such as the central business district, fees are higher to discourage long-term parking and encourage vehicle turnover. This approach has significantly reduced traffic congestion, as fewer drivers are circling to find free or cheap parking spots. Additionally, the revenue generated from these fees is reinvested into public transportation infrastructure, further enhancing the city's mobility options (Gao, 2025).

The impact of these changes has been multifaceted. Firstly, there has been a noticeable decrease in vehicles on the road during peak hours, contributing to a reduction in average commute times by approximately 10–12% (Zhang et al., 2021). Secondly, public transportation usage has increased by around 20%, with more residents opting for buses and the metro instead of driving. This shift has also reduced CO_2 emissions by about 8% in urban areas, improving air quality (Chen, 2017).

Moreover, the turnover rate for parking spaces has improved, with spaces being used more efficiently and frequently. This has eased congestion and enhanced the economic efficiency of urban space utilisation (Pengjun and Shengxiao, 2018). The introduction of parking fees has thus played a crucial role in transforming Jinan's transportation system, making it more efficient and environmentally friendly. The data after the introduction of parking fees in Jinan is presented in Table 4.

Table 4. Changes in personal and social utility after the introduction of parking fee in Jinan

Jinan, parking fee		ratio %	individual utility (m/s^2)	social utility (gCO_2/km)
down-town	PT	56	8.3	73.6
	Car	12	10	147.2
	MM	12	6	50
	walking	20	1,42	40
City	PT	45	8.3	60
	Car	25	10	140
	MM	12	6	40
	walking	17	1.42	40
rural	PT	26	13.9	60
	Car	46	19.4	115
	MM	16	5.5	60
	walking	12	0	0
motor-way	PT	5	7.7	76
	Car	95	30,5	140
	MM	0	0	0
	walking	0	0	0

5. Conclusion

This paper presents a comprehensive model to evaluate the impact of economic interventions on mobility in urban environments, specifically focusing on the introduction of parking fees in Jinan, China. The study highlights the significant differences in modal split and mobility patterns between European and Far Eastern cities, emphasising the need for region-specific adaptations in sustainability models. The crucial results of this research demonstrate that the introduction of parking fees in Jinan has led to a notable reduction in traffic congestion, increased public transportation usage, and improved air quality. The tiered pricing system has effectively discouraged long-term parking in high-demand areas, contributing to more efficient urban space utilisation and reduced CO_2 emissions.

Overall, this paper contributes to the body of knowledge by offering a refined model for evaluating economic interventions in urban mobility, highlighting the importance of region-specific adaptations, and suggesting new directions for further research.

https://doi.org/10.55343/CogSust.185

References

Bieker, G. (2021). A global comparison of the life-cycle greenhouse gas emissions of combustion engine and electric passenger cars. ICCT White Paper. URL: https://theicct.org/sites/default/files/publications/Global-LCA-passenger-cars-jul2021_0.pdf

Buzási, A., Csete, M. (2015). Sustainability indicators in assessing urban transport systems. *Periodica Polytechnica Transportation Engineering*. 43(3), 138–145. DOI: 10.3311/PPtr.7825

Buzási, A., Jäger, B. S. (2020). District-scale assessment of urban sustainability. *Sustainable Cities and Society*. 62, 102388. DOI: 10.1016/j.scs.2020.102388

Chen, C. (2017). At 20km/h you are moving only slightly faster than a donkey in Jinan, China's most gridlocked city. *South China Morning Post*, 2017, November 28. URL: https://www.scmp.com/business/china-business/article/2121979/20km/h-you-are-moving-only-slightly-faster-donkey-jinan

Gaal, G., Horváth, E., Török, Á., Csete, M. (2015). Analysis of Public Transport Performance in Budapest, Hungary. *Periodica Polytechnica Social and Management Sciences*. 23(1), pp. 68–72. DOI: 10.3311/PPso.7724

Gao, J. (2025). Research on improving traffic planning control in Jinan City, Shandong Province based on big data urban planning. *Advances in Economics Management and Political Sciences*. 148(1), 60–66. DOI: 10.54254/2754-1169/2024.LD19168

He, D., Meng, F., Wang, M. Q., He, K. (2011). Impacts of urban transportation mode split on CO_2 emissions in Jinan, China. *Energies*. 4(4), 685–699. DOI: 10.3390/en4040685

IEA (2020). GHG intensity of passenger transport modes, 2019. URL: https://www.iea.org/data-and-statistics/charts/ghg-intensity-of-passenger-transport-modes-2019

Kocziszky, Gy. 2023. Quo Vadis, Market Economy? Challenges of Sustainability and Values, Possible Answers. *Public Finance Quarterly*. 69(1), 9–28. DOI: 10.35551/PFQ_2023_1_1

Nguyen, H. P., Le, P. Q. H., Pham, V. V., Nguyen, X. P., Balasubramaniam, D., Hoang, A. T. (2025). Application of the Internet of Things in 3E (efficiency, economy, and environment) factor-based energy management as smart and sustainable strategy. *Energy Sources, Part A: Recovery, Utilization, and Environmental Effects*. 47(1), 9586–9608. DOI: 10.1080/15567036.2021.1954110

Orynycz, O., Rodrigues, G. S., Mendes dos Reis, J. G., Kulesza, E., Matijošius, J., Teixeira Machado, S. (2025). Energy and environmental benefits of in-motion charging trolleybuses: A case study of Vilnius. *Energies*, 18(12), 3015. DOI: 10.3390/en18123015

Pengjun, Z., Shengxiao, L. (2018). Suburbanisation, land use of TOD and lifestyle mobility in the suburbs. Journal of Transport and Land Use, 11(1), 195-215. DOI: 10.5198/jtlu.2018.1099

Szalmáné Csete M., Zöldy M., Török Á. (2024). Új mobilitási megoldások: technikai lehetőségek és pénzügyi aspektusok a fenntarthatóság tükrében [New mobility solutions: technical possibilities and financial aspects in the light of sustainability]. In: Kolozsi P. P. (szerk.): *A pénz jövője, a jövő pénze I: Pénzügyek történelmi perspektívában, zöld pénzügyi fordulat* [The Future of Money, the Money of the Future: Finance in Historical Perspective: the Green Financial Turn]. METU–MNB, Budapest. 183–199.

Torok, A., Torok, A., Heinitz, F. (2014). Usage of production functions in the comparative analysis of transport related fuel consumption. *Transport and Telecommunication*. 15(4), 292. DOI: https://doi.org/10.2478/ttj-2014-0025

Transport & Environment (2020). How clean are electric cars? T&E's analysis of electric car lifecycle CO2 emissions. *Briefing by Transport & Environment*. URL: https://www.transportenvironment.org/uploads/files/TEs-EV-life-cycle-analysis-LCA.pdf

Wengritzky, Z., Szabó, T. P., Dézsi-Benyovszky, A. (2024). Spatial effects of economical and infrastructural factors on BEV adoption: Evidence from an emerging market. *Review of Economic Studies & Research Virgil Madgearu*. 17(1). DOI: 10.24193/RVM.2024.17.113

World Bank. (2018). Reducing Traffic Congestion and Emission in Chinese Cities. *World Bank.* URL: https://www.worldbank.org/en/news/feature/2018/11/16/reducing-traffic-congestion-and-emission-in-chinese-cities

Yang, Z., Jia, P., Liu, W., Yin, H. (2017). Car ownership and urban development in Chinese cities: A panel data analysis. *Journal of Transport Geography*. 58, 127–134. DOI: 10.1016/j.jtrangeo.2016.11.015

Zamprogno M. M., Esztergár-Kiss D. (2024). Applying Cluster Analysis for the Investigation of Travel Behavior and User Profiles. *Periodica Polytechnica: Transportation Engineering*. 52(4), 362–371. DOI: 10.3311/PPtr.25663

Zhang, Y., Zhao, L., Zhao, H., Gao, X. (2021). Urban development trend analysis and spatial simulation based on time series remote sensing data: A case study of Jinan, China. *PLoS ONE*. 16(10), e0257776. DOI: 10.1371/journal.pone.0257776

Zöldy, M. (2024). Changes at mobility space use in the cognitive mobility era. *Acta Technica Jaurinensis*. 17(4), 163–168. DOI: 10.14513/actatechjaur.00750

Zöldy M., Kolozsi P. P. (2025). Analysis Of Economic Policy Instruments To Promote Sustainable Mobility. *Acta Universitatis Sapientiae – Economics and Business*. Online first. URL: https://acta.sapientia.ro/content/docs/ACTA-Economics-2025-13--2.pdf

Zoldy, M., Csete, M. S., Kolozsi, P. P., Bordas, P., Torok, A. (2022). Cognitive sustainability. *Cognitive Sustainability*. 1(1). DOI: 10.55343/cogsust.7

Zöldy, M., Baranyi, P., Török, Á. (2024). Trends in Cognitive Mobility in 2022. *Acta Polytechnica Hungarica*. 21(7), 189–202. DOI: 10.12700/APH.21.7.2024.7.11

https://doi.org/10.55343/CogSust.125

Study of the strength of a removable module with a container when loading it into an open wagon

Alyona Lovska
0000-0002-8604-1764
Department of Transport and Handling Machines, University of Žilina
Žilina, Slovak Republic
alyona.lovska@fstroj.uniza.sk

Juraj Gerlici
0000-0003-3928-0567
Department of Transport and Handling Machines, University of Žilina
Žilina, Slovak Republic
juraj.gerlici@fstroj.uniza.sk

Ján Dižo
0000-0001-9433-392X
Department of Transport and Handling Machines, University of Žilina
Žilina, Slovak Republic
jan.dizo@fstroj.uniza.sk

Miroslav Blatnický
0000-0003-3936-7507
Department of Transport and Handling Machines, University of Žilina
Žilina, Slovak Republic
mirolsav.blatnicky@fstroj.uniza.sk

Pavlo Rukavishnykov
0000-0002-9670-3071
Department of Heat Engineering, Heat Engines and Energy Management, Ukrainian State University of Railway Transport
Kharkiv, Ukraine
rukavishnikov@kart.edu.ua

Abstract

The main goal of this article is to present the design of a removable module that facilitates transportation of containers in open wagons. This module functions as an intermediary adapter between a wagon body and a container, and it ensures their reliable interaction. The loading of the removable module with the container into an open wagon is provided by suspended or other types of loading and unloading devices. Appropriate calculations were made to study the strength of the removable module during loading and unloading operations. The movement of the removable module using steel ropes and a spreader was considered. The calculation of the strength of the removable module was carried out in the SolidWorks Simulation software, which implements the finite element method. It was established that the strength of the removable module is ensured within the considered load schemes. The results of the conducted research will contribute to increasing the efficiency of container transportation by rail and to the development of a modular vehicle design.

Keywords

railway transport; design adaptation; removable module, structural load; container transportation

https://doi.org/10.55343/CogSust.125

1. Introduction

The increasing profitability of international transport led to the introduction of container transportation. The possibility of transporting containers by almost all types of vehicles ensures their mobility and widespread use in transport operations (Caban et al., 2021; Soloviova et al., 2020).

A significant share of container transportation is accounted for by rail transport: containers are carried on platform wagons (Haferkorn, 2022; Široky et al., 2024). The occasional lack of platform wagons in operation makes it necessary to use other types of wagons for container transportation, for example, open wagons. However, the use of open wagons for container transportation requires a reliable system of interaction, as open wagons are not designed for this purpose. The lack of compatibility might lead to damage not only of the container itself together with transported cargo, but also to the open wagon body (Medvediev et al., 2024; Milenković et al., 2023; Wang and Xie, 2024). This is also dangerous from an environmental point of view, because in the event of an accident, the release of cargo transported in unsecured containers into the environment might cause environmental hazards (Wickens et al., 2003; Norman, 2013; Graedel and Allenby, 2010; McDonough and Braungart, 2010). In this regard, the issues of situational adaptation of open wagon to transportation of containers are highly relevant and requires thorough research.

The purpose of the study presented here is to determine the load bearing structure of a removable module with a container when it is loading into an open wagon. To achieve this goal, the following tasks are defined:

- Determination of the strength of the removable module when it is lifted by steel ropes (the 1st load case)
- Determination of the strength of the removable module when it is lifted by a spreader (the 2nd load case)
- To conduct an experimental study of the strength of the hatch cover of an open wagon when loaded by the removable module.

2. Literature review

The issues of creation of railway vehicles for container transportation and their introduction into operation are quite urgent. For example, Lovska (2024) highlights the results of studies of the load concepts of the load-bearing structures of a platform wagon considering improvements to increase the efficiency of their operation in international transport. Measures are proposed to improve the load-bearing structures of platform wagons in order to extend their functions for transporting containers, timber or steel in rolls, wood chips or trailers; also to promote the use of platform wagons for military and strategic purposes. The author suggests the creation of articulated platform wagons based on existing structures. At the same time, solutions aimed at the adaptation of open wagons to the transportation of containers are not proposed in this work.

In order to increase the efficiency of container transportation by railway, Reidemeister et al. (2016) proposed to improve the supporting structure of a universal platform wagon by placing fitting stops on the longitudinal beams of the frame. The results of experimental studies of the strength of the wagon frame during shunting manoeuvres, considered the most unfavorable loading condition for the load-bearing structure of the wagon in operation, are presented. It was established that the proposed modernization is expedient. However, the authors did not investigate the feasibility of such modernization of open wagons for the purpose of transporting containers.

The work presented in Shaposhnyk et al. (2021) proposes the modernization of a universal platform wagon for enabling container transport . by applying a removable frame on a platform wagon. The results of the calculations proved the feasibility of using such a solution on platform wagons, but this study did not test open wagons for similar purposes either.

Some studies (Gerlici et al., 2023a; Lovska et al., 2024) have investigated the strength of a hatch cover of a universal open wagon when subjected to loading by a fitting stop. It was established that the transportation of containers in open wagons, whose floor is equipped with hatch covers, is not possible without additional modernization. However, the authors of this study did not propose an adaptation of an open wagon to the container transportation.

Measures for the safe transportation of containers in an RGS wagon type are proposed by Berescu et al. (2020). A special feature of the container fastening scheme on this wagon type is the use of special bolts. The authors made appropriate calculations and determined the optimal type of bolts for fixing containers. However, the authors did not examine the possibility of using such a fastening scheme for containers in open wagons.

The research by Gerlici et al. (2023b) proposes a concept of a removable module for the situational adaptation of open wagons for container transportation. The design of the removable module is multifunctional, and it can be used for

https://doi.org/10.55343/CogSust.125

transporting other types of cargo if modernized. The study provides a justification of the use of such a module for fastening containers on open wagons. It also highlights the design features of the removable module using modern software tools. However, the strength of the load-bearing structure of an open wagon and the container considering the use of this module, was not examined in the study.

Determining the load of an open wagon when transporting containers is carried out by Gerlici et al. (2023c). A solution for improving the container fastening scheme in an open wagon is proposed. However, these solutions are proposed as concepts, and no examples of their implementation are provided.

The above analysis of the literature demonstrates that the issues of situational adaptation of wagons for container transportation are highly relevant. At the same time, the adaptation of the load-bearing structures of open wagons for container transportation has not been given appropriate attention. This makes it necessary to study this issue in more detail.

3. Analysis of the strength of the removable module

It is suggested to use a removable module for safe transportation of containers in an open wagon. This module works on a principle of an intermediate adapter between the container and the open wagon body (Fig. 1). The module consists of a frame, which is made up of lateral beams (1), end beams (2), longitudinal beams (3), end structures (4) and diagonal reinforcement beams (5). Further, it is equipped with corner fittings – lower (6) and upper (7) –, which allow the module to be fastened to an open wagon. These components are supplemented by additional fittings stops (8).

A detail of container fastening in the module by fitting stops is depicted in Fig. 2.

At the same time, the interaction of suspended devices with the removable module is assumed at its upper fittings. The results of evaluating the loading of the removable module during transportation in an open wagon – considering the most unfavourable loading conditions – showed that the strength of the module is ensured, and the proposed container fastening scheme is appropriate (Panchenko et al., 2024).

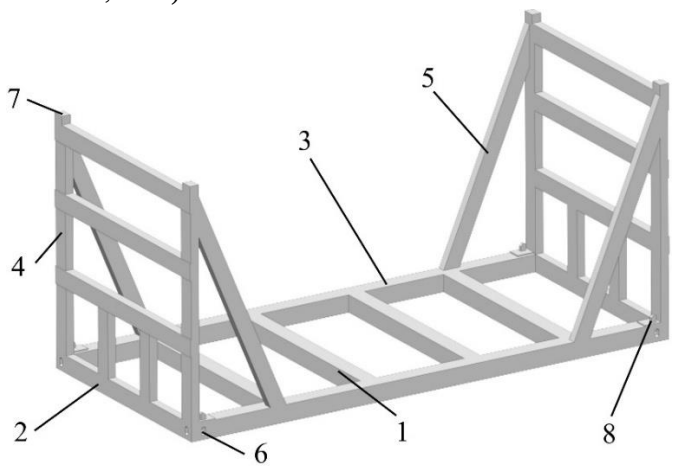

Figure 1. Removable module for container fastening in an open wagon

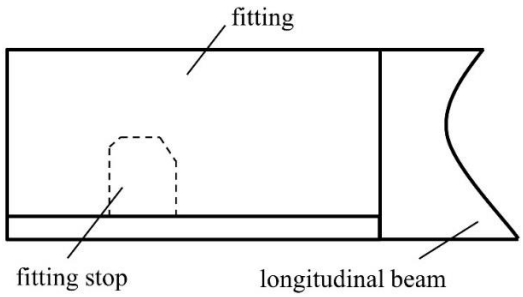

Figure 2. A scheme of interaction of the fitting stops with the fitting of the removable module

Loading of the removable module together with a container into an open wagon is achieved by suspended or other types of loading and unloading devices, as shown in Fig. 3.

https://doi.org/10.55343/CogSust.125

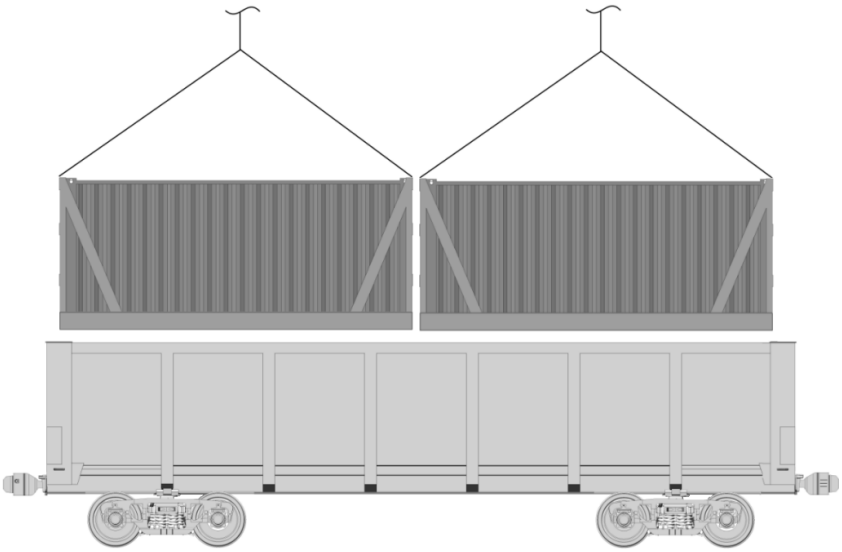

Figure 3. Loading of removable modules with containers in an open wagon

To study the strength of the removable module during loading and unloading operations, appropriate calculations were carried out. Two loading scenarios are considered:

- by means of steel ropes – the 1st loading case (Fig. 4a)
- by means of a spreader – the 2nd loading case (Fig. 4b)

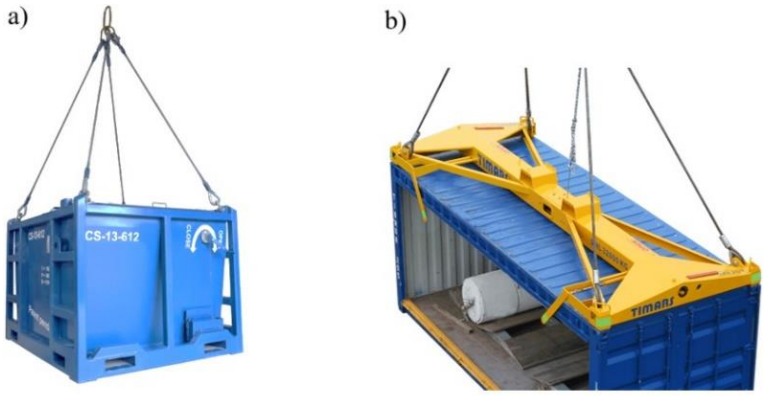

Figure 4. Suspended means of transport when interacting with containers:
a) steel ropes; b) a spreader

At the initial stage of research, the strength of the removable module was determined when it was lifted using steel ropes, i.e. for the 1st loading case. The strength calculation was carried out in the SolidWorks Simulation software using the finite element method (Kozyar et al., 2018; Pustylga et al., 2018).

A calculation scheme of the removable module for the 1st loading case is shown in Fig. 5.

It is considered that the removable module is loaded by the force P_v (the load of the own mass) as well as the gross weight of the container P_k. In the areas of interaction of the removable module with the steel ropes (upper corner fittings), the load P_s was applied. This load is divided into two components (vertical and horizontal), taking into account of the angle of inclination of steel ropes, which is assumed to be 45°.

The finite-element (FE) model of the removable module is constructed using tetrahedrons. Their optimal number was determined by a graphical-analytical method. Considering the calculations, the number of elements of the finite element mash was of 95,235 with a maximum size of 100 mm and a minimum of 20 mm. The number of nodes of the FE mesh was 33,147.

https://doi.org/10.55343/CogSust.125

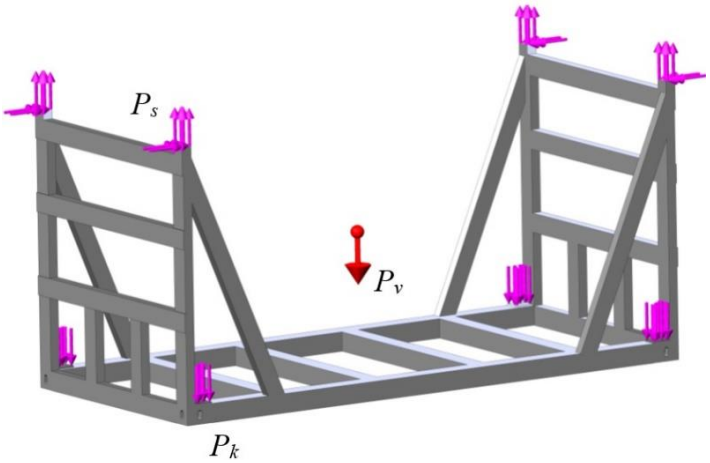

Figure 5 A calculation scheme of the removable module during its lifting by steel ropes

Steel 09G2S was selected as a construction material for the designed removable module. This steel type was chosen because it is the most common steel used for manufacturing wagon structures, and it is used not only for the load-bearing structures of wagons, but also for modular transport units. The results of strength calculations for the removable module for the 1st loading case are shown in Fig. 6 and Fig. 7.

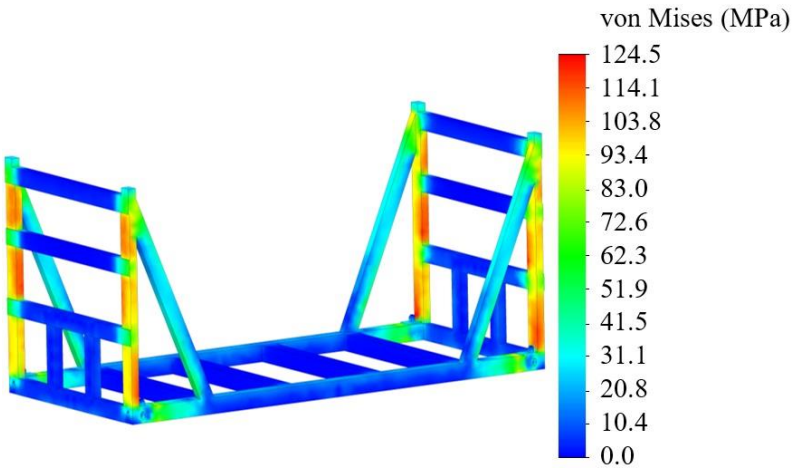

Figure 6. Stress distribution in the removable module structure in the 1st load case

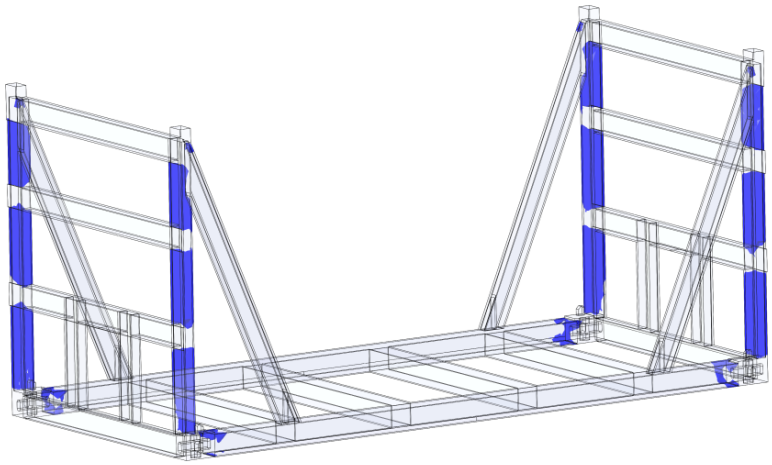

Figure 7. The most loaded areas of the removable module are the end structures in the 1st load case

https://doi.org/10.55343/CogSust.125

Maximum stresses occur in the zones of interaction of end beams with longitudinal beams. These stresses amounted to 124.5 MPa (Fig. 6). These values do not exceed the permissible values given in the standard (DSTU, 2014). Therefore, the strength of the removable module design within the applied load scheme (the 1st load case) is ensured.

The stress distribution along the height of the end beams is shown in Fig. 8.

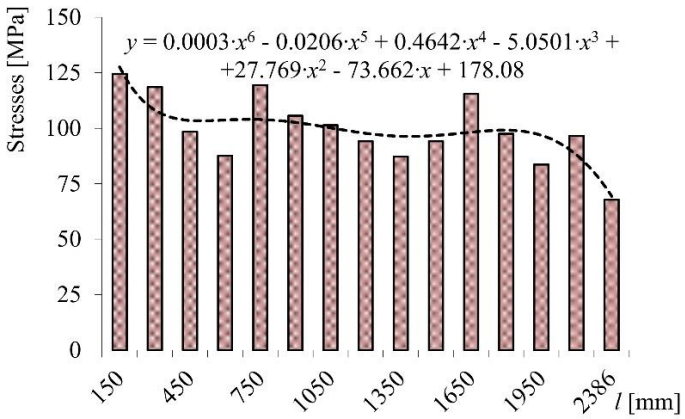

Figure 8. A distribution of stresses along the height of the removable module end structures for the 1st load case

As it can be seen in Fig. 8., the stresses distributed in the removable structure have a variable character. This phenomenon can be explained by the presence of diagonal reinforcement beams in the end superstructures, and accordingly, by the variable stiffness of end structures in height.

At the next stage, the strength of the removable module when it is lifted by a spreader, i.e. for the 2nd load case, was investigated. A calculation scheme of the removable module for the 2nd load case is shown in Fig. 9.

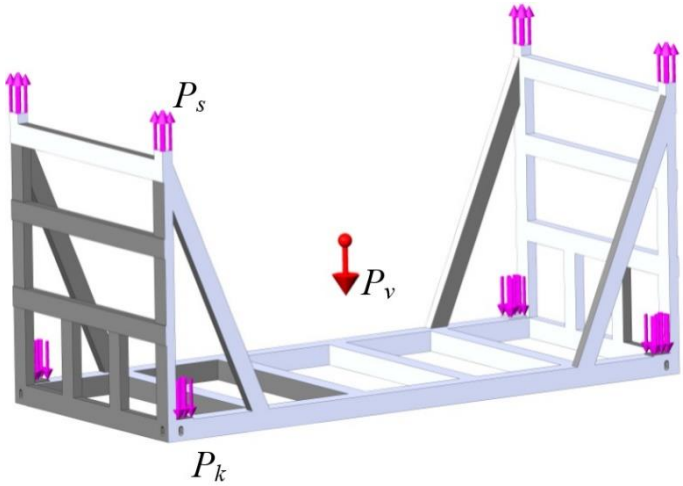

Figure 9. A calculation scheme of the removable module for the 2nd load case

The force P_v (the load of the own mass) as well as the gross weight of the container P_k are taken into account as the load of the removable module for the 2nd load case. The load of P_s is applied in the areas of interaction of the removable module with the spreader (upper corner fittings).

The results of the strength analysis of the removable module are shown in Fig. 10 and Fig. 11. The maximum stresses were identified in the zones of interaction of end structures with the longitudinal beams. These stresses amounted to the value of 135.7 MPa (Fig. 10). However, the permissible values of the strength of the used material are not exceeded (DSTU, 2014) in this case either.

https://doi.org/10.55343/CogSust.125

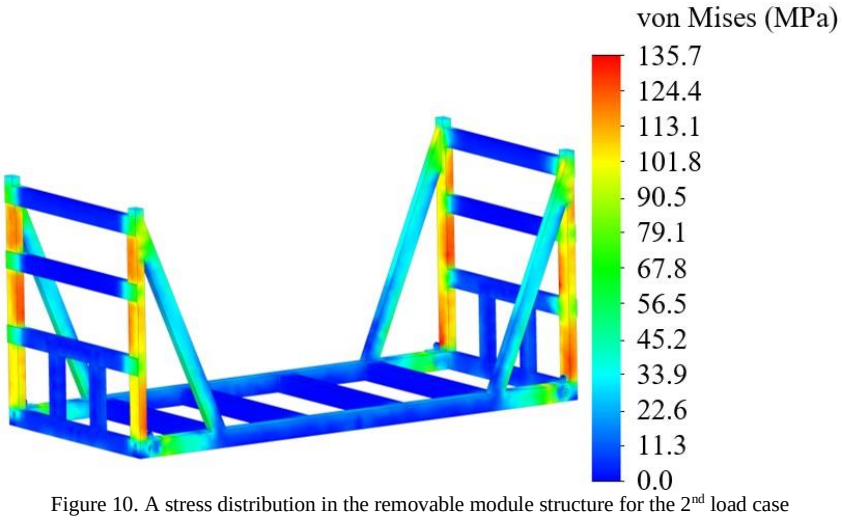

Figure 10. A stress distribution in the removable module structure for the 2nd load case

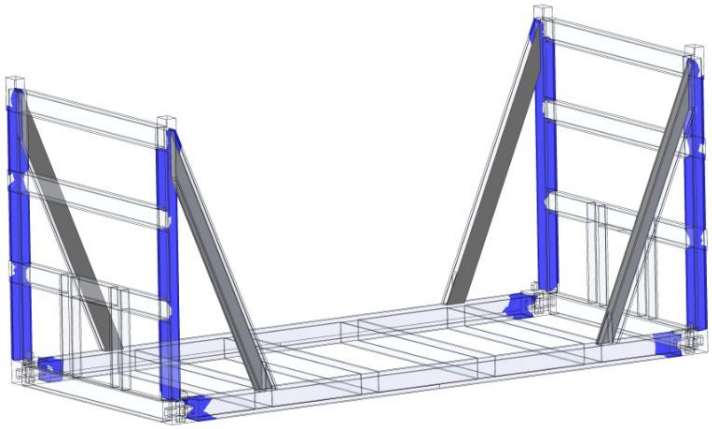

Figure 11. The most loaded areas of the removable module for the 2nd load case

The stress distribution along the removable module end structures is shown in Fig. 12. The nature of the stresses varying in height of the end structures of the removable module is explained in the same way as in the previous load case (i.e. the 1st load case).

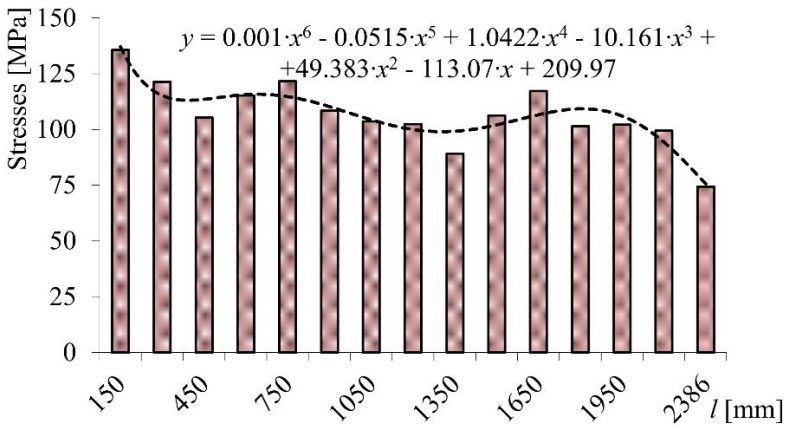

Figure 12. A distribution of stresses along the removable module end structures for the 2nd load case

The performed calculations prove that the strength of the removable module for container transport is ensured for its loading and unloading operations. The performed analyses revealed that the load of the removable module is slightly higher

https://doi.org/10.55343/CogSust.125

for the manipulation with a spreader in comparison with manipulation with steel ropes. This can be caused by the angle of inclination of steel ropes, which leads to dividing the load into two components and, accordingly, this causes a decrease of stresses in the design of the removable module.

To substantiate the use of a removable module for fastening containers in an open wagon, an experimental determination of stresses in the hatch cover of an open wagon was carried out. This structural unit of the wagon body forms its floor (Fig. 13). When the fitting stop is placed on the hatch cover, it is exposed to the load. Therefore, it is advisable to examine its strength. Bench tests were run in the research laboratory of the "Center for Diagnostics of Transport Structures" at the Ukrainian State University of Railway Transport. The determination of stresses in the hatch cover structure was carried out using the method of electrical strain gauge measurement. The strain gauges were calibrated before installing the strain gauge resistors. Strain gauge resistors with a base of 10 mm and a resistance of 100 Ohms were used in this case (Fig. 14).

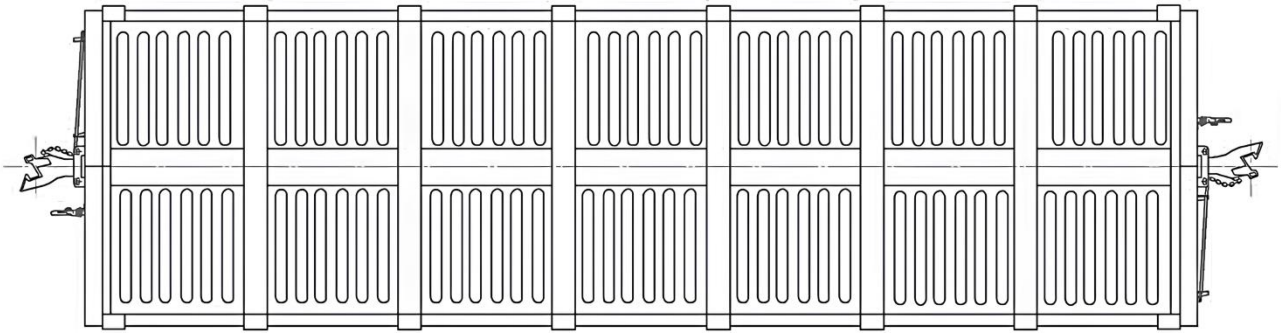

Fig. 13. A placement of hatch covers on the wagon body floor (a top view)

Figure 14. Placement of strain gauges on the hatch cover

The strain gauges were installed according to the bridge scheme. The locations of the strain gauges on the hatch cover were determined by the theoretically obtained stress fields. The scheme of the groups of strain gauges on the hatch cover is shown in Fig. 15. Strain gauges were also placed at the bottom of the hatch cover in the same areas as at the top.

https://doi.org/10.55343/CogSust.125

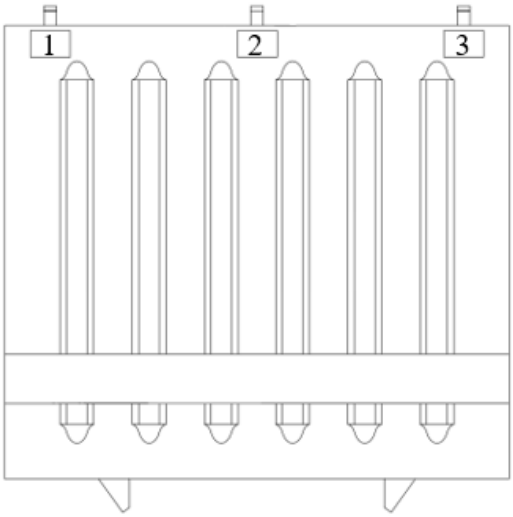

Figure 15. An arrangement of groups of strain gauges on the hatch cover: 1 – the first group; 2 – the second group; 3 – the third group

A special stand was created to test the hatch cover, which was secured by hinges using metal pins (Fig. 16).

The load was transferred to the hatch cover through a metal plate (Fig. 15, 16), whose width was equal to the width of the longitudinal beam of the removable module.

The load on the plate was transferred through an I-beam, which, in turn, perceived the load from a jack. The load value was controlled by a dynamometer. In this case, the maximum load value was 6 t (60 kN), which corresponds to the maximum loaded state of a 1CC size container.

The largest deformation readings during the tests were recorded by the strain gauges in Group 3 (Fig. 17). It can be seen in Fig. 17 that the dependence of relative deformations on the load is linear. The stresses arising in the hatch cover are shown in Fig. 18.

Figure 16. The placement of the hatch cover on the test stand

https://doi.org/10.55343/CogSust.125

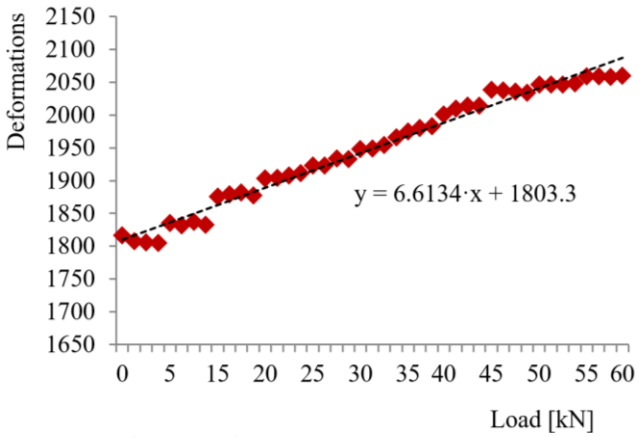

Figure 17. Dependence of relative deformations in the hatch cover on vertical load (strain gauge Group 3)

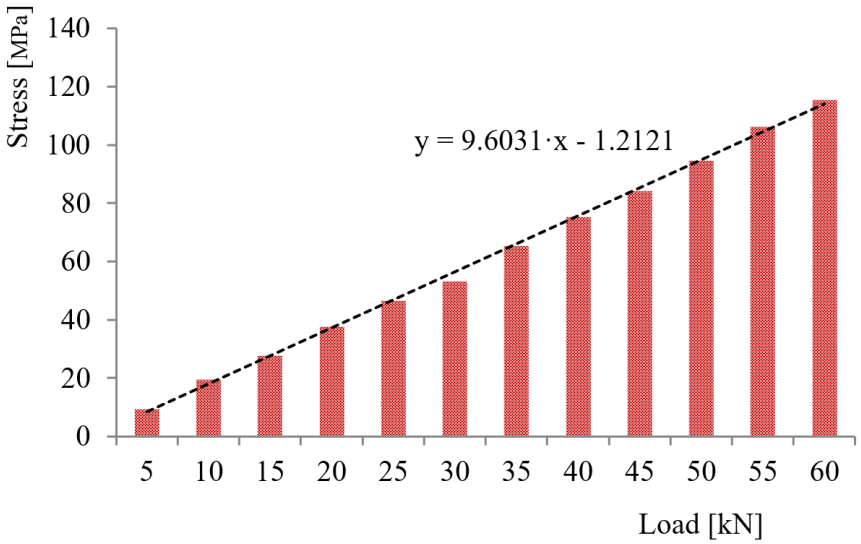

Figure 18. A dependence of stresses in the hatch cover on its load

The maximum stresses identified in the hatch cover were 103.5 MPa. These stresses are lower than the permissible ones introduced in (DSTU 7598:2014).

For a comparative analysis of the results of experimental studies with theoretical ones, the authors performed variational calculations of the strength of the hatch cover using the finite element method.

The discrepancy between the results of computer modelling of the strength of the hatch cover and experimental studies is shown in Fig. 19.

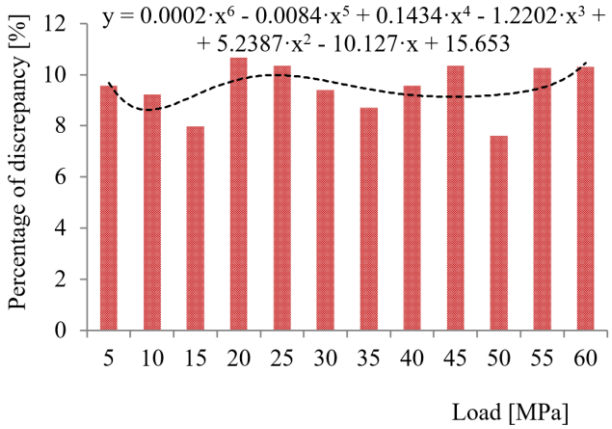

Figure 19. A discrepancy between the results of a computer simulation of the strength of the hatch cover and experimental studies

https://doi.org/10.55343/CogSust.125

It can be concluded from Fig. 17 that the largest percentage of a discrepancy is of 10.4%, and it is recorded when the load on the hatch cover is 20 kN.

Thus, the proposed scheme of fastening containers in an open wagon allows to reduce the stress in the hatch cover by three-times compared to the typical scheme of interaction of fittings with fitting stops (Rukavishnykov, 2025).

The presented study is a part of more expensive research, which includes also economic assessment of the proposed technical solution. The economic indicators are explained and calculated in details in the research work by Rukavishnykov (Rukavishnykov, 2025). Evaluation was performed on freight wagons with the number over 100,000. According to preliminary calculations, the economic effect of using the proposed technology of container transportation for the calculation period (10 years) is of 88.028 million UAH (1CC size containers) or 49.376 million UAH (1AA size containers). In this case, the economic effect is determined by the annual savings of the dependent part of operating costs compared to the basic option of using open wagons and one-time costs for their structural re-equipment for container transportation in the empty direction (Rukavishnykov, 2025).

4. Conclusion

(1) Determination of the strength of the removable module when lifting it with steel ropes was carried out (the 1st load case). The maximum stresses were recorded in the zones of interaction of the end structures with longitudinal beams. These stresses amounted to 124.5 MPa. These values did not exceed the permissible values of the used material (steel 09G2S). This distribution of stress fields is determined by a scheme of fastening and loading of the removable module.

(2) Determination of the strength of the removable module when it is lifted by a spreader was also carried out. The maximum stresses were recorded also in the zones of interaction of the end structures with longitudinal beams. These stresses amounted to 135.7 MPa, and they did not exceed the permissible values either.

(3) An experimental study of the strength of the hatch cover of an open wagon loaded by a removable module was conducted. The maximum stresses recorded in the hatch cover were of 103.5 MPa. The obtained stress value is lower than the permissible one. The largest percentage of discrepancy is of 10.4% and was recorded when the load on the hatch cover was 20 kN. The proposed scheme for fastening containers in an open wagon allows to reduce the stresses in the hatch cover by three-times compared to the typical scheme of interaction of fittings with fitting stops.

(4) The results of the conducted research will contribute to increasing the efficiency of container transportation by railway and to the development of modular rail vehicles. They will also help to improve the environmental friendliness of freight transportation by rail, that is, to the creation of sustainable transport.

Acknowledgement

This research was supported by the Slovak Research and Development Agency of the Ministry of Education, Science, Research and Sport of the Slovak Republic VEGA 1/0308/24 “Research of dynamic properties of rail vehicles mechanical systems with flexible components when running on a track” and by the Slovak Cultural and Educational Grant Agency in the project KEGA 031ŽU-4/2023 Development of key competencies of the graduate of the study program Vehicles and Engines.

Funded by the EU NextGenerationEU through the Recovery and Resilience Plan for Slovakia under the project No. 09I03-03-V01-00131.

References

Berescu, C., Fratila, C., Axinte, T., Diaconu, M., Cojocaru, R. (2020). The mechanism's study of fixing a container on a freight wagon type Rgs. *Proceedings of the 8th International Conference on Modern Technologies in Industrial Engineering (ModTech 2020)*. 916, 012010. DOI: 10.1088/1757-899X/916/1/012010

Caban J., Nieoczym A., Gardyński L. (2021). Strength analysis of a container semi-truck frame. *Engineering Failure Analysis*. 127, 105487. DOI: 10.1016/j.engfailanal.2021.105487.

DSTU (2014) – ДСТУ 7598:2014 Вагони вантажні. Загальні вимоги до розрахунків та проектування нових і модернізованих вагонів колії 1520 мм (несамохідних) [Freight wagons. General requirements for calculations and design of new and modernized 1520 mm gauge wagons (non-self-propelled)]. Kyiv.

Gerlici, J., Lovska, A., Vatulia, G., Dizo, J., Blatnicky, M. (2023a). Research into the strength of the discharge door of an open wagon transporting containers. *Proceedings of the 15th International Scientific Conference on Aeronautics, Automotive, and Railway Engineering and Technologies (BulTrans 2023)*. 3129, 060001. DOI: 10.1063/5.0201451

Gerlici, J., Lovska, A., Vatulia, G., Pavliuchenkov, M., Kravchenko, O., Solčanský, S. (2023b). Situational adaptation of the open wagon body to container transportation. *Applied Sciences*. 13(15), 8605. DOI: 10.3390/app13158605

Gerlici, J., Vatulia, G., Lovska, A., Skurikhin, D., Harušinec, J., Suchánek, A., Ishchuk, V. (2023c). The strength of the open wagon body when transporting containers. *Proceedings of 27th International Scientific Conference (Transport Means 2023)*, 440–445.

Graedel, T. E., Allenby, B. R. (2010). Industrial Ecology and Sustainable Engineering. Pearson, Boston, MA.

Haferkorn, F. (2022). Articulated train of deep well cars for high-speed container transport. *WIT Transactions on the Built Environment*. 213: *Computers in Railways XVIII*, 121–134. DOI: 10.2495/CR220111

Kozyar et al. (2018). – Козяр М. М., Фещук Ю. М. В., Парфенюк О. В. (2018). Комп'ютерна графіка: SolidWorks: Навчальний посібник [Computer graphics: SolidWorks: Study guide]. Херсон, Олді-плюс. URL: https://ep3.nuwm.edu.ua/22175/1/%D0%9A%D0%BE%D0%BC%D0%BF%27%D1%8E%D1%82%D0%B5%D1%80%D0%BD%D0%B0%20%D0%B3%D1%80%D0%B0%D1%84%D1%96%D0%BA%D0%B0.pdf

Lovska, A. (2024). *Situational adaptation of flat wagons for international traffic*. Monograph. Riga, Latvia: Baltija Publishing, 312 p. DOI: 10.30525/978-9934-26-467-2

Lovska et al. (2024) – Ловська, А. О., Мурад'ян, А. О., Рукавішников, П. В., Демидюков, О. В. (2024). Аналіз міцності кришки люка універсального напіввагона при перевезенні в ньому контейнерів [Analysis of the strength of the hatch cover of a universal open wagon when transporting containers in it]. *Academic notes of the Tavri National University named after V. I. Vernadskyi. Series: Technical Sciences*. 35(2), 304–309. DOI: https://doi.org/10.32782/2663-5941/2024.2/42

McDonough, W., Braungart, M. (2010). *Cradle to Cradle: Remaking the Way We Make Things*. North Point Press, New York, NY.

Medvediev, I., Muzylyov, D., Montewka, J. (2024). A model for agribusiness supply chain risk management using fuzzy logic. Case study: Grain route from Ukraine to Poland. *Transportation Research Part E: Logistics and Transportation Review*. 190, 103691. DOI: 10.1016/j.tre.2024.103691

Milenković, M., Bojović, N., Abramin, D. (2023). Railway freight wagon fleet size optimization: A real-world application. *Journal of Rail Transport Planning and Management*. 26, 100373. DOI: 10.1016/j.jrtpm.2023.100373

Norman, D. A. (2013). *The Design of Everyday Things*. Revised and Expanded Edition. Basic Books. Hachette, UK.

Panchenko, S., Lovska, A., Muradian, A., Pelypenko, Ye., Rukavishnykov, P., Demydiukov, O. (2024). Identifying possible ways for adapting an open wagon for transporting containers. *Eastern-European Journal of Enterprise Technologies* 5/7(131), 6–14. DOI: 10.15587/1729-4061.2024.311324

Pustylga, S. I. et al. (2018). – Пустюльга С. І., Самостян В. Р., Клак Ю. В. (2018) Інженерна графіка в SolidWorks : навчальний посібник [Engineering graphics in SolidWorks: a tutorial]. Луцьк : Вежа.

Reidemeister, O. H., Kalashnyk, V. O., Shykunov, O. A. (2016). Modernization as a way to improve the use of universal cars. *Science and Transport Progress.* 2(62), 148–156. DOI: 10.15802/stp2016/67334

Rukavishnykov, P. V. (2025). Improvement of methods of technical adaptation of an open wagon for transportation of containers (in Ukrainian). Doctoral dissertation thesis, Kharkiv, Ukraine, UkrSURT.

Shaposhnyk, V., Shykunov, O., Reidemeister, A., Leontii, M., Potapenko, O. (2021). Determining the possibility of using removable equipment for transporting 20- and 40-feet-long containers on an universal platform wagon. *Eastern-European Journal of Enterprise Technologies*. 1(7), 14–21. DOI: 10.15587/1729-4061.2021.225090

Široky, J., Nachtigall, P., Tischer, E., Schejbal, K., Michalek, T. (2024). The modelling of traction energy consumption of a container train. *Transportation Research Procedia*. 77, 76–84. DOI: https://doi.org/10.1016/j.trpro.2024.01.010

Soloviova, L., Strelko, O., Isaienko, S., Soloviova, O., Berdnychenko, Yu. (2020). Container Transport System as a Means of Saving Resources. *IOP Conference Series: Earth and Environmental Science 459 (2020).*. 052070. DOI: 10.1088/1755-1315/459/5/052070

Wang, D., Xie, Ch. (2024). A descriptive and prescriptive analysis of rail service subsidies in the China–Europe freight transportation market. *International Journal of Transportation Science and Technology*. 1–16. DOI: 10.1016/j.ijtst.2024.06.003

Wickens, C. D., Lee, J. D., Liu, Y., Gordon-Becker, S. E. (2003). *An Introduction to Human Factors Engineering*. 2nd edition. Pearson. 587 p.